

Utah State University

DigitalCommons@USU

All Graduate Theses and Dissertations

Graduate Studies

5-2015

High Resolution Multi-Spectral Imagery and Learning Machines in Precision Irrigation Water Management

Leila Hassan-Esfahani
Utah State University

Follow this and additional works at: <https://digitalcommons.usu.edu/etd>



Part of the [Civil and Environmental Engineering Commons](#)

Recommended Citation

Hassan-Esfahani, Leila, "High Resolution Multi-Spectral Imagery and Learning Machines in Precision Irrigation Water Management" (2015). *All Graduate Theses and Dissertations*. 4480.
<https://digitalcommons.usu.edu/etd/4480>

This Dissertation is brought to you for free and open access by the Graduate Studies at DigitalCommons@USU. It has been accepted for inclusion in All Graduate Theses and Dissertations by an authorized administrator of DigitalCommons@USU. For more information, please contact digitalcommons@usu.edu.



HIGH RESOLUTION MULTI-SPECTRAL IMAGERY AND LEARNING MACHINES
IN PRECISION IRRIGATION WATER MANAGEMENT

by

Leila Hassan-Esfahani

A dissertation submitted in partial fulfillment
of the requirements for the degree

of

DOCTOR OF PHILOSOPHY

Civil Engineering

Approved:

Mac McKee, PhD.
Major Professor

Douglas Ramsey, PhD.
Committee Member

David Stevens, PhD.
Committee Member

Todd Moon, PhD.
Committee Member

David Rosenberg, PhD.
Committee Member

Mark R. McLellan, Ph.D.
Vice President for Research and
Dean of the School of Graduate Studies

UTAH STATE UNIVERSITY

Logan, Utah

2015

Copyright © Leila Hassan Esfahani 2015

All Rights Reserved

ABSTRACT

High-Resolution Multi-Spectral Imagery and Learning Machines in Precision Irrigation
Water Management

by

Leila Hassan Esfahani, Doctor of Philosophy

Utah State University, 2015

Major Professor: Mac McKee

Department: Civil and Environmental Engineering

The current study has been conducted in response to the growing problem of water scarcity and the need for more effective methods of irrigation water management. Remote sensing techniques have been used to match spatially and temporally distributed crop water demand to water application rates. Remote sensing approaches using Landsat imagery have been applied to estimate the components of a soil water balance model for an agricultural field by determining daily values of surface/root-zone soil moisture, evapotranspiration rates, and losses and by developing a forecasting model to generate optimal irrigation application information on a daily basis. Incompatibility of coarse resolution Landsat imagery (30m by 30m) with heterogeneities within the agricultural field and potential underestimation of field variations led the study to its main objective, which was to develop models capable of representing spatial and temporal variations within the agricultural field at a compatible resolution with farming management activities. These models support establishing real-time management of irrigation water scheduling and application. The

AggieAir™ Minion autonomous aircraft is a remote sensing platform developed by the Utah Water Research Laboratory at Utah State University. It is a completely autonomous airborne platform that captures high-resolution multi-spectral images in the visual, near infrared, and thermal infrared bands at 15cm resolution. AggieAir flew over the study area on four dates in 2013 that were coincident with Landsat overflights and provided similar remotely sensed data at much finer resolution. These data, in concert with state-of-the-art supervised learning machine techniques and field measurements, have been used to model surface and root zone soil volumetric water content at 15cm resolution. The information provided by this study has the potential to give farmers greater precision in irrigation water allocation and scheduling.

(153 pages)

PUBLIC ABSTRACT

High-Resolution Multi-Spectral Imagery and Learning Machines in Precision Irrigation
Water Management

by

Leila Hassan Esfahani, Doctor of Philosophy

Utah State University, 2015

Major Professor: Mac McKee

Department: Civil and Environmental Engineering

The goals of preserving scarce water resources, cultivating more lands, and saving on irrigation water bills have directed the attention of water resources managers toward the concepts of precision agriculture and, in particular, to precision irrigation. The purpose of precision irrigation is to increase irrigation efficiency to avoid crop water stress, avoid yield reduction due to under-irrigation and leaching of nutrients, runoff, and reduce soil erosion due to over-irrigation. In this study, irrigation efficiency has been defined in terms of irrigation uniformity and the response of the crop to irrigation. Crop water demand, soil moisture, evapotranspiration rate, and potential water losses to deep percolation and runoff have been calculated by using remotely sensed data, field measurements, and learning machines. Sub-field level irrigation water allocation and scheduling have been examined for an agricultural field in Utah. These calculations have been carried out at 30 m by 30 m resolution, which is commensurate with the applied remotely sensed data (Landsat

imagery). In addition to a focus on the use of satellite data for irrigation scheduling, this study has developed a similar irrigation water allocation model at a much finer resolution (15 cm by 15 cm) using a different set of remotely sensed data (acquired through use of an autonomous, unmanned remote sensing aircraft called AggieAirTM) to create surface and root zone soil moisture maps at 15 cm resolution. The high-resolution information provides the capability to represent spatial variations within the agricultural field at a compatible resolution with farming management activities. Instead of farmers visually perceiving agricultural field conditions, specifically soil moisture, this study provides a means whereby farmers might gain information about actual soil moisture distribution over the field, which could help in scheduling irrigation and enabling greater precision in the application of irrigation water by identifying dry/wet spots.

To my parents,
Fereshteh and Mohammad
My love and best friend,
Mahdi Maher
And my little angels,
Araad and unborn Maher

ACKNOWLEDGMENTS

I would like to express my sincere appreciation to Dr. Mac McKee for his valuable advice and encouragement. I sincerely appreciate the words of wisdom of Dr. McKee and his role in directing my attention toward the practical utility of my present and future work. Dr. McKee allowed me to develop academically in a free environment, allowing me to explore my edge of research.

Special thanks to my friend and coworker, Dr. Alfonso Torres-Rua, for his guidance throughout the research. Special thanks to Utah Water Research Laboratory, Utah State University, and the Provo Office of the US Bureau of Reclamation that supported my research financially through an MLF Seed Grant

I acknowledge the extraordinary efforts of the AggieAir flight team and Dr. Andres Ticlavilca, Dr. Roula Bachour, and Manal Elarab and the support of Ivan Robins, the agricultural farm owner, whose cooperation greatly improved the data collection procedure.

And last but not least, I give my special thanks to my husband, Mahdi Maher, for his help, encouragement, and moral support throughout this time at Utah State University.

Leila Hassan-Esfahani

CONTENTS

	Page
ABSTRACT	iii
PUBLIC ABSTRACT.....	v
ACKNOWLEDGMENTS.....	viii
LIST OF TABLES.....	xi
LIST OF FIGURES	xii
CHAPTER	
1. INTRODUCTION	1
1.1. Problem Statement	2
1.2. Purpose and Objectives.....	2
1.3. Research Motivation.....	3
1.4. Research Contributions.....	4
1.5. Remote Sensing Data.....	4
1.6. References.....	5
2. ASSESSMENT OF SURFACE SOIL MOISTURE USING HIGH- RESOLUTION MULTI-SPECTRAL IMAGERY AND ARTIFICIAL NEURAL NETWORKS	6
2.1. Introduction	7
2.2. Materials and Methods.....	10
2.3. Results and Discussion.....	22
2.4. Conclusions	31
2.5. Future Work.....	34

2.6.	References.....	34
3.	HIGH-RESOLUTION ROOT-ZONE SOIL WATER CONTENT ESTIMATION USING BAYESIAN-BASED MODEL AND HIGH-RESOLUTION VISUAL, NIR, AND THERMAL IMAGERY: A CASE STUDY.....	42
3.1.	Introduction	43
3.2.	Materials and Methods.....	47
3.3.	Results and Discussion.....	60
3.4.	Conclusions	76
3.5.	References.....	78
4.	ASSESSMENT OF OPTIMAL IRRIGATION WATER ALLOCATION FOR PRESSURIZED IRRIGATION SYSTEM USING WATER BALANCE APPROACH, LEARNING MACHINES, AND REMOTELY SENSED DATA.....	86
4.1.	Introduction	87
4.2.	Model Components Review.....	89
4.3.	Materials and Methods.....	92
4.4.	Results.....	100
4.5.	Conclusions	105
4.6.	References.....	107
5.	CONCLUSIONS.....	112
5.1.	General Conclusions.....	112
5.2.	Future Work.....	117
6.	Appendices.....	118

LIST OF TABLES

Table	Page
2.1 Temporal and spatial changes in normalized difference vegetation index (NDVI) values during the study period.....	23
2.2 Goodness-of-fit statistics from Wrapper selection results (1 to 10 inputs) with highest predictive power using ANN	26
2.3. Comparison between measured and estimated soil moisture values for different crop type zones.....	30
3.1. Comparison between measured and estimated soil moisture values for different crop type zones.....	61
3.2. Temporal and spatial changes in NDVI values during the study period related to the different crops present in the area of study.....	62
3.3. P-values presented as the results of correlation test.....	63
3.4. Goodness-of-fit statistics from wrapper selection results (1 to 10 inputs) for surface soil moisture estimations (SM-0) with highest predictive power using Bayesian artificial neural networks.....	65
3.5. Goodness-of-fit statistics from wrapper selection results (1 to 10 inputs) for soil moisture estimations at 15 cm (SM-15) with highest predictive power using Bayesian artificial neural networks.....	68
4.1. Components of the model based on a water balance approach.....	98
4.2. Components of the ANN model for surface and deep soil moisture estimation.....	100
4.3. Comparison of volume of water in the root zone for current irrigation management and water balance simulation model for three sample arcs.....	101
4.4. Comparison of volume of water in the root zone for current and optimized irrigation management for three sample arcs (objective one).....	102
4.5. Comparison of volume of water in the root zone for current and optimized irrigation management for three sample arcs (objective two).....	103

LIST OF FIGURES

Figure	Page
2.1. The location of the study area in Utah (schematic Utah counties map (on the left) and cropping pattern for 2013 irrigation season (on the right)), (39°14'N, 112°6'W).....	14
2.2. (a) Some raw natural color images from the unmanned aerial vehicle (UAV) taken from the study area (39°14'N, 112°6'W); (b) Orthorectified image using position and orientation of UAV aircraft during image capture; and (c) Accurate orthorectified mosaic image from EnsoMOSAIC	16
2.3. Spatial distribution of soil moisture sample locations in the study area.....	17
2.4. Map of field capacity based on soil texture type and plot of the location of soil samples.....	18
2.5. Schematic view of possible performance by 5-input dataset using wrapper selection method and artificial neural network (ANNs).....	25
2.6. (a) The measured soil moisture values versus the estimated values of the selected model; (b) one-by-one scatter plot; (c) residual plot; and (d) residual histogram.....	28
2.7. Performance plot of the selected ANN model with 8 inputs showing Mean Squared Error (MSE) trend during the leaning procedure for three data sets (training, testing and validation).....	29
2.8. Estimated soil moisture maps (Volumetric Water Content (%)), with ANNsmodel for four different dates (a) 16 May; (b) 1 June; (c) 9 June and (d) 17 June 2013 (Res. 15 cm) (right), false color images (left).....	32
3.1. The location of the study area in Utah (schematic Utah counties map (on the left) and cropping pattern for 2013 irrigation season (on the right)), (39°14'N 112°6'W).....	53
3.2. Spatial distribution of soil moisture sample locations in the study area.....	56
3.3. Map of field capacity based on soil texture type and plot of the location of soil samples.....	57
3.4. Volumetric root zone water content calculation procedure.....	60
3.5. Measured surface soil moistures versus estimated values of the selected model, the corresponding one-by-one plot, residual plot, and histogram of error.....	67

3.6. Measured soil moistures at 15 cm versus predicted values of the selected model, the corresponding one-by-one plot, residual plot, and histogram of error.....	72
3.7. Volumetric soil water content variation in the root zone profile at sample locations for each flight.....	73
3.8. Pixelwise measured root zone VWC versus pixelwise estimated root zone VWC....	74
3.9. Pixelwise VWC in the root zone for the four flights.....	75
4.1. The location of the study area in Utah, USA (schematic Utah counties map (on the right) and cropping pattern for 2013 irrigation season (on the left)), (39°14'N 112°6'W).....	93
4.2. Flowchart of soil moisture water balance calculation (SMWB) for the first time step.....	94
4.3. Map of field capacity based on soil texture type and plot of the location of soil moisture sensors.....	97
4.4. Evapotranspiration map (mm/day).....	101
4.5. a. Comparison of volume of water in the root zone for current irrigation management and water balance simulation model, b. Comparison of volume of water in the root zone for current and optimized irrigation management (objective one), c. Comparison of volume of water in the root zone for current and optimized irrigation management(objective two).....	104
4.6. Spatial distribution of soil water balance components in the field for a sample day during the growing cycle (day 17 with Landsat overpass) for objectives one (A) and two (B).....	105

CHAPTER 1

INTRODUCTION

Rapidly growing population levels and the need for drinking water and food are increasing global water demand drastically. Water use has been growing at more than twice the population rate, and a number of regions are already chronically short of water. Agricultural, industrial, and domestic consumption represent the major water withdrawals. Irrigated agriculture, responsible for nearly 40% of world food production, uses about 70% of total water withdrawals (FAO, 2006). Water shortage is a key concern for the future of agricultural production. This is more pressing when viewed in conjunction with climate change that is expecting to bring more extreme climatic conditions including droughts. Thus, as the population grows, more efficient use of water in the production of food will be of key importance.

Since water scarcity threatens both rain-fed and irrigation farming, water managers must seek new and sustainable solutions to water supply problems. Water shortage in irrigated farming has been a common problem, bordering on the norm rather than the exception, and irrigation management will shift from emphasizing production per unit area towards maximizing the production per unit of water consumed (Feres and Soriano, 2007).

Managers, planners, engineers, consultants, policymakers, and irrigators are cooperating to investigate new methods to cope with water scarcity issues. They are interested in effective methods to observe, measure, and respond to agricultural field conditions to forecast water demand and schedule optimally water allocation based on available water supplies.

1.1. Problem Statement

Of all sectors of the economy, agriculture is the most sensitive to water scarcity, which can have a huge impact on food production. Many researches have worked to combat this growing problem with more effective methods of water management. Irrigation patterns play an essential role in the productivity of a farm, especially in arid areas. Gains in water use efficiency can only be achieved by precisely matching water applications operations to the spatially and temporally distributed crop water demand.

1.2. Purpose and Objectives

The purpose of this study is to develop adaptable methods that allow for better response to agricultural farm conditions in terms of irrigation water scheduling and allocation. Remote sensing approaches (Landsat/Airborne imagery) have been applied to estimate surface/root-zone soil moisture and evapotranspiration rates, and state-of-art supervised learning machine techniques have been used to model these phenomena at different spatial scales. Incompatibility of coarse resolution of Landsat imagery with heterogeneities within the agricultural farms led us to our main objective which was developing models with the capability of representing spatial and temporal variations within the agricultural field at a compatible resolution with farming management activities. These models support establishing real-time management of irrigation water scheduling and application.

Chapter 2 presents a study in which Landsat imagery, field measurements, and crop-related remote sensing algorithms were applied to demonstrate the adequacy and accuracy of a model for optimizing irrigation water allocation and simulating soil moisture

conditions for a center pivot irrigation system in the study area. The accuracy of the model was checked using a soil water balance approach for the crop growing cycle (Chapter 2).

Chapter 3 uses high-resolution remote sensing imagery to develop accurate surface soil moisture estimates as main component of an agricultural water balance that could be used to enhance the quality of calculations in irrigation scheduling and water allocation. High resolution multi spectral imagery have been used to develop a data mining model that resulted in high resolution surface soil moisture estimations (Chapter 3).

Chapter 4 applies the same methodology used in Chapter 3 to estimate spatially distributed root-zone soil moisture values. It uses surface soil moisture information from chapter 3 as a boundary condition. An intensive calculation procedure was adopted in Chapters 3 and 4 to quantify the quality of soil moisture estimates at different calculation levels (Chapter 4).

1.3. Research Motivation

Recent literature has shown encouraging studies in a variety of agricultural water management problems through the use of remote sensing approaches and data mining algorithms. This initiated the idea that this methodology could be potentially applied for soil moisture estimation and irrigation water allocation models at a fine scale (at 0.15m) and at a comparatively coarse scale of Landsat imagery (30m). The information at these scales helps in identifying and understanding heterogeneities, variability, and correlations within the agricultural field in terms of soil moisture, evapotranspiration, and loses. Also the Bayesian based algorithm used to estimate root-zone soil moisture provided additional information about the variability of the results obtained.

1.4. Research Contributions

The current research has demonstrated the applicability of remote sensing approaches in monitoring agricultural field conditions to provide a solution to the objectives mentioned earlier. The information derived from this study provides high resolution surface and root zone soil moisture maps that are compatible with farming management activities. Also at Landsat level the developed models present information on optimizing center pivot operation in terms of saving water. This is the first study that combines learning machines with optimization algorithms to adjust the settings of a programmable irrigation facility while attempts to support more efficient irrigation water allocation schedules. Based on this study farmers can get the information to:

- Keep a record of their farm in terms of soil water content.
- Improve decision making on irrigation rates and applications.
- All of which improves the quality of the crops and enhances marketing.

1.5. Remote Sensing Data

AggieAir Minion is a remote sensing platform developed by Utah Water Research Laboratory at Utah State University. This completely autonomous airborne platform, equipped with multi-spectral cameras (red, green, blue, near infrared, and infrared/thermal) flew over the study area on May 16, June 1, June 9 and June 17, 2013, capturing the images at 15 cm resolution.

The flights were scheduled to coincide with Landsat over passes (either Landsat 7 ETM+, Landsat 8 OLI, that have similar spectral coverage at a spatial resolution of 30m) so that high-resolution products could be compared to the standard Landsat outputs. In order to acquire sufficient training and testing data to establish the learning algorithms at both spatial scales (AggieAir and Landsat), intensive ground sampling was accomplished at precisely determined locations. The data collection procedure was designed to cover maximum spatial distribution of soil moisture, crop type, and soil texture characteristics.

In addition, field data were collected for three dates in 2012, September 2 and 18 and October 4. The information from this part of study is used to develop an optimal water allocation model.

1.6. References

- FAO., 2006. Water Monitoring-Mapping Existing Global Systems & Initiatives. Prepared by FAO on behalf of the UN-Water Task Force on Monitoring, Rome (Italy).
- Fereres E., Soriano M.A., 2007. Deficit irrigation for reducing agricultural water use. *J. Exp. Bot.* 58 (2), 147-159.

CHAPTER 2

ASSESSMENT OF SURFACE SOIL MOISTURE USING HIGH-RESOLUTION
MULTI-SPECTRAL IMAGERY AND ARTIFICIAL NEURAL NETWORKS¹

ABSTRACT

Many crop production management decisions can be informed using data from high-resolution aerial images that provide information about crop health as influenced by soil fertility and moisture. Surface soil moisture is a key component of soil water balance, which addresses water and energy exchanges at the surface/atmosphere interface; however, high-resolution remotely sensed data is rarely used to acquire soil moisture values. In this study, an artificial neural network (ANN) model was developed to quantify the effectiveness of using spectral images to estimate surface soil moisture. The model produces acceptable estimations of surface soil moisture (root mean square error (RMSE) = 2.0, mean absolute error (MAE) = 1.8, coefficient of correlation (r) = 0.88, coefficient of performance (e) = 0.75 and coefficient of determination (R^2) = 0.77) by combining field measurements with inexpensive and readily available remotely sensed inputs. The spatial data (visual spectrum, near infrared, infrared/thermal) are produced by the AggieAir™ platform, which includes an unmanned aerial vehicle (UAV) that enables users to gather aerial imagery at a low price and high spatial and temporal resolutions. This study reports

¹ Reprinted from Remote Sensing Journal, Vol. 7(3), Leila Hassan-Esfahani, Alfonso Torres-Rua, Austin Jensen, Mac McKee, “Assessment of Surface Soil Moisture Using High-Resolution Multi-Spectral Imagery and Artificial Neural Networks” pages 2627-2646, © 2015 by the authors; licensee MDPI, Basel, Switzerland. This article is an open access article distributed under the terms and conditions of the Creative Commons Attribution license (<http://creativecommons.org/licenses/by/4.0/>)

the development of an ANN model that translates AggieAir™ imagery into estimates of surface soil moisture for a large field irrigated by a center pivot sprinkler system.

2.1. Introduction

Soil moisture content (SMC) is an important factor in managing irrigated farms. SMC includes two main components: surface soil moisture (SSM) (held in the upper 10 cm of soil) and root zone soil moisture (held in the upper 200 cm of soil). Surface soil moisture is a key component for addressing energy and water exchanges at the land surface/atmosphere interface and can be estimated using different techniques, such as *in situ* measurements, physically based models, remote sensing, etc. Grayson and Western addressed the estimation of soil moisture by applying: (1) field (or *in situ*) measurements; (2) remote sensing techniques; and (3) soil water balance simulation models [1,2]. Soil moisture constitutes a very small volume in terms of the total global water balance, but it plays a significant role in water resources planning and management [2]. Many current crop production management decisions that are made by growers, production managers, and crop advisors in precision agriculture are already based on observation from remotely sensed data such as satellite imagery. The objective of this research is to generate surface soil moisture (SSM) estimates using high-resolution, remotely sensed data, collected at 15 cm pixel resolution, as inputs to a learning machine algorithm (Artificial neural networks (ANNs)) developed under supervised learning procedures. ANNs are used to build the SSM estimation model. To our knowledge, this is the first study to document estimation of surface soil moisture using remotely sensed data at such a fine spatial resolution and readily available in the sense of temporal resolution. The results will contribute not only to efficient

and reliable high-resolution multi-spectral remote sensing validation, but also to better utilization of remotely sensed soil moisture products for enhanced irrigation modeling and scheduling.

Various techniques for retrieving soil moisture content have been the subject of research for almost four decades. Gravimetric measurements of soil moisture are very reliable but are laborious. Measuring SMC with imbedded sensors, such as time and frequency domain reflectometers (TDRs and FDRs), does not require a huge investment of time or facilities; however, most of these methods suffer from some of these same disadvantages. *In situ* measurements can be exhaustive and expensive if large areas are involved, as these measurements are mainly “local,” with a particular footprint representing moisture conditions in only a fraction of a cubic meter of soil [3]. Because of the spatial heterogeneity of soil moisture due to different soil conditions, vegetation, topography, or impact of human activities, local measurements when are carried out on a larger scale such as fields or watersheds, might result in inaccuracies [4]. Remote-sensing techniques might provide a useful tool to address these data acquisition difficulties.

Some of the early work in estimating SMC using remote sensing [5–10] established that thermal remote sensing, in concert with *in situ* measurements, can be used to measure, or at least quantitatively infer, soil moisture content. The possibility of estimating SSM (0–7.6 cm) from visible and near-infrared (NIR) reflectance data has also been demonstrated [11]. Optical and thermal remote-sensing techniques or passive and active microwave sensors offer large-scale monitoring of SSM [11–13]. Some meteorological satellites, such as the Advanced Microwave Scanning Radiometer (AMSR-E), the European Remote Sensing (ERS) satellite scatterometer or the Meteorological Satellite (METEOSAT), offer the

possibility of monitoring operational SSM [3]. However, the coarse spatial resolutions (ERS-Scat: 50 km, AMSR-E: 56 km and METEOSAT: visible and infrared (IR) 5 km) of the instruments are often not consistent with the scale of hydrologic processes of interest [14, 15].). A number of studies on soil moisture estimations introduced the error sources that have degraded the accuracy of satellite remotely sensed soil moisture content such that it is critical to calibrate soil moisture estimation algorithms and to validate derived products using ground-truth data. The error sources comprise radio-frequency interference (RFI) [16], vegetation water content [13, 17], surface roughness [16], and land surface heterogeneity [18]. It has been stated in the literature that a space-borne sensor designed to interpret SMC on the basis of soil microwave emission, and therefore the relationship between soil dielectric constant and water content, will show considerable systematic uncertainty of around 4% with maximum figures at relatively low water content in SMC retrieval [19].

Remote-sensing measurements in the thermal IR band has given rise to the thermal inertia (TI) approach for SMC retrieval. The TI approach relates SMC to the magnitudes of the differences between daily maximum and minimum soil and crop canopy temperatures [6]. This approach retrieves SMC from models that describe TI as a function of water content [20,21]. The implementation of the TI approach is simple because knowledge of soil physical properties and climate can produce representative SMC profiles up to a depth of 1 m. The limitation of the approach, however, is its sensitivity to the uncertainty of soil physical properties, which are complex to determine spatially and are typically obtained with point measurements [22]. The TI method provides large-scale spatial coverage, but the functions are empirical and have the drawback of being site- and

time-specific, such that none of them are general enough to be applied extensively [21]. Monitoring soil moisture by remote sensing includes another set of approaches that permits SSM retrieval from the information contained in satellite-derived surface temperature (T_s) and vegetation index (VI). However, one of the major drawbacks of the T_s -VI method is that, in order to have enough points in a remote-sensing image to use in the determination of the boundaries of extreme conditions, a sufficiently large number of pixels must be sampled. This limitation is a handicap when dealing with smaller scale imagery on the order of the size of a typical farm field [11].

The difficulties associated with the above introduced approaches have led researchers to look for data-driven modeling tools, such as artificial neural networks (ANNs), support vector machines (SVMs), and relevance vector machines (RVMs), to estimate soil moisture [2,3,23–27]. For example, Landsat data has been used for soil moisture estimation using relevance vector and support vector machines [3]. One of the major advantages of the machine learning approach to SMC estimation is that it can provide estimates having resolutions commensurate with remotely sensed data [3].

2.2. Materials and Methods

2.2.1. Artificial Neural Networks (ANNs)

This section presents a brief description of ANNs relevant to this study. A three-layered feed-forward neural network (FFNN) model was developed that includes “I” input neurons, “h” hidden neurons, and “o” output neurons, which can be shown symbolically as ANNs (i,h,o) [28]. Connection weights and bias connect these neurons. Input is multiplied by the connection weights. These products are simply summed, fed

through a transfer function to generate a result, and then output. The hidden layer neurons usually use a sigmoidal activation function, while the output layer neurons utilize a linear activation function. The activation functions are used to transform inputs to targeted outputs with a nonlinear regression procedure. Each ANN model requires training and testing operations. In the training operation, by minimizing the cost function (Mean Squared Error (MSE) in this study), the connection weights and bias values are optimized. Once trained, an independent set of data that was not used for training is applied to test the neural network model [26]. The issue that threatens the application of ANN-based models is the randomness of predicted output, which is fixed in this study [29]. This was carried out by applying seed generation function. Since weights are initialized randomly, seed generation function was reset to overcome the randomness of the results by fixing the weights initialization and make the results reproducible. Also the models were run for a wide range of seed values. The training operation of ANNs was performed by a back-propagation algorithm, which is the most commonly used supervised training algorithm in the multilayer feed-forward networks. The network weights are simultaneously modified by the back-propagation algorithm which seeks to minimize the difference between the targets and the computed outputs. In this kind of algorithm the processing operation is performed in a forward direction, from inputs to hidden layers and eventually to an output layer [30]. A back-propagation method uses a least-mean-square-error method and generalized-delta rule to optimize the network weights. The derivative chain rule and the gradient-descent method are utilized to adjust the network weights [31]. Forward pass and reverse pass are two main phases of the training operation. In the first phase, the input data are multiplied by the initial weights, forming weighted inputs that then are added to

yield the net to each neuron. This net generates the output of the neuron after passing through an activation or transfer function.

In back-propagation networks, a derivative of the activation function modifies the network weights. Therefore, continuous-transfer functions are targeted. The Log-sigmoid transfer function and Hyperbolic tangent sigmoid transfer function are the most common continuous-transfer functions in back-propagation networks [32]. The Log-sigmoid transfer function was used in this study. The output of the neuron is transmitted to the next layer as an input, and this procedure is repeated until it reaches the output layer. The error between the network outputs and the target outputs is computed at the end of each forward pass and it is checked with a specific value. If the error passed this value, the procedure continues with a reverse pass; otherwise, training is stopped [33]. In the reverse pass, the weights in the network are modified using the error value. The modification of weights in the output layer is different from the modification of weights in the hidden layers. In the output layer, the target outputs are provided, whereas in the intermediate layers, target values do not exist [31]. Therefore, back propagation uses the derivatives of the objective function regarding the weights in the entire network to distribute the error to neurons in each layer in the entire network [33].

2.2.2. Selection of Possible Input Variables

One of the critical issues in training learning machine algorithms such as ANNs is to select the appropriate input variables. The idea is to choose the combination of variables that are highly correlated with soil moisture. Previous studies have shown good correlation between soil water content and infrared (IR) skin temperature and normalized difference

vegetation index (NDVI), and between IR heating rate and thermal images [34,35]. Optical and microwave remotely sensed data have been used for surface soil energy balance modeling [6,11,12,36]. After collecting these variables from independent datasets, the correlation and dependency among these variables were evaluated in the study reported here. Some Vegetation Indices (VIs) are considered as input variables with some contributions in soil moisture estimations [4,37–39].

2.2.3. Study Area, Instrumentation, Techniques and Data

2.2.3.1. Study Area

The study area is a farm in Scipio, Utah ($39^{\circ}14'N$, $112^{\circ}6'W$), equipped with a center pivot irrigation system covering an area of approximately 84 acres. The main crops are alfalfa and oats, grown from April to October. Figure 2.1 shows the location of the farm in Utah, and provides information about the heterogeneity within the farm due to different crop types and the presence of an access road. Generally the center pivot lateral rotates clockwise and supplies irrigation water to the field at a constant rate from an upstream reservoir. In the current study a full rotation of the center pivot takes three days and six hours to irrigate the field fully to field capacity. This study was carried out for the crop growing cycle starting 16 May 2013 and ending 17 June 2013 (4 days).

2.2.3.2. Instrumentation: AggieAir Minion (Remote Sensing Platform)

AggieAir is the remote sensing platform applied in the current study. This platform is comprised of an autonomous unmanned aerial vehicle (UAV) that carries a multispectral sensor payload.

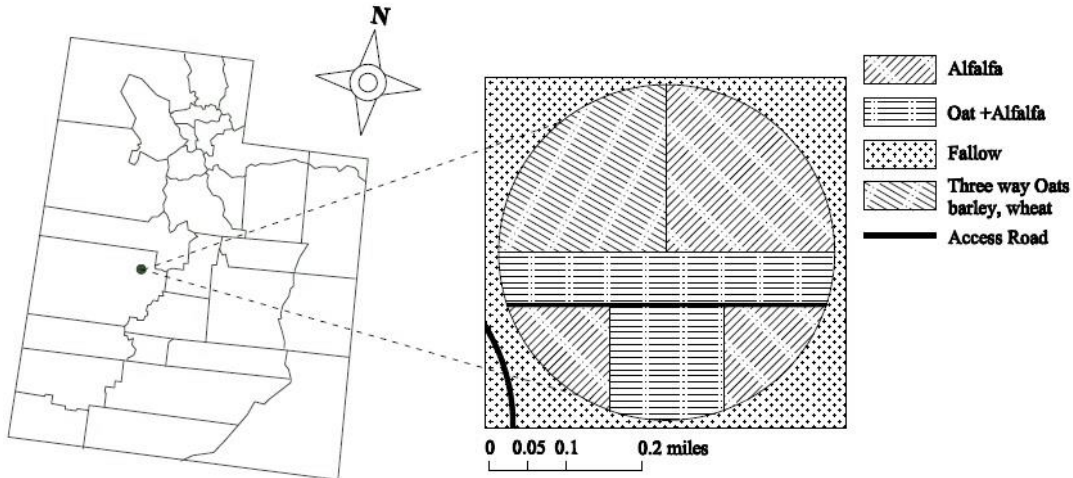


Figure. 2.1. The location of the study area in Utah (schematic Utah counties map (on the left) and cropping pattern for 2013 irrigation season (on the right)), ($39^{\circ}14'N$, $112^{\circ}6'W$).

The UAV navigates over the area of interest based on a pre-programmed flight plan and captures images using the on-board sensor payload system. The UAV is a small aircraft (8 feet wing span, 14-pound take-off weight) that can fly for an hour at a speed of 30 miles per hour. In this study, the UAV was equipped with visual, near-infrared, and thermal cameras and flew over the study area on four dates in 2013 (16 May, 1 June, 9 June, and 17 June), acquiring imagery with the optical cameras at 0.15 m resolution and with the thermal camera at about 60 cm. The wavelength range peaks around 420, 500, 600 and 800 nm, respectively, for blue, green, red and NIR sensors. Detailed information about the operation of the AggieAir system has been previously published by Jensen [40].

After the AggieAir UAV completes a flight mission, the aircraft may have acquired 300–400 images from each camera: visual, near-infrared, and thermal (Figure 2.2a). The images can be georeferenced directly using the position and orientation of the UAV when the image was exposed (Figure 2.2b) [40]. EnsoMOSAIC is used to orthorectify the AggieAir imagery with high accuracy [40,41]. EnsoMOSAIC generates hundreds of tie-

points between overlapping images and uses photogrammetry and block adjustment to refine the position and orientation information for each image, thereby accurately georeferencing each image (Horizontal Accuracy: 1–2 pixels Vertical Accuracy: 1.5–2 pixels (when all error sources are controlled)). EnsoMOSAIC also generates an internal digital elevation model (DEM) to compensate for distortions in the imagery caused by changing elevations. The resulting product is an orthorectified mosaic (Figure 2.2c) that is in 8-bit digital format. AggieAir uses a modified “reflectance mode” method to convert the digital numbers of the mosaic to reflectance values [40]. This radiometric normalization is the ratio of the digital number from the mosaic to the digital number from a spectralon white reflectance panel with known reflectance coefficients, multiplied by the reflectance factor which accounts for the zenith angle of the sun at the time, date, and location of the photos. The product of this method is an orthorectified mosaic in reflectance values. The reflectance values (for all four flights) range from 0.11 to 0.36, 0.20 to 0.49, 0.15 to 0.51 and 0.51 to 0.61 for blue, green, red and NIR, respectively. Thermal values range from 10.2 to 43.3 degrees Celsius.

2.2.3.3. Ground-Based Data Collection

In order to perform ground truthing, at the same time the AggieAir UAV flew over the study area, intensive ground sampling was conducted at precisely determined locations in the field [42]. Soil samples were collected based on a pre-defined spatial distribution map that was developed in light of the crop types and soil characteristics in the field.

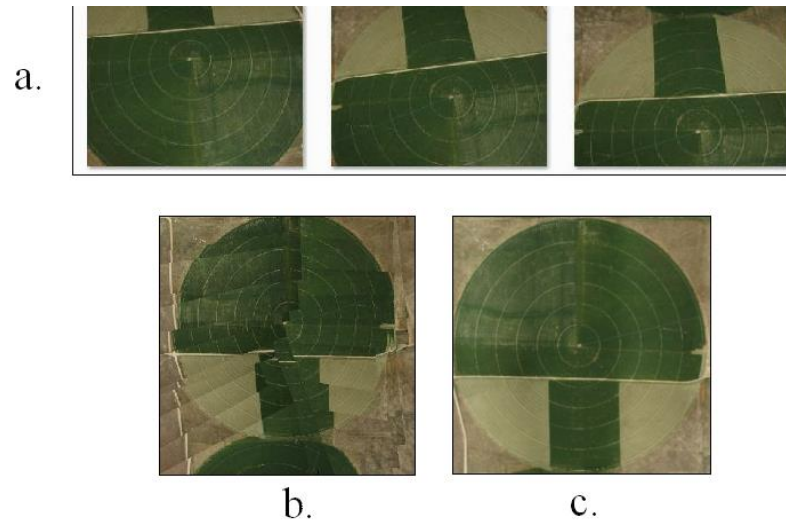


Figure. 2.2. (a) Some raw natural color images from the unmanned aerial vehicle (UAV) taken from the study area ($39^{\circ}14'N$, $112^{\circ}6'W$); (b) Orthorectified image using position and orientation of UAV aircraft during image capture; and (c) Accurate orthorectified mosaic image from EnsoMOSAIC.

The data collection included almost 50 samples per AggieAir flight scattered all over the field (minimum of 12 in each quarter) to cover the soil condition properties. Further, the unusable samples were discarded and the data collected from the four days were pooled (making a data set of 184 points) and utilized in the modeling procedure. The research crew collected soil samples from the surface soil and determined gravimetric soil moisture values after the samples were oven dried and weighted. The crew also used a hand-held measuring device to make in-field measurements and double-check the laboratory soil moisture results. The device, manufactured by Decagon Inc. (Pullman, WA, USA), includes a sensor read-out and storage system for real-time readings. Called “Procheck,” it was connected to a GS3 soil moisture, temperature, and EC sensor from Decagon Inc as well [43]. Figure 2.3 illustrates the location of soil moisture samples in the study area.

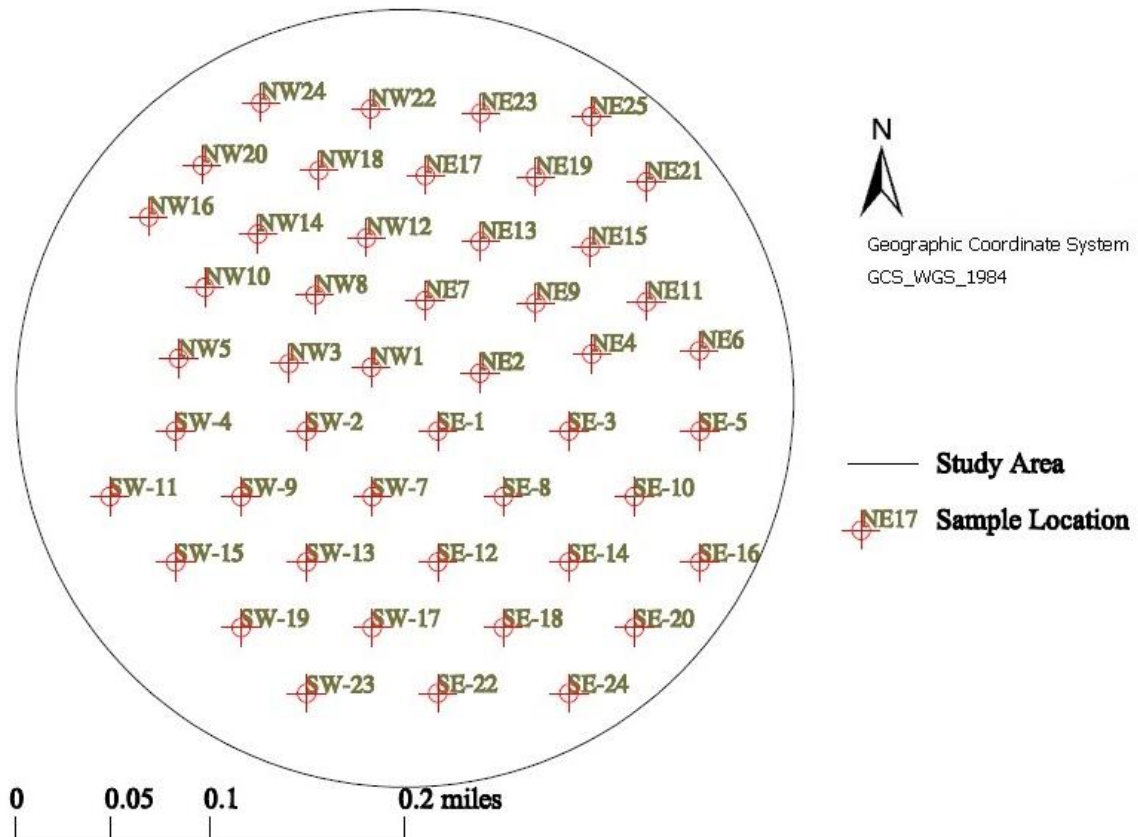


Figure. 2.3. Spatial distribution of soil moisture sample locations in the study area.

2.2.3.4. Soil Texture Analysis

The upper and lower limits of soil moisture storage in the root zone are a function of soil texture. After the soil has been saturated and drained by gravity, the soil is said to be at “field capacity,” and the amount of water that remains in the root zone but which the crop can no longer extract is called the “wilting point” [44]. In order to take these two parameters in to account, 14 different points from around the field were selected for soil texture sampling. After soil type determination, the corresponding field capacity values were acquired from previously published values and considered as model inputs [45].

Figure 2.4 illustrates the soil field capacity map developed by utilizing a Spherical Kriging interpolation method for the information from the 14 available sampling locations.

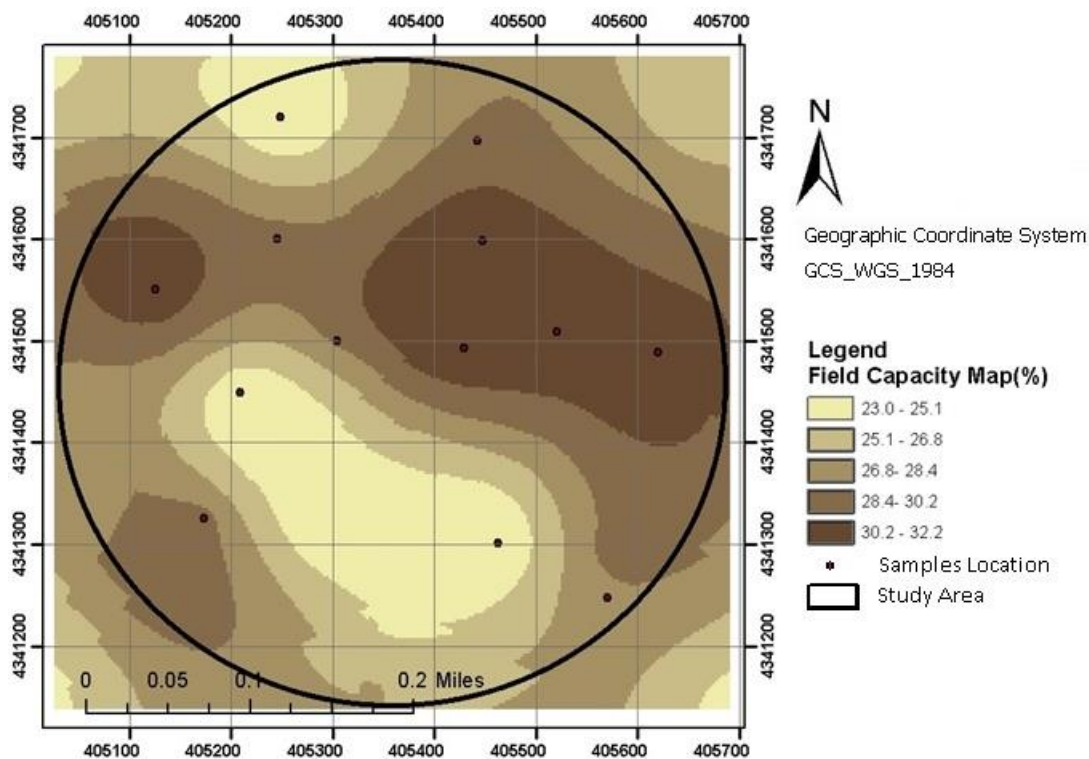


Figure. 2.4. Map of field capacity based on soil texture type and plot of the location of soil samples.

2.3.5. Relevant Vegetation Indices (VIs) from AggieAir Imagery

Visual spectrum (red, green, and blue, or RGB), near-infrared (NIR), and infrared/thermal remotely sensed data and some vegetation indices (VIs) are used as input variables for the soil moisture model. All AggieAir data (RGB, NIR, and thermal imagery), normalized difference vegetation index (NDVI), vegetation condition index (VCI), enhanced vegetation index (EVI), vegetation health index (VHI), and field capacity were chosen as model inputs with surface soil moisture as the target or output. The VHI was

proposed by Kogan (1995), which is an additive combination of VCI and Temperature Condition Index (TCI) [36]. Equations (1)–(5) represent the vegetation indices included in this study:

$$\text{NDVI} = \frac{\rho_{\text{NIR}} - \rho_{\text{RED}}}{\rho_{\text{NIR}} + \rho_{\text{RED}}} \quad 1)$$

$$\text{VCI} = 100 \times \frac{\rho_{\text{NDVI}} - \rho_{\text{NDVI}_{\text{min}}}}{\rho_{\text{NDVI}_{\text{max}}} - \rho_{\text{NDVI}_{\text{min}}}} \quad 2)$$

$$\text{EVI} = 2.5 \times \frac{\rho_{\text{NIR}} - \rho_{\text{RED}}}{\rho_{\text{NIR}} + C_1 \times \rho_{\text{RED}} - C_2 \times \rho_{\text{BLUE}} + L} \quad 3)$$

$$\text{TCI} = 100 \times \frac{\text{BT}_{\text{max}} - \text{BT}}{\text{BT}_{\text{max}} - \text{BT}_{\text{min}}} \quad 4)$$

$$\text{VHI} = 0.5 \times \text{VCI} + 0.5 \times \text{TCI} \quad 5)$$

where ρ_{NIR} , ρ_{RED} and ρ_{BLUE} are NIR, red, and blue reflectance bands; C_1 , C_2 and L are the coefficients of the aerosol resistance term, which uses the blue band to correct for aerosol influences in the red band; and BT is the thermal brightness, which is the thermal band reflectance.

2.2.3.6. Model Validation

A K-fold cross validation was used as the model validation technique in order to generalize an independent dataset. In general, in K-fold cross validation the original dataset (including all samples) is partitioned into K sub-data sets. Each time, a single sub-data set is retained for evaluation and the remaining (K-1) sub-data sets are used for training. This process repeats K times, and the errors for each time are estimated. Furthermore, the K

model errors are averaged to represent the best model [46,47]. Since the authors were not confident about the optimal percentage of data being considered for training, testing and validation to avoid over-fitting, a 5-fold cross validation technique is applied to the original data set and Mean Squared Error (MSE) is the calculated evaluation criterion. The 5-fold cross-validation was done repeatedly, and during the training phase different values for the training technique's parameters were used in concert with different network architectures. Further, the authors ended up with the best values for number of hidden nodes and training parameters. Then with these in hand, finally the network was trained using all the data, with the best number of hidden nodes and training parameters.

2.2.3.7. Wrapper Selection

For model construction, it is necessary to identify the best combination of input variables from the available data. A wrapper selection method was used to accomplish this. Guyon (2003) introduced the advantages of applying this method with reference to three main aspects: (1) improving the performance of predictors; (2) obtaining faster and more cost-effective predictors; and (3) providing a better understanding of the underlying process that generated the data [48]. This method is recommended over the backward selection method and is applicable to cases with a small number of inputs. Wrapper selection considers all possible combinations of input variables and develops a separate model for each combination. The models are then scored based on their predictive power, and the best model can be selected based on the corresponding score [48,49]. In order to check the goodness of fit, root mean square error (RMSE), mean absolute error (MAE), coefficient of correlation (r), coefficient of performance (e), and coefficient of

determination (R^2) are the statistical parameters that were calculated to evaluate the performance of the many alternative models and score their predictive power [50].

2.2.3.8. Division Set Up in ANN Model Architecture

The input data division set up can have a significant influence on the performance of an ANN model. Bowden (2002) presented two methodologies for dividing data into representative subsets (training, testing and validation) with similar statistical properties. These methods were proven to develop more robust results compared to conventional approaches in which the dataset was simply divided into arbitrary subsets [51]. The methods were applied by using a 5-fold cross validation method for data generalization. Other water resources related studies have utilized Bowden's approach and concluded that it ensures that the training, testing, and validation sets are representative of the same population [52–57].

It is difficult to assess beforehand how large an artificial neural network model should be for a specific application to avoid over-fitting. Model size strongly relates to sample size, and collecting more data and increasing the size of the training set or reducing the size of a network are recommended as solutions [28]. In this study, collecting more data was impossible; therefore, the error of the validation data set was checked as alternative method of investigation [28]. As training initiates, the error for all three data sets (training, testing, and validation) decreases, and in the case of over-fitting, the error for validation set increases while the error in the training set maintains a decreasing trend. If the error in the validation set continues in a reducing trend, there is no danger of over-fitting.

2.3. Results and Discussion

2.3.1. Input Data

2.3.1.1. Soil Moisture Data Calculation Results

In order to ground truth data and relate soil moisture values to remotely sensed data, gravimetric soil moisture measurements were checked with the corresponding in-field measurements of volumetric soil moisture using soil bulk density values that were extracted from soil texture data. A t-test comparing the gravimetric soil moisture measurements against the volumetric soil moisture measurements showed these two data sets are not statistically different at a 95 percent confidence level with P-value of 0.3. The results from the t-test indicates that either of these data sets can be used for further calculations. Finally, the gravimetric soil moisture values from four flight dates were pooled representing the maximum, minimum and mean values of 30.6, 10.1 and 19.7, respectively, and used as model targets. Also, the spatial distribution of soil moisture from high to low values is in accordance with time after irrigation. The highest values occur immediately behind the center pivot lateral, and the driest spots were concentrated in front of the lateral.

3.1.2. Spatial Information of Vegetation Indices

Due to heterogeneity within the field because of the different crop types, an access road, wheel tracks, the center pivot station, and historic locations of fence lines and ditch banks that once occupied the modern field, spatial analysis was required. The significance of spatial information comes from the ability of the human brain to detect spatial patterns in a map or an image. Table 2.1 represents the temporal and spatial changes of NDVI during

the study period. The same information is provided for other three VIs in the supplementary material.

Table. 2.1. Temporal and spatial changes in normalized difference vegetation index (NDVI) values during the study period.

Crop Type/Date	NDVI(Mean)			
	5/17/2013	6/1/2013	6/9/2013	6/17/2013
Three way, Oat, Barley , Wheat	0.09 Planting	0.34 continued growth	0.43 continued growth	0.53 full growth
Alfalfa	0.42 continued growth	0.47 continued growth	0.53/0.08 full growth/ after cut	0.59/0.13 full growth/ after cut
Oat, Alfalfa	0.43 germination	0.48 continued growth	0.53 full growth	0.57 full growth

2.3.2. Wrapper Selection Outcome

Goodness-of-fit statistics were used to test the degree of association between the observed and estimated data. As noted previously, root mean square error (RMSE), mean absolute error (MAE), coefficient of correlation (r), coefficient of performance (e) and coefficient of determination (R^2) were calculated for the models to score their predictive power. In the scoring phase, the authors referred to RMSE and judged the models predictive power based on them, further MAE and R^2 were considered and finally e and r came to account.

The models with high but similar predictive power were compared spatially against thermal, NIR and false color images. Also the research crew has collected a set of notes

about their observations during the data collection procedure. The notes paid attention to crop types, crops growing stage, location of lateral, irrigation uniformity, wet and dry spots (created due to deficiencies in the irrigation sprinkler system), existence of wind (wind direction if it scatters the water) and weather condition. After the models with high but similar predictive power were developed, the best model was selected visually to accommodate the spatial distribution of above information. Figure 2.5 illustrates how schematically wrapper selection would evaluate the models for the inputs from AggieAir (RGB, NIR, and Thermal) as an example of wrapper scoring. for this study, 1023 models in 10 sets for all possible combinations of 10 inputs were developed (10 combinations of 1, 45 combinations of 2, 120 combinations of 3, 210 combinations of 4, 252 combinations of 5, 210 combinations of 6, 120 combinations of 7, 45 combinations of 8, 10 combinations of 9 and 1 combination of 10 inputs), and the model results were compared.

A trial-and-error approach was utilized to select those models that worked on different numbers of neurons (up to $2 \times (\text{number of inputs}) + 1$ to avoid over-fitting issues), hidden layers, training functions, and division setups [32]. Finally, the model with 8 inputs (red, blue, NIR, thermal, NDVI, VCI, EVI, and field capacity) was selected because it had the best predictive power and best spatial pattern, which was checked visually. Table 2.2 shows the best model results for all 10 sets of combinations along with their highest predictive power statistics.

2.3.3. Results Extracted from Artificial Neural Networks (ANNs)

After the intensive trial and error selection procedure using cross validation procedure, a network architecture with one hidden layer and 17 nodes and a division set up of 80:10:10 with trainlm (Levenberg-Marquardt backpropagation) as a training function was selected.

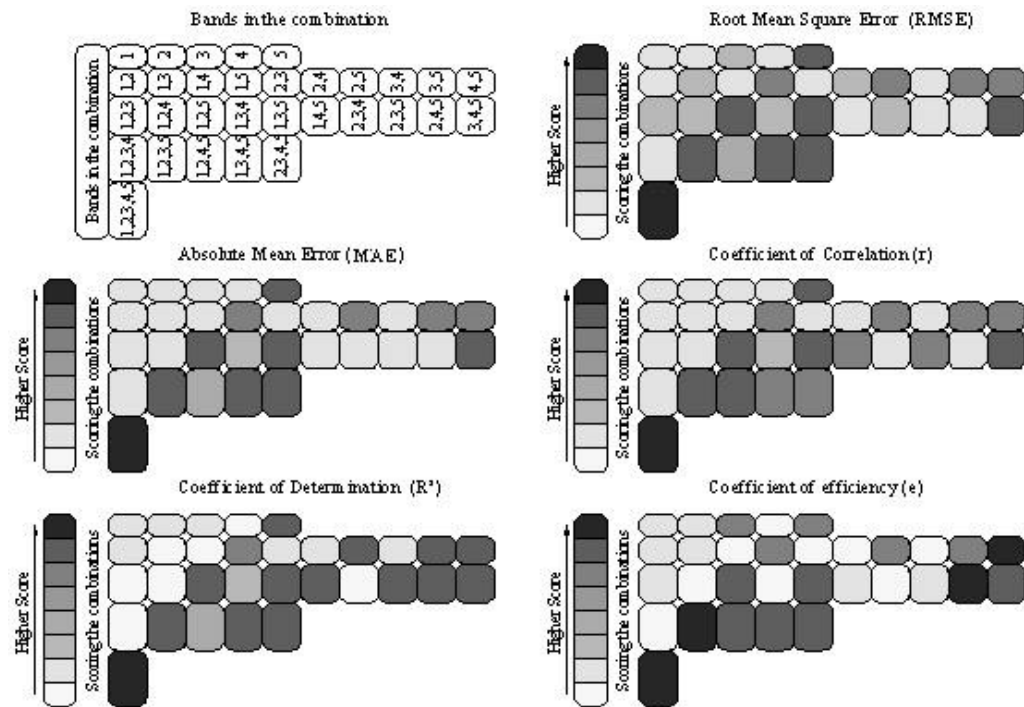


Figure. 2.5. Schematic view of possible performance by 5-input dataset using wrapper selection method and artificial neural network (ANNs).

Figure 2.6 illustrates (a) the measured versus the estimated soil moisture values of the selected model; (b) the corresponding one-by-one scatter plot (showing that all the points are clustered along the 45° line); (c) residual plot; and (d) residual histogram to demonstrate the validation of the model in the sense of normality, linearity, and equality of variances. Figure 2.7 represents the performance plot of the selected ANN model with 8

inputs, showing Mean Squared Error (MSE) trend during the learning procedure for the training, testing and validation sets to evaluate possible over-fitting issues. The decreasing trend of the validation set confirms that there is no over-fitting in the model. Figure 2.8 shows estimated surface soil moisture maps (Volumetric Water Content (%)) (right column), at four different dates (a) 16 May, (b) 1 June, (c) 9 June and (d) 17 June 2013 (Res. 15 cm) alongside false color composite images (NIR–Green–Blue) (left column). The false color map (NIR-Green-Blue) is related to the relative density of vegetation in the image. Exposed soil (bare) is expected to have lower soil moisture content while areas with high vegetation density the opposite. The concept of using false color composite images was taken from previously published studies [56,58].

Table. 2.2. Goodness-of-fit statistics from Wrapper selection results (1 to 10 inputs) with highest predictive power using ANN.

ANN Inputs		Division Set up	# of Neurons	RMSE	MAE	r	e	R ²
One Input	Thermal	80/10/10	4	3.0	2.4	0.64	0.4	0.41
Two Inputs	Thermal, Field capacity	75/15/10	5	2.5	1.8	0.78	0.60	0.61
Three Inputs	Red, Blue, Thermal	70/15/15	7	2.7	2.1	0.74	0.54	0.55
Four Inputs	Red, NDVI, VCI, VHI	70/15/15	7	2.5	1.8	0.77	0.59	0.60

Five Inputs	Green, Thermal, VCI, EVI, Field Capacity	80/10/10	9	2.1	1.6	0.84	0.71	0.71
Six Inputs	NIR, Thermal, NDVI, EVI, VHI, Field Capacity	80/10/10	11	2.1	1.5	0.84	0.70	0.71
Seven Inputs	Red, Blue, NIR, Thermal, NDVI, VCI, Field Capacity	80/10/10	12	2.1	1.6	0.86	0.73	0.73
Eight inputs	Red, Blue, NIR, Thermal, NDVI, EVI, VCI, Field Capacity	80/10/10	17	2.0	1.3	0.85	0.75	0.77
Nine Inputs	Red, Green, Blue, Thermal, NDVI, EVI, VCI, VHI, Field Capacity	80/10/10	17	2.0	1.4	0.87	0.75	0.75
Ten Inputs	Red, Green, Blue, NIR, Thermal, NDVI, EVI, VCI,	80/10/10	19	2.0	1.3	0.85	0.73	0.73

	VHI, Capacity	Field							
--	------------------	-------	--	--	--	--	--	--	--

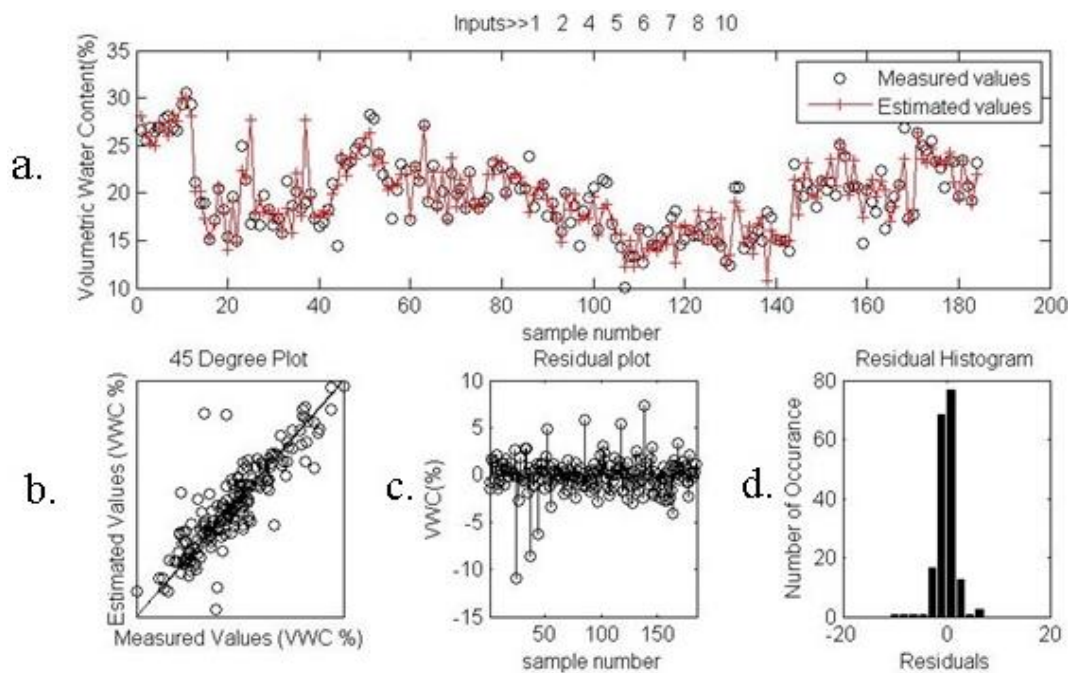


Figure. 2.6. (a) The measured soil moisture values versus the estimated values of the selected model; (b) one-by-one scatter plot; (c) residual plot; and (d) residual histogram.

As shown in Figure 2.8, the soil moisture maps have a direct association with the false color composite maps. The field exterior area was not irrigated during the growing cycle and was expected to be less moist. Although the wheel tracks and the access road are located within the irrigation zone, they are expected to be drier since they are covered by bare soil, become more compacted due to traffic over them, and lose moisture rapidly. This assumption also applies to the zones where the crops have been cut.

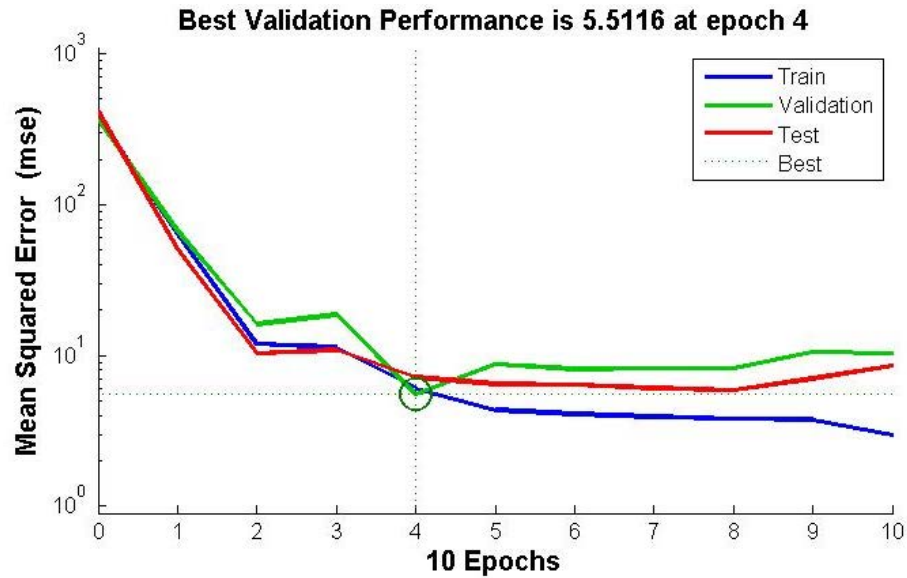


Figure. 2.7. Performance plot of the selected ANN model with 8 inputs showing Mean Squared Error (MSE) trend during the learning procedure for three data sets (training, testing and validation).

Different crop types have different water demands and water up-take rates that cause surface soil moisture heterogeneity even after a uniform irrigation event. This heterogeneity appeared in the form of cropping patterns in the soil moisture maps. According to the clockwise rotation of the lateral, the spots with the maximum soil moisture values are expected to fall near the lateral and in a counterclockwise direction. This status is clearest in Figure 2.7a where the field was under a heavy irrigation event at the time the aerial imagery was captured. Table 2.3 shows the comparison between measured and estimated soil moisture values for different crop type zones. Soil moisture numerical values are presented in the supplementary materials.

Table. 2.3. Comparison between measured and estimated soil moisture values for different crop type zones.

Crop Type/Date	Soil Moisture (Volumetric Water Content (%)) (Zonal Mean)							
	5/17/2013		6/1/2013		6/9/2013		6/17/2013	
	Measur ed	Estimat ed	Measur ed	Estimat ed	Measur ed	Estimat ed	Measur ed	Estimat ed
Three way, Oat, Barley , Wheat	18.9	20.1	21.5	19.0	14.9	15.7	19.3	17.6
Alfalfa	27.6	25.9	25.0	23.5	18.4	18.9	21.2	20.4
Oat, Alfalfa	18.0	18.3	20.5	18.1	15.7	15.8	22.5	18.9

The main problem with such modeling procedures is being dependent to site and time. This implies that ground sampling and modeling will be required for every flight to ensure accurate and quality data. So far this is a handicap and should be strengthened with more studies over different types of crops, in different areas at different stages of growth. Having such a model (or a collection of models) makes this practical for routine use (independent of site and time). In addition, the current study was targeted toward showing the detailed information that can be interpreted from high resolution data. Even though such a high resolution might not be required for monitoring agricultural farm conditions that are cropped with inexpensive crops such as alfalfa and oats, this resolution presents its value for other crops that require high resolution data (e.g., vineyards, orchards). These results essentially help to justify future work to look at the value of high resolution data for precision farming activities.

One step forward in generalizing the presented modeling methodology in temporal scale could be the idea of pooling the soil moisture data collected from different dates. In the case of the current study, every single sampling location experiences four different conditions of soil moisture level, which provides a wide range of information about soil moisture status through time. This type of information makes the model more robust in its ability to simulate previously unseen soil moisture conditions through time.

2.4. Conclusions

This paper demonstrates the application of a high resolution remote sensing technology (AggieAir) for estimating surface soil moisture as a key piece of information in irrigation water management. High-resolution multi-spectral imagery, in combination with ground sampling, provided enough information for the modeling approaches to accurately estimate spatially distributed surface soil moisture.

This paper presents the results of a modeling approach utilizing ANN in concert with time and site specific information. Parallel to other modeling approaches, such as data mining algorithms or linear regression, the ANN model is calibrated for this study within the conditions of the information collected including soil moisture measurements, soil texture, crop type information, and high resolution multi-spectral imagery.

This paper presents the results of a modeling approach utilizing ANN in concert with time and site specific information. Parallel to other modeling approaches, such as data mining algorithms or linear regression, the ANN model is calibrated for this study within the conditions of the information collected including soil moisture measurements, soil texture, crop type information, and high resolution multi-spectral imagery.

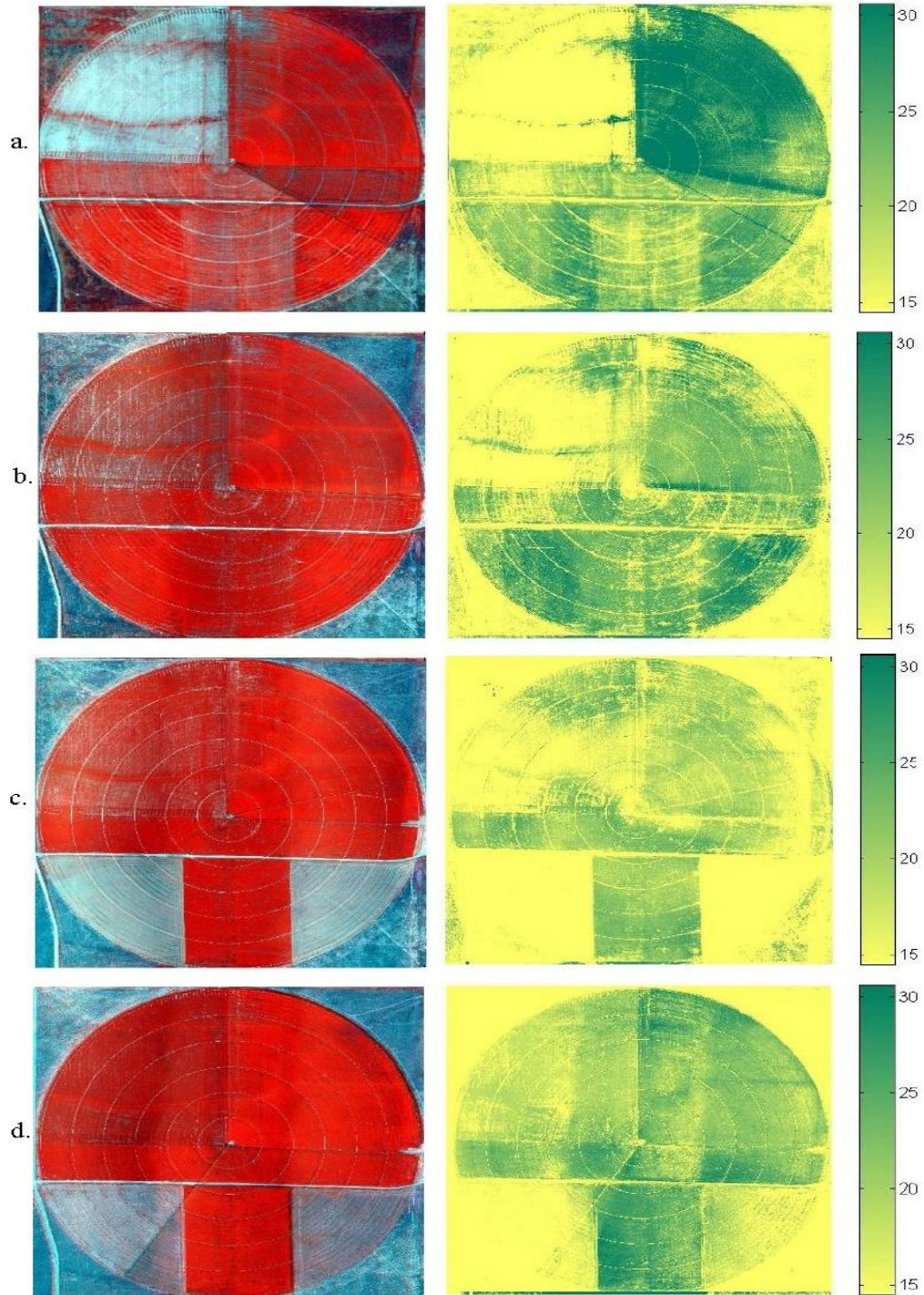


Figure. 2.8. Estimated soil moisture maps (Volumetric Water Content (%)), with ANNsmodel for four different dates (a) 16 May; (b) 1 June; (c) 9 June and (d) 17 June 2013 (Res. 15 cm) (right), false color images (left).

While the site-specific calibrated ANN in this study cannot be used immediately in another location, the modeling procedure (identifying spatial information with the most significant contribution to soil moisture estimation (Table 2.2)) along with similar field measurements and high resolution multi-spectral imagery and the data mining algorithm, are transferable from this study.

Surface soil moisture estimation was accomplished with an ANN model (RMSE: 2.0, MAE: 1.3, r: 0.87, e: 0.75, R2:0.77) for four dates in 2013 (16 May, 1 June, 9 June, and 17 June). These results show the capability of the model to accurately estimate surface soil moisture. Compared to the traditional soil moisture estimations that are based on a farmer's visual perceptions or a few soil moisture samples averaged across the farm, the modeling approach presented enables greater precision in the application of water and identifies dry/wet spots and water stressed crops.

AggieAir imagery, combined with appropriate analytic tools, allows spatial estimation of surface soil moisture. These estimates were made at much finer resolutions in space and time than those available from conventional remote sensing technologies (e.g., satellite or commercial aerial photography services). Also, the application of data mining algorithms to AggieAir aerial imagery allows for quantification of actionable information for precision agriculture (soil moisture values across the field). The soil moisture maps that are produced can then be related to irrigation water management for scheduling and application rates.

The results from the wrapper selection (Table 2.2) prove the significance of thermal imagery as the most relevant information in surface soil moisture estimations. In the case of one input, a model with thermal imagery can estimate the soil moisture values with

RMSE of approximately 3% (thermal images are provided in supplementary material section).

Soil water holding capacity as a function of soil texture plays an important role in soil moisture values. This parameter was observed by utilizing field capacity as an input to the models. Table 2.2 shows that field capacity is a component of most of the models. The effect of this parameter is confounded by other important inputs in the spatial distribution of soil moisture in Figure 2.8. Based on the information presented in Table 2.2, among the available vegetation indices, NDVI and VCI have a greater explanatory contribution in surface soil moisture estimates. The soil moisture maps have a good association with false color composite maps that allows for distinction of agricultural features in the field.

2.5. Future Work

Further studies will involve the estimation of surface soil moisture using other data mining algorithms and its application as a boundary condition to produce remotely sensed estimates of root zone soil moisture. In addition, Pixel-wise estimation of soil moisture could also be applied in a water balance models.

2.6. References

1. Grayson, R.B.; Western, A.W. Towards areal estimation of soil water content from point measurements: Time and space stability of mean response. *J. Hydrol.* **1998**, *207*, 68–82.

2. Gill, K.; Kemblowski, M.; McKee, M. Soil moisture data assimilation using support vector machines and ensemble Kalman filter. *JAWRA J. Am. Water Resour. Assoc.* **2007**, *43*, 1004–1015.
3. Zaman, B.; McKee, M.; Neale, C.M.U. Fusion of remotely sensed data for soil moisture estimation using relevance vector and support vector machines. *Int. J. Remote Sens.* **2012**, *33*, 6516–6552.
4. Liu, W.; Baret, F.; Gu, X.; Zhang, B.; Tong, Q.; Zheng, L. Evaluation of methods for soil surface moisture estimation from reflectance data. *Int. J. Remote Sens.* **2003**, *24*, 2069–2083.
5. Idso, S.; Jackson, R.; Reginato, R. Estimating evaporation: A technique adaptable to remote sensing. *Science* **1975**, *189*, 991–992.
6. Idso, S.; Jackson, R.; Reginato, R. Compensating for environmental variability in the thermal inertia approach to remote sensing of soil moisture. *J. Appl. Meteorol.* **1976**, *15*, 811–817.
7. Reginato, R.; Idso, S.; Jackson, R.; Vedder, J.; Blanchard, M.; Goettelman, R. Soil water content and evaporation determined by thermal parameters obtained from ground-based and remote measurements. *J. Geophys. Res.* **1976**, *81*, 1617–1620.
8. Reginato, R.; Jackson, R.; Pinter, P. Evapotranspiration calculated from remote multispectral and ground station meteorological data. *Remote Sens. Environ.* **1985**, *18*, 75–89.
9. Jackson, T. Soil water modeling and remote sensing. *IEEE Trans. Geosci. Remote Sens.* **1986**, *24*, 37–46.

10. Quattrochi, D.; Luvall, J. Thermal infrared remote sensing for analysis of landscape ecological processes: Methods and applications. *Landsc. Ecol.* **1999**, *14*, 577–598.
11. Kaleita, A.; Tian, L.; Hirschi, M. Relationship between soil moisture content and soil surface reflectance. *Trans. ASAE* **2005**, *48*, 1979–1986.
12. Humes, K.; Kustas, W.; Jackson, T.; Schmugge, T.; Moran, M. Combined use of optical and microwave remotely sensed data for the estimation of surface energy balance components over a semi-arid watershed. In *Proceedings of the IEEE Topical Symposium on Combined Optical-Microwave Earth and Atmosphere Sensing*, Albuquerque, NM, USA, 22–25 March **1993**; pp. 86–89.
13. Njoku, E.G.; Jackson, T.J.; Lakshimi, V.; Chan, T.K.; Nghiem, S.V. Soil moisture retrieval from AMSR-E. *IEEE Trans. Geosci. Remote Sens.* **2003**, *41*, 215–229.
14. Aritola, J.F.; Pepper, I.L.; Brusseau, M.L. *Environmental Monitoring and Characterization*; Elsevier Academic Press: San Diego, CA, USA, **2004**.
15. Das, N.N.; Mohanty, B.P. Root zone soil moisture assessment using remote sensing and vadose zone modeling. *Vadose Zone J.* **2006**, *5*, 296–307.
16. Njoku, E.G.; Ashcroft, P.; Chan, T.K.; Li, L. Global survey and statistics of radio-frequency interference in AMSR-E land observations. *IEEE Trans. Geosci. Remote Sens.* **2005**, *43*, 938–947.
17. Crosson, W.L.; Limaye, A.S.; Laymon, C.A. Parameter sensitivity of soil moisture retrievals from airborne C- and X-band radiometer measurements in SMEX02. *IEEE Trans. Geosci. Remote Sens.* **2005**, *43*, 2842–2853.
18. Crow, W.T.; Chan, T.K.; Entekhabi, D.; Houser, P.R.; Hsu, A.Y.; Jackson, T.J.; Njoku, E.G.; O'Neill, P.E.; Shi, J.; Zhan, X. An observing system simulation

- experiment for hydros radiometer-only soil moisture products. *IEEE Trans. Geosci. Remote Sens.* **2005**, 43, 1289–1303.
19. Fernandez-Galvez, J. Errors in soil moisture content estimates induced by uncertainties in the effective soil dielectric constant. *Int. J. Remote Sens.* **2008**, 29, 3317–3323.
 20. Cai, G.; Xue, Y.; Hu, Y.; Wang, Y.; Guo, J.; Luo, Y.; Wu, C.; Zhong, S.; Qi, S. Soil moisture retrieval from MODIS data in northern China plain using thermal inertia model. *Int. J. Remote Sens.* **2007**, 28, 3567–3581.
 21. Lu, S.; Ju, Z.; Ren, T.; Horton, R. A general approach to estimate soil water content from thermal inertia. *Agric. For. Meteorol.* **2009**, 149, 1693–1698.
 22. Verstraeten, W.W.; Veroustraete, F.; van der Sande, C.J.; Grootaers, I.; Feyen, J. Soil moisture retrieval using thermal inertia, determined with visible and thermal spaceborne data, validated for European forests. *Remote Sens. Environ.* **2006**, 101, 299–314.
 23. Gill, M.; Asefa, T.; Kemblowski, M.; McKee, M. Soil moisture prediction using support vector machines. *J. Am. Water Resour. Assoc.* **2006**, 42, 1033–1046.
 24. Jiang, H.; Cotton, W. Soil moisture estimation using an artificial neural network: A feasibility study. *Can. J. Remote Sens.* **2004**, 30, 827–839.
 25. Hassan-Esfahani, L.; Torres-Rua, A.; Jensen, A.; McKee, M. Topsoil moisture estimation for precision agriculture using unmanned aerial vehicle multispectral imagery. In *Proceedings of the 2014 IEEE International Geoscience and Remote Sensing Symposium (IGARSS)*, Quebec City, QC, Canada, 13–18 July **2014**; pp. 3263–3266.

26. Elshorbagy, A.; Parasuraman, K. On the relevance of using artificial neural networks for estimating soil moisture content. *J. Hydrol.* **2008**, 362, 1–18.
27. Khalil, A.; Gill, M.K.; McKee, M. New applications for information fusion and soil moisture forecasting. In *Proceedings of the 8th International Conference on Information Fusion*, Philadelphia, PA, USA, 25–28 July **2005**; IEEE: Piscataway, NJ, USA; pp. 1622–1628.
28. Haykin, S. *Neural Networks: A Comprehensive Foundation*, 2nd ed.; MacMillan: New York, NY, USA, **1999**.
29. Khan, M.; Coulibaly, P. Streamflow forecasting with uncertainty estimate using Bayesian learning For ANN. In *Proceedings of the 2005 IEEE International Joint Conference on Neural Networks*, Montreal, QC, Canada, 31 July–4 August **2005**; Volume 5, pp. 2680–2685.
30. Tokar, S.A.; Johnson, P.A. Rainfall-runoff modeling using artificial neural networks. *J. Hydrol. Eng.* **1999**, 4, 232–239.
31. Rumelhart, D.E.; McClelland, J.L.; PDP Research Group. *Parallel Distributed Processing. Volume 1: Foundations*; The MIT Press: Cambridge, MA, USA, **1986**.
32. Hecht-Nielsen, R. *Neurocomputing*; Addison-Wesley Publishing Company: Reading, MA, USA, **1990**.
33. Wasserman, P.D. *Neural Computing Theory and Practice*; Van Nostrand Reinhold: New York, NY, USA, **1989**.
34. Gillies, R.R.; Carlson, T.N. Thermal remote sensing of surface soil water content with partial vegetation cover for incorporation into climate models. *J. Appl. Metrol.* **1995**, 34, 745–756.

35. Wetzel, P.J.; Woodward, R.H. Soil moisture estimation using GOES-VISSR infrared data: A case study with a simple statistical method. *J. Clim. Appl. Meteorol.* **1987**, *26*, 107–117.
36. Kogan, F.N. Droughts of the late 1980s in the United States as derived from NOAA polar-orbiting satellite data. *Bull. Am. Meteorol. Soc.* **1995**, *76*, 655–668.
37. Mallick, K.; Bhattacharya, B.K.; Patel, N.K. Estimating volumetric surface moisture content for cropped soils using a soil wetness index based on surface temperature and NDVI. *Agric. For. Meteorol.* **2009**, *149*, 1327–1342.
38. Liang, S.; Rui, S.; Xiaowen, Li.; Shunlin, L.; Renhua, Z. Monitoring surface soil moisture status based on remotely sensed surface temperature and vegetation index information. *Agric. For. Meteorol.* **2012**, *166*, 175–187.
39. Bhuiyan, C.; Singha, R.P.; Koganc, F.N. Monitoring drought dynamics in the Aravalli region (India) using different indices based on ground and remote sensing data. *Int. J. Appl. Earth Observ. Geoinf.* **2006**, *8*, 289–302.
40. Jensen, A.M. A Geospatial Real-Time Aerial Image Display for a Low-Cost Autonomous Multispectral Remote Sensing. Master's Thesis, Utah State University, Logan, UT, USA, **2009**.
41. MosaicMill EnsoMOSAIC. Available online: <http://www.ensomosaic.com> (accessed on 6 May **2012**).
42. Long, D.; Longuevergne, L.; Scanlon, B.R. Uncertainty in evapotranspiration from land surface modeling, remote sensing, and GRACE satellites. *Water Resour. Res.* **2014**, *50*, 1131–1151.

43. Decagon Devices, Inc. Available online: <http://www.decagon.com/> (accessed on 20 November **2014**).
44. Israelson, O.W.; West, F.L. Water holding capacity of irrigated soils. *Utah State Agric. Exp. Station Bull.* **1922**, 183, 1–24.
45. Costa, A.; Albuquerque, J.A.; Costa, A.; Pértile, P.; Silva, F.R. Water retention and availability in soils of the State of Santa Catarina-Brazil: Effect of textural classes, soil classes and lithology. *Braz. Soil Sci. Soc.* **2013**, 37, 1535–1548.
46. Kohavi, R. A study of cross-validation and bootstrap for accuracy estimation and model selection. In *Proceedings of the Fourteenth International Joint Conference on Artificial Intelligence*, Montreal, QC, Canada, 20–25 August **1995**; Volume 12, pp. 1137–1143.
47. Geisser, S. *Predictive Inference*; Chapman and Hall: New York, NY, USA, **1993**.
48. Guyon, I. An introduction to variable and feature selection. *J. Mach. Learn. Res.* **2003**, 1157–1182.
49. Kohavi, R.; John, G.H. Wrappers for feature subset selection. *Artif. Intell.* **1997**, 12, 273–324.
50. Glover, D.M.; Jenkins, W.J.; Doney, S.C. *Least Squares and Regression Techniques, Goodness of Fit and Tests, Non-Linear Least Squares Techniques*; Woods Hole Oceanographic Institute: Woods Hole, MA, United States, **2008**.
51. Bowden, G.J.; Maier, H.R.; Dandy, G.C. Optimal division of data for neural network models in water resources applications. *Water Resour. Res.* **2002**, doi:10.1029/2001WR000266.

52. Bowden, G.J.; Maier, H.R.; Dandy, G.C. Input determination for neural network models in water resources applications. Part 2. Case study: Forecasting salinity in a river. *J. Hydrol.* **2005**, 301, 93–107.
53. Anctil, F.; Lauzon, N. Generalisation for neural networks through data sampling and training procedures, with applications to stream flow predictions. *Hydrol. Earth Syst. Sci.* **2004**, 8, 940–958.
54. Jia, Y.; Culver, T.B. Bootstrapped artificial neural networks for synthetic flow generation with a small data sample. *J. Hydrol.* **2006**, 331, 580–590.
55. Lauzon, N.; Anctil, F.; Petrinovic, J. Characterization of soil moisture conditions at temporal scales from a few days to annual. *Hydrol. Process.* **2004**, 18, 3235–3254.
56. Whalley, W.R.; Leeds-Harrison, P.B.; Bowman, G.E. Estimation of soil moisture status using near infrared reflectance. *Hydrol. Process.* **1991**, 5, 321–327.
57. Hassan-Esfahani, L.; Torres-Rua, A.; McKee, M. Assessment of optimal irrigation water allocation for pressurized irrigation system using water balance approach, learning machines, and remotely sensed data. *Agr. Water Manage.* **2015**, 153, 42–50. [doi:10.1016/j.agwat.2015.02.005](https://doi.org/10.1016/j.agwat.2015.02.005)
58. Yin, Z.; Lei, T.; Yan, Q.; Chen, Z.; Dong, Y. A near-infrared reflectance sensor for soil surface moisture measurement. *Comput. Electron. Agric.* **2013**, 99, 101–107.

CHAPTER 3
HIGH-RESOLUTION ROOT-ZONE SOIL WATER CONTENT ESTIMATION USING
BAYESIAN-BASED MODEL AND HIGH-RESOLUTION VISUAL, NIR, AND
THERMAL IMAGERY: A CASE STUDY

ABSTRACT

Soil moisture information is important for various research applications including weather and climate prediction, hydrological forecast applications, and watershed and agricultural management. For precision agriculture, it is considered a key parameter in irrigation scheduling and application. Knowledge of root zone volumetric water content supports more efficient irrigation management by enabling estimation of required water application rates at appropriate temporal and spatial scales. High-resolution multispectral imagery provides an adequate set of data to obtain a remotely sensed estimate of soil moisture at three different depth in the root zone soil profile as well as root zone soil volumetric water content due to the fact that spectral reflectance of vegetation and vegetation indices are indicators of crop status influenced by soil water content and fertility. The remote sensing platform used in this study, called AggieAir™, was developed by the Utah Water Research Laboratory at Utah State University. It consists of an autonomous unmanned aerial system (UAS) that is equipped with visual, near-infrared, and thermal cameras. Bayesian data mining algorithms (Bayesian Artificial Neural Networks) were tested and calibrated to combine the remotely sensed spatial information with field measurements. The integrated data mining approach was developed to obtain high-resolution soil moisture maps at the surface and 15 cm below the surface using the multispectral information from AggieAir. Since soil moisture variations were negligible

at 30 cm, a uniform soil moisture value was assumed at this depth. Finally, a trapezoidal integration method was utilized to estimate volumetric water content in the root zone using the results of the modeling approach.

3.1. Introduction

Surface and deep soil moisture (SM) can be important information in climate prediction, hydrological forecast applications, and watershed and agricultural management (Manfreda and Fiorentino 2008; Seneviratne et al. 2010). Soil moisture monitoring may enhance the understanding of water and energy exchange rate in the atmosphere/ground interface. Soil moisture content (SMC) includes two main components: surface soil moisture (SSM) (almost held in the upper 10 cm of soil) and root zone soil moisture (almost held in the upper 200 cm of soil) (Gill et al. 2007). SMC can be estimated using different techniques, such as *in situ* measurements, physically based models, and remote sensing (Gill et al. 2007; Abdallah and Mohamed 2013). Although *in situ* measurements are precise and reliable, they are time- and energy-intensive and are not available over large spatial scales. Satellite remote sensing of soil moisture has recently become a consistent alternative that can provide continuous and large scale monitoring of the SSM state. Though it is only able to provide surface information, it is still a good source of data for hydrological and agricultural applications (Gao et al. 2006; Escorihuela et al. 2010). Remote sensing of soil moisture in the visual domain, thermal infrared and microwave portion of the electromagnetic spectrum, at different spatial scales has drawn a great deal of attention. A growing need for regional- to global-scale observations of the spatial distribution of soil moisture has motivated the development of airborne and satellite

microwave sensors (Famiglietti et al. 2008). Satellite remote sensing approaches in particular have engendered much enthusiasm and interest with their promise of global data coverage, leading Vinnikov et al. (1999) to speculate that, in regard to long-term soil moisture monitoring, “The future obviously belongs to remote sensing of soil moisture from satellites.” In fact, the intervening decades of research on remote sensing of soil moisture are now beginning to bear fruit in terms of operational satellites for large-scale soil moisture monitoring. Great advances have been made in satellite remote sensing approaches for estimating surface soil moisture, but the coarse spatial resolution and the shallow sensing depth are significant limitations for many applications (Wagner et al. 2007).

3.1.1. Dedicated soil moisture missions

The National Aeronautics and Space Administration (NASA) Advanced Microwave Scanning Radiometer (AMSR-E) provides moisture content estimates for near surface soils (0–2 cm) at approximately a 43-km by 75-km footprint scale (Njoku et al. 2003) (AMSR-E is not currently producing any data since the antenna stopped spinning in October 2011) the European Space Agency (ESA) Soil Moisture Ocean Salinity (SMOS) mission maps 0–5 cm surface soil moisture every three days, achieving an accuracy of 4% at a spatial resolution of about 50 km across the globe since its launch on 2 November 2009 (Kerr et al. 2010; ESA 2015); and NASA’s Soil Moisture Active Passive (SMAP) mission uses an L-band radar and an L-band radiometer for soil moisture mapping of the top ~5 cm and is clearly sensitive to soil moisture in regions having vegetation water contents up to ~5 kg m⁻² averaged over the radiometer resolution footprint of ~40 km; it was launched on

January 31, 2015 and is designed to measure soil moisture over a three-year period (SMAP hand book, Entekhabi et al. 2010). These satellites all use sensors in the microwave portion of the spectrum.

3.1.2. Satellite remote sensing of SM

Since the coarse spatial resolution of dedicated satellite missions are not commensurate with many hydrological, agricultural and ecological contexts, and are mainly developed for Earth system monitoring and observations, researchers have carried out several studies on remote sensing estimations of SM at other frequencies using satellite imagery with finer resolution compared (Hassan et al. 2007; Mallick et al. 2009; see chapter 4). Generally a number of error sources can degrade the accuracy of satellite remotely sensed soil moisture content such that it is critical to calibrate retrieval algorithms and to validate derived products using ground-truth data. The error sources include radio-frequency interference (a problem of microwave remote sensing missions) (RFI) (Njoku et al. 2005), vegetation water content (Crosson et al. 2005; Njoku et al. 2003), surface roughness (Crosson et al. 2005), and land surface heterogeneity (Crow et al. 2005). Future research advances in this area will require the use of new observation data at suitable spatial and temporal scales (Seneviratne et al. 2010).

The growing need for high-resolution remotely sensed data and appropriate field data to calibrate and validate applications of these data to the solution of practical questions are the motivations of the current research. The researchers investigated existing data-driven models to estimate soil moisture and found several studies analogous to the current work that have been conducted under different (much coarser) resolutions in time and space

(Gill et al. 2007; Zaman et al 2012; Jiang and Cotton 2004; Khalil et al. 2005). Several approaches to estimating root-zone soil moisture in conjunction with surface measurements have been introduced. They mainly consider surface soil moisture as a boundary condition or model input in root zone soil moisture estimations (Ragab 1995; Laio 2006; Sabater et al. 2007; Albergel et al. 2008; Zaman et al. 2012; Manfreda et al. 2014; Hirschi et al. 2014; see chapter 4).

In this study, the soil is assumed to be composed of three layers: one at the surface with a depth of a few centimeters (SM-0), the second layer below it with an average depth of 15 cm (SM-15), and the third layer with an average depth of 30 cm that may be assumed to be coincident with the rooting depth of many types of crops or vegetation (1 foot) (SM-30).

To our knowledge, this is the first study to document estimation of root zone soil moisture (SM-RZ) using remotely sensed data at a fine spatial resolution (at 15 cm), that is readily available at customized temporal intervals (essentially, flights available on demand), and that uses these estimates to provide a high-resolution map of root zone soil volumetric water content. The results can contribute to efficient and reliable high-resolution multi-spectral remote sensing validation and, potentially, to better utilization of remotely sensed soil moisture products for enhanced irrigation modeling and scheduling.

In examining the issue of root zone soil moisture, the current study is the logical next step from a previous study (see chapter 2) in which the authors applied Artificial Neural Networks (ANNs) as a data mining tool to estimate surface soil moisture (SM-0). The current paper adapts the same methodology to estimate root zone soil moisture using a modeling approach for three layers at soil vertical profile (SM-0, SM-15, and SM-30).

Also, the present study uses Bayesian Artificial Neural Networks (Bay-ANNs) as the data mining tool to enhance the quality of estimations. Bay-ANN is an adaptive regularization method that adds one term to the cost function to be minimized. The regularized cost function contains two terms: a mean squared errors MSE term and the weights. The idea is that this cost function will penalize large weights and the prediction capabilities of the ANN algorithm could be increased as the Bay-ANNs would have smoother behavior than ANNs. In the case of the Bayesian regularization, instead of fixing the relative weights (alpha and beta parameters) the weights and biases of the network are considered as random variables with specified distributions, and the regularization parameters alpha and beta are obtained from the variances associated with these distributions. The Bayesian technique is described in more detail in Section 2.1.

3.2. Materials and Methods

3.2.1. Bayesian Artificial Neural Networks (Bay-ANNs)

Artificial neural networks (ANNs) have proven to be valuable tools in the field of water resources engineering (Koksal et al. 2011). Maier and Dandy (2000) have published a review of 43 papers in which ANNs are used for prediction and forecasting of water resources variables. The multi-layer perceptron (MLP) is the most commonly used architecture for these practical applications due to its capability to approximate any smooth function as long as enough data are provided to estimate the MLP parameters (Nabney 2001; Torres et al. 2011). In this study, the multi-layer perceptron (MLP) networks were implemented and trained using MATLABTM and the associated NETLAB toolbox

developed by Nabney (2001). The data was presented to a series of MLP networks with variable numbers of hidden nodes and a single hidden layer. Each network had a variable number of input nodes ranging from 1 to 10 and a single output node corresponding to the value of either soil moisture at 15 cm depth or at the surface.

MLP networks determine nonlinear transformations from the vector of inputs to the output (either soil moisture at 15 cm depth or surface in this study) by parameterizing a set of network weights. In contrast to traditional ANN network training, where an optimal set of weights is selected by minimizing a suitable error function, the Bayesian approach deals with a probability distribution of network weights (Titterton 2004).

The idea of using a Bayesian approach comes from the fact that it produces probabilistic results rather than the deterministic results of traditional ANNs. In this approach, the trained network is represented by a posterior distribution of weights rather than a single set of weights. An array of inputs, combined with the posterior weight distribution, creates a distribution of network outputs. The mean variance of a Gaussian approximation to this predictive distribution can then be calculated to provide error bars of the mean prediction. This is a feature that is difficult to achieve with other ANN training methods (MacKay 1994).

The MLP architecture can be described as given by Pierce et al. (2008):

$$\text{Equation (1)} \quad y_k = \sum_{m=1}^M w_{km}^{\text{II}} \tanh\left(\sum_{d=1}^D w_{md}^{(1)} x_d + b_m\right) + b_k$$

where y_k is the k^{th} component of the output vector in an MLP ($y^{(n)}$; $y_k \in 1 \leq k \leq K$); x_d is the d^{th} component of the input vector in an MLP ($x^{(n)}$; $x_d \in 1 \leq d \leq D$); w_{km}^{II} , $w_{md}^{(1)}$ are weight matrices for the second and first layer, respectively; K is the number of outputs

or predicted values; D is the number of inputs; M represents the number of hidden nodes; and b_m, b_k are the bias vectors for the first and second layer, respectively.

Using input target pairs with N training samples, $\Lambda = [x^n, t^n]$, while $n = 1, \dots, N$. The learning procedure runs by optimizing the network parameters $W = (w, b)$ and seeking to minimize the overall error function, which can be described as:

$$\begin{aligned} \text{Equation(2)} \quad E &= \frac{\beta}{2} \sum_{n=1}^N (t^{(n)} - y^{(n)})^2 + \frac{\alpha}{2} \sum_{i=1}^W w_i^2 \\ &= \beta \times E_{\Lambda} + \alpha \times E_W \end{aligned}$$

where E_{Λ} is the data error function; E_W is the penalty term; W is the number of biases and weights in the network and α and β are the Bayesian hyperparameters.

Applying a network optimization function is one option available for network training. A helper function can be used with any function that searches in parameter space using error and gradient functions which is called optimization function (Nabney 2001). The helper function facilitates the training of networks using the general purpose optimizers, as well as sampling from the posterior distribution of parameters using general purpose Markov chain Monte Carlo sampling algorithms. The models perform forward, targeted toward estimating the probability of the weights and biases of the MLP model, given the dataset (MacKay 1992).

$$\text{Equation (3)} \quad p(W|t^{(n)}) = \frac{p(t^{(n)}|W) \times p(W)}{p(t^{(n)})}$$

where $p(W|t^{(n)})$ is the posterior probability of the weights; $p(t^{(n)}|W)$ represents the likelihood function; $p(W)$ is the prior probability of the weights; and $p(t^{(n)})$ is the evidence for the dataset.

Nabney (2001) expressed the likelihood and the prior probabilities by assuming a Gaussian distribution for the error term $\xi^{(n)} = t^n - y^n$ and the weights, W .

$$\text{Equation (4)} \quad p(t^{(n)}|W, \beta) = (2\pi\beta^{-1})^{-N/2}\exp(-\beta E_\Lambda)$$

$$\text{Equation (5)} \quad p(t^{(n)}|W, \alpha) = (2\pi\alpha^{-1})^{-N/2}\exp(-\alpha E_W)$$

Assuming Gaussian zero-mean noise, E_Λ shows the uncertainty (or error) of the target variables with variance equal to β^{-1} ($\sigma^2 \equiv \beta^{-1}$). The conditional probability of W is defined by E_W with variance equal to α^{-1} ($\sigma_W^2 \equiv \alpha^{-1}$). Then Equation (3) can be modified as:

$$\text{Equation (6)} \quad p(W|t^{(n)}, \alpha, \beta) = \frac{p(t^{(n)}|W, \beta)p(W|\alpha)}{p(t^{(n)}|\alpha, \beta)}$$

$$\text{Equation (7)} \quad p(W|t^{(n)}, \alpha, \beta) = \frac{\exp(E(W^{MP})(1/2)\Delta W^T H \Delta W)}{\exp(E(W^{MP}))(2\pi)^{W/2}|H|^{1/2}}$$

where $E(W^{MP})$ is the expected or most probable values for the weights and bias matrices and H is a Hessian matrix of dimension $W \times W$, where W is the number of weights (Nabney 2001).

$$\text{Equation (8)} \quad H = \beta \nabla \nabla E_\Lambda^{MP} + \alpha I$$

$$\text{Equation (9)} \quad \Delta W = W - W^{MP}$$

Once the maximizing of likelihood for α and β is used to estimate the distribution of W , an integrating method can be applied to the prediction and the variance of the predictions (Neal 1996).

$$\text{Equation (10)} \quad p(y_k | x^{(n)}, t^{(n)}) = \int (t^{(n)} | x^{(n)}, W) p(W | t^{(n)}) dW$$

which can be approximated by:

$$\begin{aligned} \text{Equation (11)} \quad & p(y_k|x^{(n)}, t^{(n)}) \\ & \propto (2\pi\sigma_y^2)^{-1/2} \exp\left(-\frac{1}{2}\sigma_y(y_{MP}^{(n)} - t^{(n)})^2\right) \end{aligned}$$

where σ_y^2 is the output or estimated variance array, which is $\sigma_y^2 = (\sigma_1^2, \dots, \sigma_k^2, \dots, \sigma_K^2)$.

Then the variance of output can be assessed as (Torres-Rua 2011):

$$\text{Equation (12)} \quad \sigma_y^2 = \beta_{MP}^{-1} + g^T H^{-1} g$$

where g represents the gradient of $y^{(n)}$ with respect to the weights, which is $g = \nabla W y^{(n)}|_{W_{MP}}$

The variance of output is due to both the intrinsic noise in the target data and the posterior distribution of the ANN weights. It can be captured using confidence interval estimations (Pierce et al. 2008).

3.2.2. Selection of possible input variables

The appropriate selection of input variables is crucial in training data mining algorithms. The intent of this research was to develop surface soil moisture estimates and a model of soil moisture at 15 cm depth that uses the surface soil moisture measurements as a boundary condition. The efficiency of models could then be improved by choosing the most effective combination of input variables, many of which are remotely sensed. One previous study has presented a good correlation between soil water content and infrared (IR) skin temperature and normalized difference vegetative index (NDVI), another one presented a good correlation between soil water content and IR heating rate and thermal

(Wetzel and Woodward 1987; Gillies and Carlson 1995). Remotely sensed optical and microwave data have been used for surface soil energy balance modeling (Kogan 1995; Kaleita et al. 2005). After these variables were collected from independent datasets, they were evaluated for correlation and dependency. Some vegetation indices (VIs) are considered as parameters that have some contributions in soil moisture estimations (Liu et al. 2003; Bhuiyan et al. 2006; Haubrock et al. 2008; Ben-Dor et al. 2009; Mallick et al. 2009; Liang et al. 2012; Hassan-Esfahani et al. 2014; see also chapters 2 and 4).

3.2.3. Study area, instrumentation, techniques and data

3.2.3.1. Study area

The study area is an 84-acre agricultural field located in Scipio, Millard County in Central Utah at 39°14'N 112°6'W (Figure 3.1). The field is equipped with a modern center pivot irrigation sprinkler system to supply water for crops such as oats, alfalfa, barley, and wheat grown from April to October. Figure 3.1 shows the location of the farm and presents the heterogeneity within the field due to different crop types and the presence of an access road. The irrigation system is fed by an upstream reservoir and rotates clockwise when functioning. In order to irrigate the field fully to field capacity with the current settings of the center pivot, a full lateral rotation takes three days and six hours. In order to monitor the dynamic properties of soil moisture, the experiment was designed based on flights with eight days offset during the full growing cycles of alfalfa, which was the main crop in the field. For the first growing cycle, the feasibility of five consecutive flights was investigated, but one of the flights was removed from the experiment plan due to the presence of haze

and clouds. Although monitoring more growing cycles would be beneficial to produce a more generalized data set, this was beyond the budget limitations of the project. The study reported here was carried out for the crop growing cycle starting May 16, 2013 and ending June 17, 2013, and included four flights.

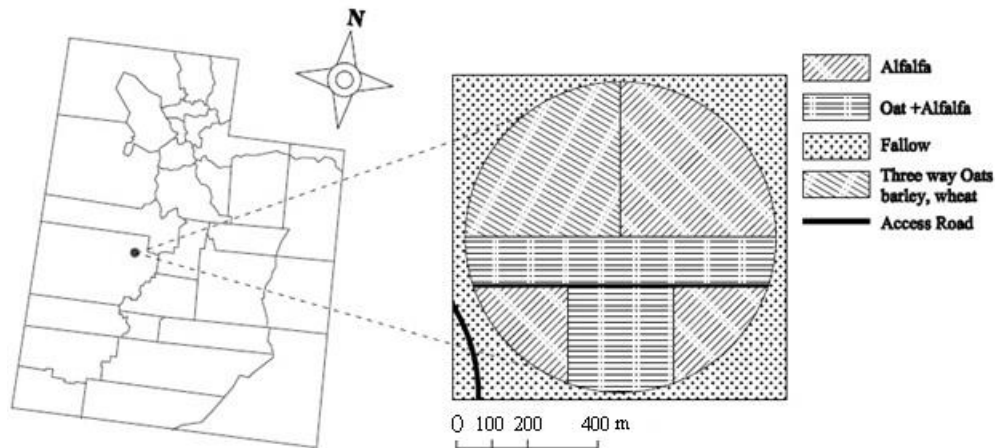


Figure 3.1. The location of the study area in Utah (schematic Utah counties map (on the left) and cropping pattern for 2013 irrigation season (on the right)), ($39^{\circ}14'N$ $112^{\circ}6'W$)

3.2.3.2. Instrumentation: Aggieair minion (the remote sensing platform)

The remote sensing platform that was utilized in this study, AggieAir, is comprised of three main subsystems: (1) the UAV aircraft, (2) the sensor payload, and (3) the ground control station (GCS). The aircraft is completely autonomous and navigates over the area of interest using a pre-programmed flight plan that can be easily designed to capture images of the desired area. The UAV is small with an 8-ft wing span and a 14-pound take-off weight. It can travel at 30 miles per hour for up to one hour. The GCS utilizes a wireless connection to monitor the flight and transmit high-level commands to the aircraft, which in turn sends flight information (location, speed, etc.) back to the GCS. In this study, the

UAV was equipped with visible, near-infrared, and thermal infrared cameras, and flew over the study area on four dates in 2013, May 16, June 1, June 9, and June 17, to acquire imagery at 0.15m resolution for the visible and near infrared bands and 0.6 m resolution for the thermal infrared band which was processed to 0.15m resolution for further calculations. The wavelength range peaks around 420, 500, 600 and 800 nm for blue, green, red and NIR sensors, respectively.

During an AggieAir flight, the aircraft may acquire 300 to 400 images from each camera. The images can be georeferenced directly by simply applying the position and orientation of the UAV when the image was exposed (Jensen 2009; AggieAir 2015). To produce an orthomosaic with highest accuracy, EnsoMOSAIC is used to orthorectify the AggieAir imagery (MosaicMill 2012). EnsoMOSAIC creates hundreds of tie-points between overlapping images and applies photogrammetry and block adjustment to refine the position and orientation information for each image, thereby accurately georeferencing each image (Horizontal Accuracy: 1-2 pixels Vertical Accuracy: 1.5-2 pixels (when all error sources are controlled)). EnsoMOSAIC also creates an internal digital elevation model (DEM) to compensate for distortions in the imagery caused by changing elevations. The resulting product is an orthorectified mosaic with 8-bit digital number format. The method used for absolute radiometric normalization of AggieAir imagery is called the “reflectance mode” method (Jensen 2009). AggieAir uses a modified “reflectance mode” method which uses the ratio of the digital number from the mosaic to the digital number from a Spectralon standard white reference panel with known reflectance coefficients multiplied by the reflectance factors. The method also uses the zenith angle of the sun for

the time and date of flight. The product of this method is an orthorectified mosaic in reflectance values (see chapter 2).

3.2.3.3. In-field data collection

In order to ground-truth the data and acquire sufficient training and testing data for constructing the Bay-ANN models, at the same time that AggieAir flew over the study area an intensive ground sampling was performed at precisely determined locations over the field. The data collection activity was designed in consideration of heterogeneity of crop types and soil characteristics. To guarantee that a wide range of physical conditions were sampled to improve the statistical representativeness of the dataset, the four flight dates were chosen to be at different crop growth stages and at the same time that Landsat passed over the farm. The availability of Landsat data provides independent information for studies on downscaling and upscaling issues. The data collection procedure was carried out by including around 50 samples per AggieAir flight at locations across the field (12 sample points in each quarter of the center pivot coverage). The data that were collected were pooled and utilized as model targets. Since the effective rooting depth (FAO 56) was seen to be around 30 centimeters in the field, in order to acquire the root zone soil moisture information, the research crew collected soil samples from the surface, 15 centimeters, and 30 centimeters depth (since the crop root development was concentrated near the surface because the sprinkler irrigation pattern produced a coincident 30 cm rooting depth) and determined gravimetric soil moisture values after the samples were oven dried and weighed. In order to make in-field measurements and verify the laboratory results, the crew employed a hand-held sensor read-out and storage system for real-time readings from

Decagon Inc. This device was connected to a GS3 soil moisture, temperature, and EC sensor from Decagon as well. Figure 3.2 illustrates the locations of soil moisture samples in the study area (Decagon Devices Inc.).

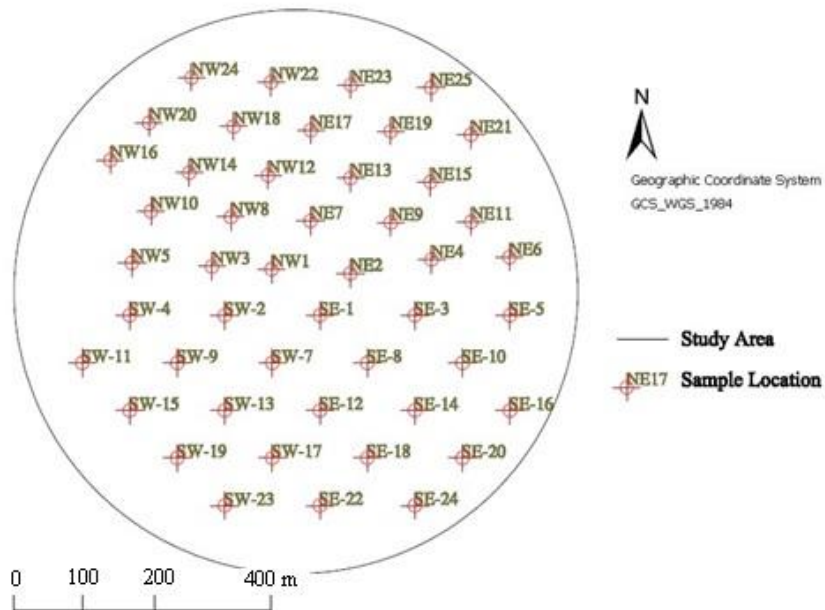


Fig. 3.2. Spatial distribution of soil moisture sample locations in the study area

3.2.4. Soil texture analysis

To estimate root zone soil moisture, soil water infiltration and conductivity must be considered. In order to define soil water characteristics, soil variables such as texture are required. After the soil has been irrigated to saturation and drained by gravity, the soil is said to be at “field capacity,” and crops can readily use the soil moisture held until total water potentials approach the permanent wilting point (Donahue et al. 1983). In order to consider field capacity and the permanent wilting point, 14 different points throughout the

field were chosen for soil texture sampling. After soil type determination, the corresponding field capacity values were derived from previously published studies and considered as model inputs (Costa et al. 2013). Figure 3.3 shows the soil field capacity map developed by applying a Spherical Kriging interpolation method (GIS package) for the information from the 14 available data points.

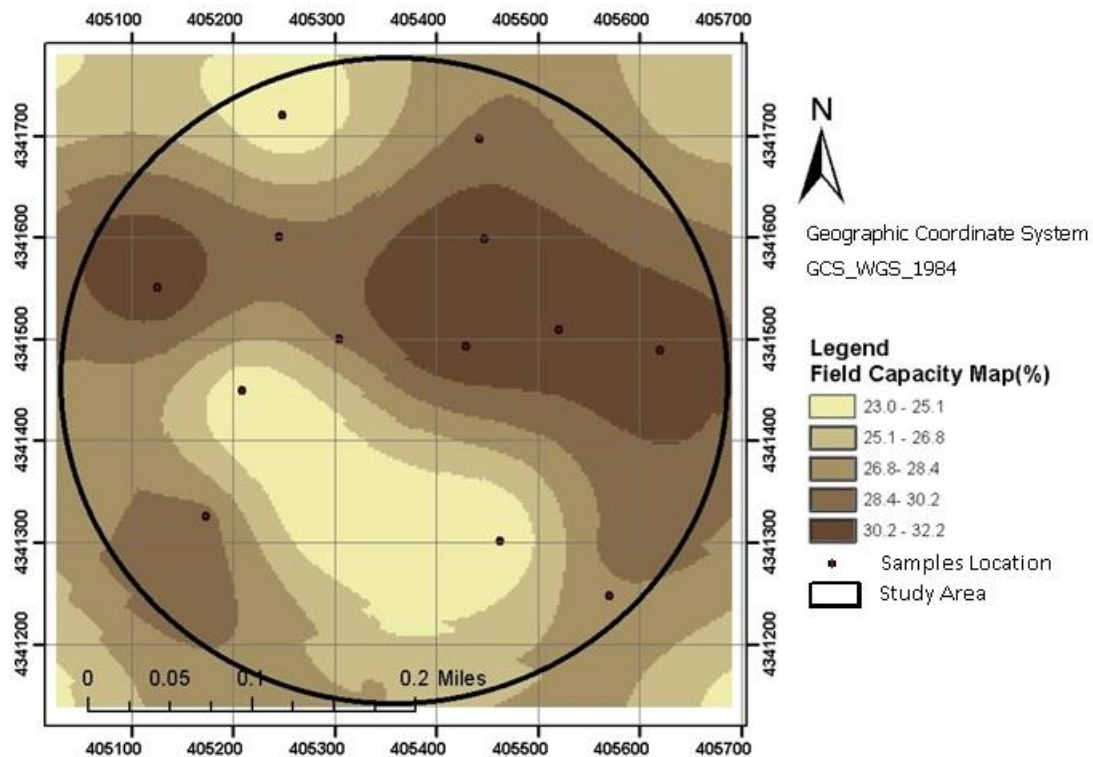


Fig. 3.3. Map of field capacity based on soil texture type and plot of the location of soil samples

3.2.5. Relevant Vegetation Indices (VIs) for surface soil moisture estimation

Visual (visible) spectrum (red, green, and blue, or RGB), near-infrared (NIR), and infrared/thermal remotely sensed data and some vegetation indices (VIs) were used as input variables for the artificial neural network (ANN) surface soil moisture estimation model (Hassan-Esfahani et al. 2014, see also chapters 2 and 4). All AggieAir data (RGB, NIR,

and thermal imagery), normalized difference vegetation index (NDVI), vegetation condition index (VCI), enhanced vegetation index (EVI), vegetation health index (VHI), and field capacity were chosen as model inputs (see chapter 2). Proposed by Kogan (1995), the VHI is an additive combination of VCI and Temperature Condition Index (TCI). Equations 13–16 represent the vegetation indices:

$$\text{Equation (13)} \quad NDVI = \frac{\rho_{NIR} - \rho_{RED}}{\rho_{NIR} + \rho_{RED}}$$

$$\text{Equation (14)} \quad VCI = 100 \times \frac{\rho_{NDVI} - \rho_{NDVI_{min}}}{\rho_{NDVI_{max}} - \rho_{NDVI_{min}}}$$

$$\text{Equation (15)} \quad EVI = 2.5 \times \frac{\rho_{NIR} - \rho_{RED}}{\rho_{NIR} + C_1 \times \rho_{RED} - C_2 \times \rho_{BLUE} + L}$$

$$\text{Equation (16)} \quad TCI = 100 \times \frac{BT_{max} - BT}{BT_{max} - BT_{min}}$$

$$\text{Equation (17)} \quad VHI = 0.5 \times VCI + 0.5 \times TCI$$

where ρ_{NIR} , ρ_{RED} and ρ_{BLUE} are NIR, red, and blue reflectance bands; C_1 , C_2 and L are the coefficients of the aerosol resistance term, which uses the blue band to correct for aerosol influences in the red band and are equal to 6, 7.5, and 1, respectively; and BT is the thermal brightness, which is the thermal band reflectance.

3.2.6. Model Validation

A K-fold cross validation technique was used in this study to validate the model's generalization. Generally in a K-fold cross validation, the original data set is partitioned into K (almost equal size) subsets. Each time a subset is retained for testing and the remaining K-1 subsets are kept for training. This procedure iterates K times and every time

an evaluation criterion is calculated. Mean squared error (MSE) is calculated as the evaluation criterion in a 5-fold cross validation in the current study. Further, the MSE for the 5 models are averaged to represent the best model. During the training phase different values for the training parameters were utilized in concert with different network architectures (Geisser 1993; Kohavi 1995). Finally the calibrated network was trained using all the data, with the best number of hidden units and training parameters.

3.2.7. Input variable wrapper selection

The model construction procedure utilized a wrapper selection method to identify the most relevant information from among the models developed. Guyon (2003) introduced the advantages of applying this method with respect to three main aspects: (1) enhancing the performance of predictors, (2) acquiring faster and more cost-effective predictors, and (3) providing a better understanding of the underlying process that generated the data. This method is recommended over the backward selection method and is applicable to cases with a small number of inputs. In a wrapper selection approach, all possible combinations of input variables are considered, and a separate model is developed for each of the combinations. The models are then scored based on their predictive power, and the best model can be selected based on the corresponding score (Kohavi and John 1997). Root mean square error (RMSE), mean absolute error (MAE), coefficient of correlation (r), coefficient of performance (e), and coefficient of determination (R^2) are the statistical parameters that were calculated to evaluate the performance of the many alternative models and score their predictive power in order to check the goodness of fit (Glover et al. 2008).

3.2.8. Root zone soil water content estimation

Estimated soil moisture values at 30cm, 15 cm, and the surface were integrated into the root zone to yield root zone soil water content estimate. The flowchart presented in Figure 3.4 illustrates the entire procedure, from the initial high-resolution multi-spectral imagery and *in situ* data collection to the final calculation of volumetric root zone soil water content.

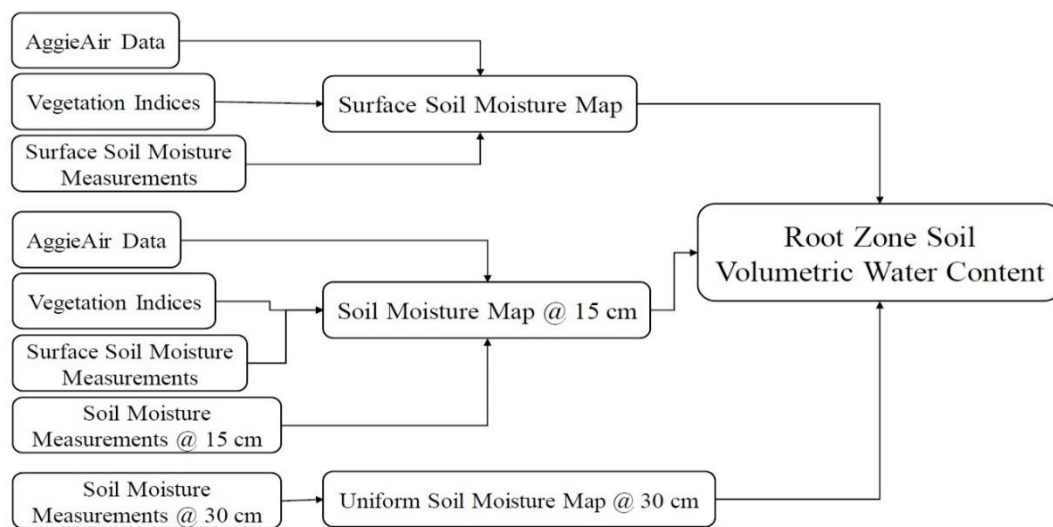


Fig. 3.4. Volumetric root zone water content calculation procedure

3.3. Results and discussion

3.3.1. Surface soil moisture (SM-0)

3.3.1.1. Surface soil moisture data

For surface soil, the gravimetric soil moisture measurements were compared with the dataset of in-field volumetric soil moisture measurements using a paired t-test. This

comparison was carried out by considering bulk density values derived from the soil texture information. The t-test results showed that the two datasets are not statistically different at a 95 percent confidence level. The t-test results imply that either of the initial data sets can be used for further calculations. Then the gravimetric soil moisture values from four flight dates were pooled representing the maximum, minimum and mean values of 30.6, 10.1 and 19.7 (VWC(%)), respectively, were considered as model targets. Table 3.1 shows the comparison between measured and estimated soil moisture values for different crop type zones.

Table. 3.1. Comparison between measured and estimated soil moisture values for different crop type zones

Crop Type/Date	Soil Moisture (Volumetric Water Content (%)) (Zonal Mean)							
	5/17/2013		6/1/2013		6/9/2013		6/17/2013	
	Measur ed	Estimat ed	Measur ed	Estimat ed	Measur ed	Estimat ed	Measur ed	Estimat ed
Three way, Oat, Barley , Wheat	18.9	20.1	21.5	19.0	14.9	15.7	19.3	17.6
Alfalfa	27.6	25.9	25.0	23.5	18.4	18.9	21.2	20.4
Oat, Alfalfa	18.0	18.3	20.5	18.1	15.7	15.8	22.5	18.9

3.3.1.2. Spatial information

The significance of the spatial information originates from the ability of the human brain to detect spatial patterns in a map or an image. In order to enhance interpretation of

results, a spatial analysis was done using NDVI as a common vegetation index that describes field condition in terms of crop type and growing stage. Spatial information magnifies the heterogeneity within the field due to different crops, the access road, wheel tracks, the center pivot station, and older fence lines and ditch banks that once occupied the modern field decades ago but that are no longer visible from the ground. Table 3.2 represents the temporal and spatial changes of NDVI during the study period.

Table 3.2. Temporal and spatial changes in NDVI values during the study period related to the different crops present in the area of study

Crop Type/Date	NDVI(Mean)			
	5/17/2013	6/1/2013	6/9/2013	6/17/2013
Three way, Oat, Barley , Wheat	0.09 Planting	0.34 continued growth	0.43 continued growth	0.53 full growth
Alfalfa	0.42 continued growth	0.47 continued growth	0.53/0.08 full growth/ after cut	0.59/0.13 full growth/ after cut
Oat, Alfalfa	0.23 germination	0.38 continued growth	0.53 full growth	0.57 full growth

3.3.1.3. Correlation test of the potential inputs

After selecting the potential inputs for the model, a correlation test has been carried out on the data set to ensure the necessity of each input parameter. The highly correlated inputs would be removed on the favor of each other to support the models' simplicity. Table 3.3 presents the p-values of the correlation test that proves the potential contributions of each input in the models. The criterion of deciding on the existence of correlation between the inputs was having a p-value close to 1 or -1 to present the direct or inverse correlations. As it has been shown in Table 3.3, none of the parameters are highly correlated and they are recommended to get involved in the modeling procedure.

Table. 3.3. P-values presented as the results of correlation test.

Potential Inputs	Red	green	Blue	NIR	Thermal	NDVI	VCI	EVI	VHI	Field Capacity
Red	1.00	0.00	0.00	0.00	0.03	0.00	0.00	0.00	0.00	0.39
green	0.00	1.00	0.00	0.00	0.00	0.00	0.00	0.00	0.00	0.55
Blue	0.00	0.00	1.00	0.08	0.00	0.00	0.00	0.00	0.00	0.13
NIR	0.00	0.00	0.08	1.00	0.00	0.00	0.00	0.00	0.00	0.76
Thermal	0.03	0.00	0.00	0.00	1.00	0.64	0.06	0.01	0.14	0.71
NDVI	0.00	0.00	0.00	0.00	0.64	1.00	0.00	0.00	0.00	0.66
VCI	0.00	0.00	0.00	0.00	0.06	0.00	1.00	0.00	0.00	0.39
EVI	0.00	0.00	0.00	0.00	0.01	0.00	0.00	1.00	0.00	0.79
VHI	0.00	0.00	0.00	0.00	0.14	0.00	0.00	0.00	1.00	0.43
Field Capacity	0.39	0.55	0.13	0.76	0.71	0.66	0.39	0.79	0.43	1.00

3.3.1.4. Input variables wrapper selection

The goodness-of-fit measures were applied to test the degree of association between the observed and estimated data. As noted previously, root mean square error (RMSE), mean absolute error (MAE), coefficient of correlation (r), coefficient of performance (e) and coefficient of determination (R^2) were calculated for the models to score their predictive power. The results of models with the greatest predictive power were compared spatially. This was carried out based on the notes that the research crew had made about field observations and were consistent with the field measurements. They paid attention to crop types, crops growing stage, location of lateral, irrigation uniformity, wet and dry spots (created due to deficiencies in the irrigation sprinkler system), existence of wind (wind direction if it scatters the water) and weather conditions. After the models with high but similar predictive power were developed (models with close quality metrics), the best model was selected on the basis of visual inspection of its ability to accommodate the spatial distribution of the above information. In total, 1023 models in 10 sets for all possible combinations of 10 inputs were established (10 combinations of 1, 45 combinations of 2, 120 combinations of 3, 210 combinations of 4, 252 combinations of 5, 210 combinations of 6, 120 combinations of 7, 45 combinations of 8, 10 combinations of 9 and 1 combination of 10 inputs), and the model results were analyzed and compared. A trial-and-error approach was utilized to select the number of hidden units and optimization algorithm for each model (Nabney 2001). The model with 8 inputs (red, green, blue, NIR, NDVI, EVI, VHI, and field capacity) was ultimately selected because it had the highest predictive power and produced the best spatial patterns. Table 3.4 shows the best model results for all 10 sets of combinations along with their highest predictive power.

Table 3.4. Goodness-of-fit statistics from wrapper selection results (1 to 10 inputs) for surface soil moisture estimations (SM-0) with highest predictive power using Bayesian artificial neural networks

Bayesian ANN Inputs		# hidden units	Optimization algorithm	RMSE	MAE	r	e	R ²
One Input	Thermal	5	QUASINEW	3.0	2.4	0.64	0.41	0.41
Two Inputs	Thermal, Field Capacity	5	QUASINEW	2.8	2.2	0.70	0.49	0.50
Three Inputs	Thermal, VHI, Field Capacity	13	QUASINEW	2.5	1.7	0.78	0.59	0.61
Four Inputs	NDVI, VCI, EVI, VHI, Field Capacity	14	QUASINEW	2.3	1.5	0.82	0.66	0.67
Five Inputs	Red, NIR, Thermal, EVI, Field Capacity	16	QUASINEW	1.9	1.3	0.87	0.76	0.77
Six Inputs	Red, Green, Thermal, NDVI, VCI, VHI	16	QUASINEW	1.77	1.3	0.89	0.80	0.80
Seven Inputs	Red, Green, NIR, Thermal, VCI, VHI, Field Capacity	15	QUASINEW	1.78	1.25	0.89	0.79	0.80
<u>Eight inputs</u>	<u>Red, Green, Blue, NIR, NDVI, EVI,</u>	<u>14</u>	<u>QUASINEW</u>	<u>1.6</u>	<u>1.1</u>	<u>0.92</u>	<u>0.84</u>	<u>0.84</u>

	VHI, Field Capacity							
Nine Inputs	Green, Blue, NIR, Thermal, NDVI, VCI, EVI, VHI, Field Capacity	14	QUASINEW	2.1	1.3	0.86	0.74	0.74
Ten Inputs	Red, Green, Blue, NIR, Thermal, NDVI, VCI, EVI, VHI, Field Capacity	12	QUASINEW	2.1	1.4	0.84	0.70	0.70

* The best model is presented in bold

3.3.1.5. Bayesian artificial neural networks (Bayesian ANN) model for surface soil moisture (SM-0)

After an intensive trial and error selection procedure, a network architecture with 14 hidden units and the Matlab QUASINEW optimization algorithm was selected. Figure 3.5 illustrates the measured surface soil moistures versus estimated values of the selected model, a one-by-one plot (showing that all the points are clustered along the 45° line), a residual plot, and a histogram of error to represent the validation of the model in the sense of normality, linearity, and equality of variances. The points in the residual plot are randomly dispersed around the horizontal line (zero error line), that confirms the regression model is appropriate for the data. The error histogram is bell-shaped, confirming the conclusions that random errors inherent in the process have been drawn from a normal distribution.

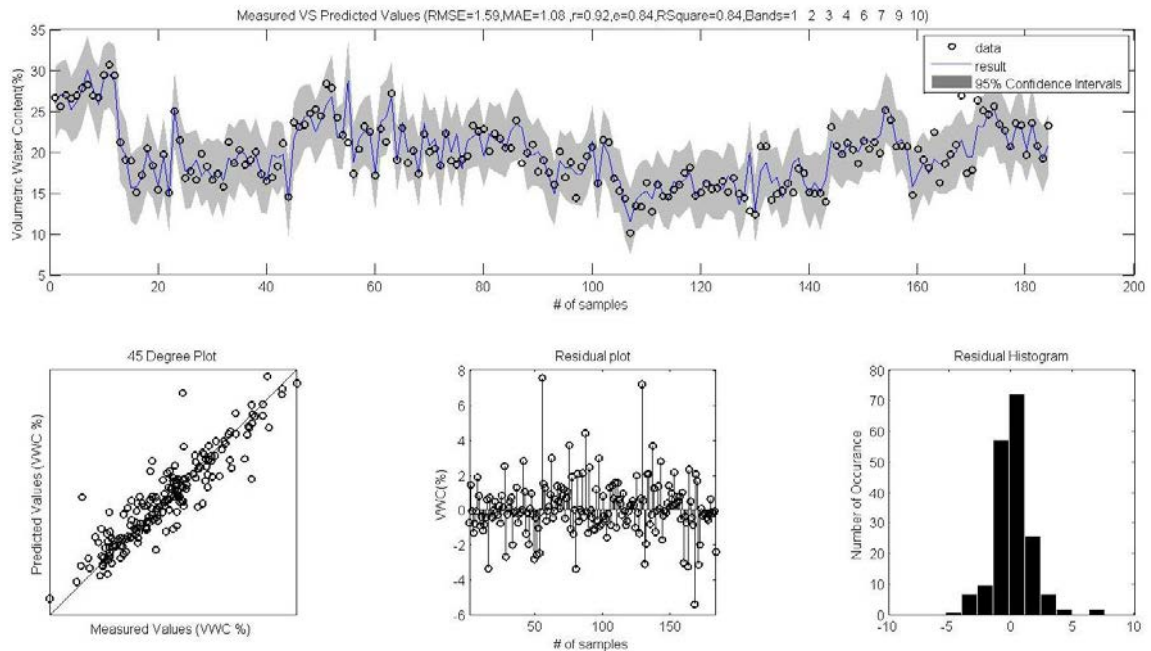


Fig. 3.5. Measured surface soil moistures versus estimated values of the selected model, the corresponding one-by-one plot, residual plot, and histogram of error

3.3.2. Soil moisture at 15 centimeters depth (SM-15)

3.3.2.1. Soil moisture data

For soil moisture measurements at 15-cm depth, soil samples were collected simultaneously with surface soil moisture samples. The volumetric soil moisture content at 15 cm was determined using gravimetric measurements of moisture in the soil samples and bulk density values from the soil texture test.

3.3.2.2. Wrapper selection

The goodness-of-fit evaluation measures were utilized to test the degree of association between the surface soil moisture as a boundary condition in concert with high-resolution remotely sensed data and soil moisture values at 15 cm depth. As mentioned

previously, the predictive power of the models was determined using root mean square error (RMSE), mean absolute error (MAE), coefficient of correlation (r), coefficient of performance (e) and coefficient of determination (R²). The same quantitative and qualitative evaluations were conducted to identify the models with best predictive power for soil moisture at 15 cm. In this set of calculations, a total of 1023 models in 10 sets for all possible combinations of 10 inputs were established with surface soil moisture values as the boundary condition, and the model results were analyzed and compared. A trial-and-error approach was applied to select model properties such as the number of hidden units and optimization algorithm (Nabney 2001). The model with 9 inputs (surface soil moisture, red, green, blue, thermal, NDVI, EVI, VHI, and field capacity) was ultimately selected because it had the highest score and best spatial pattern, which was checked visually. Table 3.4 shows the best model results for all 10 sets of combinations along with corresponding statistical parameters and model properties.

Table. 3.5. Goodness-of-fit statistics from wrapper selection results (1 to 10 inputs) for soil moisture estimations at 15 cm (SM-15) with highest predictive power using Bayesian artificial neural networks

Bayesian ANN Inputs		# hidden units	Optimization algorithm	RMSE	MAE	r	e	R ²
One Input	Surface Soil Moisture	6	QUASINEW	1.7	1.3	0.81	0.61	0.61
Two Inputs	Surface Soil Moisture, NIR	8	QUASINEW	1.6	1.2	0.82	0.68	0.68

Three Inputs	Surface Soil Moisture, Thermal, NDVI	14	QUASINEW	1.2	1.0	0.91	0.82	0.82
Four Inputs	Surface Soil Moisture, Thermal, NDVI, EVI	15	QUASINEW	1.2	0.9	0.91	0.81	0.82
Five Inputs	Surface Soil Moisture, Thermal, NDVI, VHI, Field Capacity	15	QUASINEW	1.2	0.9	0.90	0.82	0.82
Six Inputs	Surface Soil Moisture, Green, Blue, NIR, Thermal, Field Capacity	15	QUASINEW	1.2	0.8	0.91	0.82	0.83
Seven Inputs	Surface Soil Moisture, Red, Green, Blue, NIR, EVI, Field Capacity	11	QUASINEW	1.1	0.8	0.92	0.84	0.83
Eight inputs	Surface Soil Moisture, Red, Green, Blue, NIR, Thermal, EVI, Field Capacity	13	QUASINEW	1.1	0.7	0.91	0.84	0.84
<u>Nine Inputs</u>	<u>Surface Soil Moisture, Red,</u>	<u>11</u>	<u>QUASINEW</u>	<u>1.1</u>	<u>0.7</u>	<u>0.92</u>	<u>0.85</u>	<u>0.85</u>

	<u>Green, Blue,</u>								
	<u>Thermal, NDVI,</u>								
	<u>EVI, VHI, Field</u>								
	<u>Capacity</u>								
Ten Inputs	Surface Soil Moisture, Red, Green, Blue, NIR, Thermal, NDVI, VCI, EVI, VHI, Field Capacity	9	QUASINEW	1.2	0.9	0.91	0.82	0.82	
Eleven Inputs	Surface Soil Moisture, Red, Green, Blue, NIR, Thermal, NDVI, VCI, EVI, VHI, Field Capacity	5	QUASINEW	1.4	1.0	0.87	0.77	0.77	

*The best model is presented in bold

As it is shown in Table 3.5, surface soil moisture (SM-0) is the main input to the Bay-ANN models for soil moisture estimations at 15 cm depth (SM-15). Adding thermal and NDVI (a function of red and NIR bands) magnifies the quality of statistical parameters mainly because they convey some information about evapotranspiration rates and green vegetation coverage (which is related to SM content under the surface). Adding more VIs does not increase the quality of the results in a significant way because they are functions of components which have already played their effective role (NIR, red, and thermal). The

quality of the models increases slightly by adding field capacity, which is a function of soil texture and essentially influences soil water holding capacity. An obvious conclusion from the above model could be the physical correlation of soil moisture at surface (SM-0) and 15 cm depth (SM-15) which is derived from the first model developed with only one input (SM-0).

3.3.2.3. Bayesian artificial neural networks model for soil moisture at 15 cm depth (SM-15)

After an intensive trial and error selection procedure, a network architecture with 11 hidden units and the QUASINEW optimization algorithm was selected. Figure 3.6 illustrates the measured soil moisture values at 15 cm versus the estimated values of the selected model, along with the corresponding one-by-one scatter plot (showing that all the points are clustered along the 45° line), residual plot, and error histogram to represent the validation of the model in the sense of normality, linearity, and equality of variances. The points in the residual plot are randomly dispersed around the horizontal line (zero error line), that confirms the regression model is appropriate for the data. The error histogram is bell-shaped, confirming the conclusions that random errors inherent in the process have been drawn from a normal distribution.

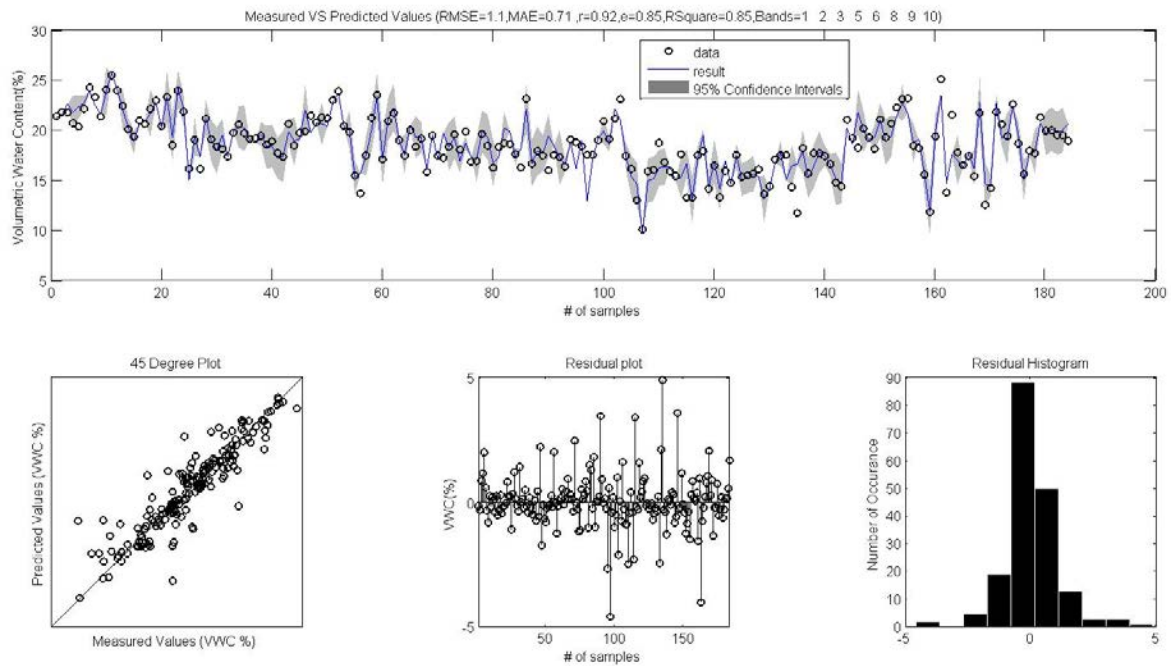


Fig. 3.6. Measured soil moistures at 15 cm versus predicted values of the selected model, the corresponding one-by-one plot, residual plot, and histogram of error

3.3.3. Soil moisture at 30 centimeters depth (SM-30)

3.3.3.1. Soil moisture data

For soil moisture measurements at 30 cm depth, soil samples were collected simultaneously with surface and 15 cm soil moisture samples. The volumetric soil moisture content at 30 cm was determined using the same method as at 15 cm depth. Since the results of the measurements presented a very negligible range of soil moisture variation throughout the growing cycle (3 percent) at 30 cm depth, an average volumetric water content of 19.6% was assumed to be constant over the entire field. Figure 3.7 shows how volumetric soil water content at 30 cm is almost constant, regardless of the shape of the root zone volumetric soil water content profile for four sample locations. Figure 3.7 illustrates volumetric soil water content variation in the root zone profile for four points

(one in each quarter of the study area). NE 4 is a point located in the northeast (NE) quarter which had been just irrigated for the first two flights. The irrigation was totally stopped for a day at the time of third flight to make the farm ready to harvest. Since a full irrigation event takes more than three days, the location of the lateral in the last flight (Figure 3.8) creates the impression that the NE quarter was irrigated almost a day before the AggieAir mission. In the case of third and fourth flights, irrigation water had penetrated the soil profile. For an example case of NW5 (located in northwest quarter), almost two days passed after the last irrigation and before the flight, which implies a drier surface soil due to higher evaporation rate of the surface layer.

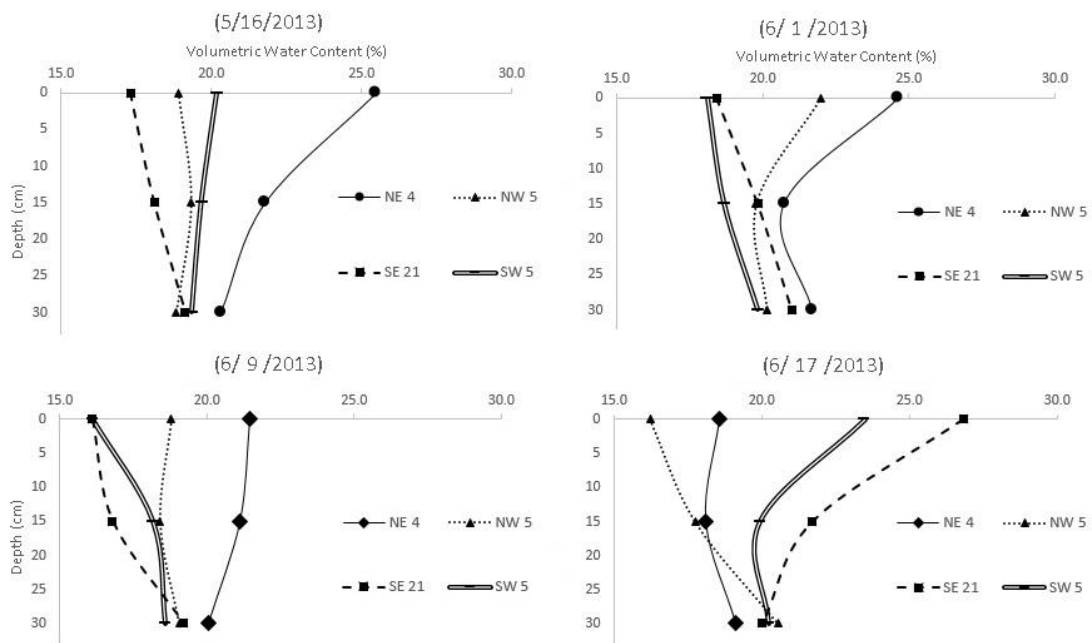


Fig. 3.7. Volumetric soil water content variation in the root zone profile at sample locations for each flight

3.3.4. Volumetric Water Content (VWC) in the root zone soil (SM-RZ)

After estimating volumetric water content values at the three different depths to cover the crop root zone (surface, 15 cm and 30 cm), these values were integrated over the

root zone to present an estimate of the VWC in the soil vertical profile. Figure 3.8 illustrates the measured VWC in the root zone versus estimated VWC. It shows that the model could estimate the root zone VWC with good accuracy (RMSE= 0.05, MAE=0.04, $r=0.97$, $e=0.92$, $R^2=0.94$) and that the estimations strongly follow the trends and fluctuations in the measured values. Figure 3.9 illustrates the pixelwise root zone VWC values for the four flights.

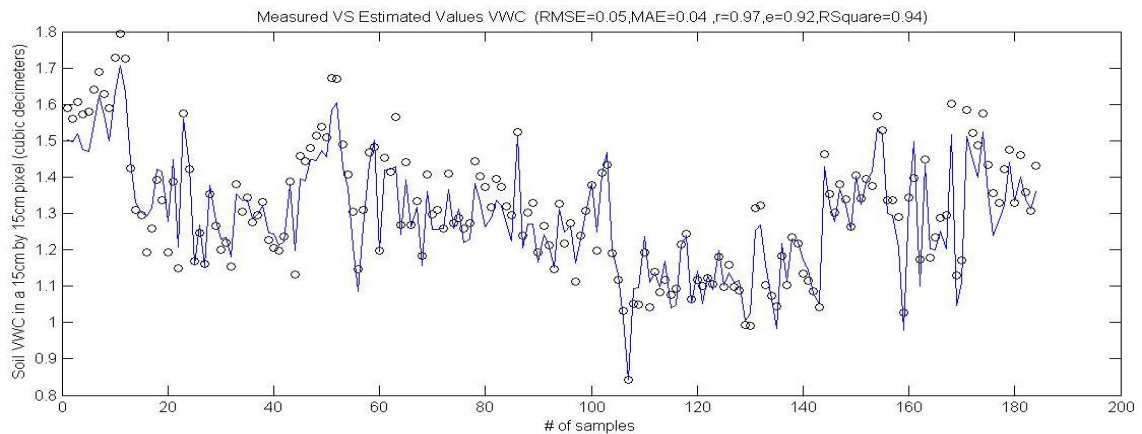


Fig. 3.8. Pixelwise measured root zone VWC versus pixelwise estimated root zone VWC

The Bayesian ANN models for soil moisture at the surface and 15 cm depth generated accurate soil moisture estimations (RMSE: 1.6, MAE: 1.08, r : 0.92, e : 0.84, R^2 :0.84 for surface and RMSE: 1.1, MAE: 0.71, r : 0.92, e : 0.85, R^2 :0.85 at 15 cm depth) for the four flights. These results in the agricultural soil profile could provide a source of information for irrigators as a main component of a soil water balance model. Figure 3.9 shows the association of root zone VWC with the crop type. The Bayesian ANN models for soil moisture at the surface and 15 cm depth generated accurate soil moisture estimations (RMSE: 1.6, MAE: 1.08, r : 0.92, e : 0.84, R^2 :0.84 for surface and RMSE: 1.1, MAE: 0.71, r : 0.92, e : 0.85, R^2 :0.85 at 15 cm depth) for the four flights.

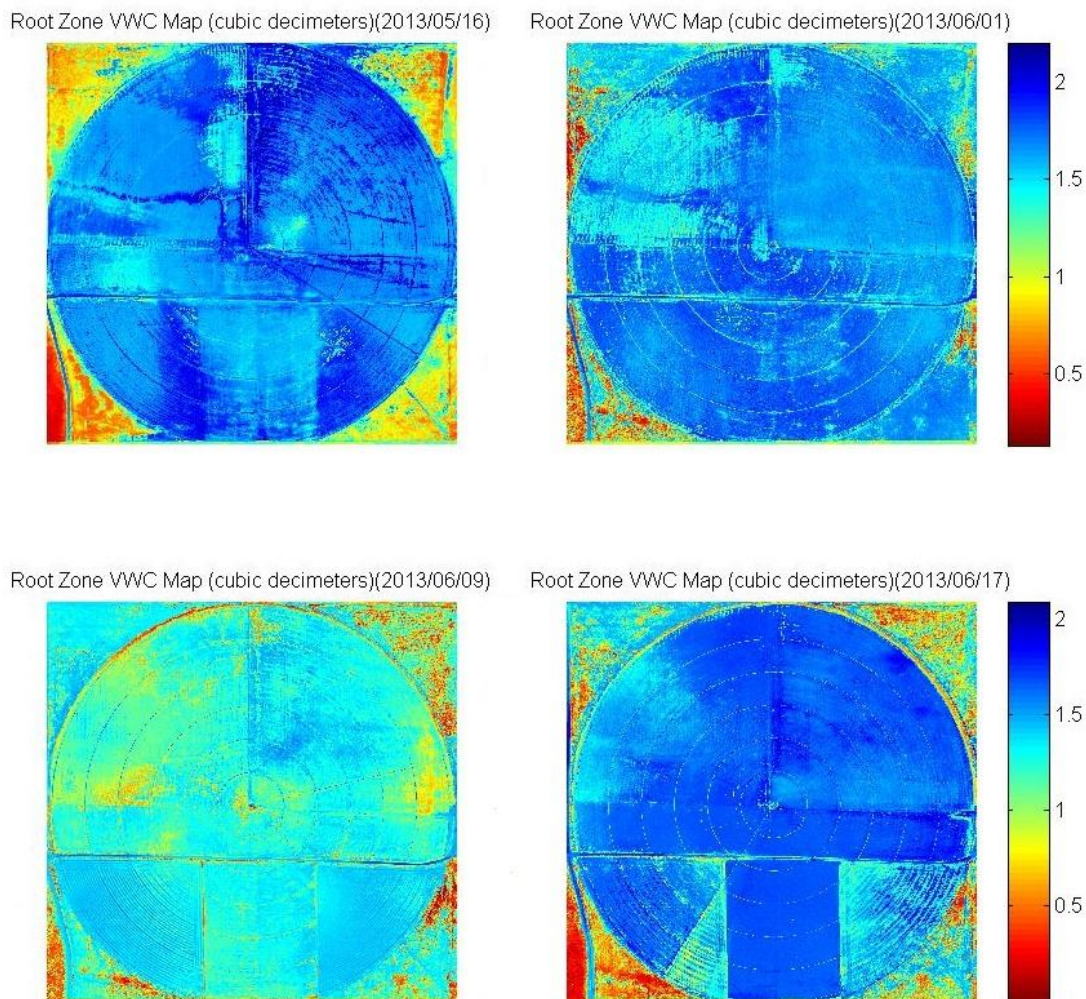


Fig. 3.9. Pixelwise VWC in the root zone for the four flights

These results in the agricultural soil profile could provide a source of information for irrigators as a main component of a soil water balance model. Figure 3.9 shows the association of root zone VWC with the crop type. The variation in the colors confirms that crops have different water requirements and absorption rates that lead to heterogeneity in the maps, even after a uniform irrigation event. Also, the field exterior area was not under irrigation, and the maps illustrate a lower soil VWC. Though no ground-based

measurements were made in these areas, the results qualitatively match expectations. The access road and wheel tracks are covered by bare soil and also show lower soil VWC.

One step forward in generalizing the current results in the temporal scale could be the idea of pooling the soil moisture data collected from different dates. In the case of the current study, every single data point experiences four different conditions of soil moisture level, which provides a wide range of information about soil moisture status through time. This type of information makes the model more robust in its ability to simulate previously unseen soil moisture conditions through time.

3.4. Conclusions

This paper presented the application of a new remote sensing technology (AggieAir) for estimating root zone soil water content as a potentially useful piece of information for a water balance model that supports irrigation water management. High-resolution multi-spectral imagery, in conjunction with surface and root zone ground sampling, provided enough information for the modeling approaches. Bayesian ANN models that utilize the remotely sensed information to quantify spatially distributed root zone soil volumetric water content.

This paper presents the results of a modeling approach applying Bayesian ANN in concert with time and site specific information. Parallel to other modeling approaches, such as data mining algorithms or linear regression, the ANN model is calibrated for this study within the conditions of the information collected including soil moisture measurements, soil texture, crop type information, and high resolution multi-spectral imagery. While the site-specific calibrated Bay-ANN in this study cannot be used immediately in another

location, the modeling procedure (identifying the information with the most significant contribution to soil moisture estimation (Table 3.4 and 3.5) along with similar field measurements and high resolution multi-spectral imagery and the data mining algorithm, are transferable from this study to other areas and applications.

Surface and 15 cm depth soil moisture estimations were accomplished with Bay-ANN models (RMSE: 1.6, MAE: 1.08, r: 0.92, e: 0.84, R^2 :0.84 for surface and RMSE: 1.1, MAE: 0.71, r: 0.92, e: 0.85, R^2 :0.85 at 15 cm depth) for four dates in 2013 (May 16, June 1, June 9, and June 17). The statistical measurements of the behavior of these models indicate good accuracy in their geospatial estimation of soil moisture. Generally, irrigation scheduling is traditionally based on the farmer's visual perceptions of soil moisture or a few soil moisture samples averaged across the farm. Irrigation scheduling can be greatly improved by the modeling approach used in this study as it enables greater precision in the application of irrigation water by identifying dry/wet spots.

AggieAir imagery, in conjunction with Bay-ANN, provided accurate estimation of root zone (30 cm) soil moisture. Compared to the traditional remote sensing technologies, e.g., satellite or commercial aerial photography services, this estimation method, with high spatial (15 cm by 15 cm pixels) and temporal resolution, is a potential step forward for possible future use in precision agriculture and irrigation scheduling. The actionable information derived here produces root zone soil water content maps (Figure 3.9) that can result in more efficient irrigation water allocation.

The results from the wrapper selection (Table 3.4) prove the significance of thermal imagery and soil texture data, which appeared as field capacity in the model inputs, as these were the most relevant information in surface soil moisture estimations. The same applies

to the information derived from Table 3.5, which shows that thermal band and field capacity are the most repeated information in the wrapper selection of appropriate model inputs for soil moisture estimations at 15 cm. In the case of one input, a model with thermal imagery can estimate the surface soil moisture values with a RMSE of approximately 3%, and a model with surface soil moisture estimations can estimate the soil moisture values at 15 cm with RMSE of approximately 1.7%.

Vegetation indices were applied as model inputs to magnify the AggieAir data. Tables 3.4 and 3.5 illustrate the significance of these indices and how they improve the model statistics as they come into account. Figure 3.9 presents the heterogeneities across the farm in terms of crop type, access road, and field exterior area, which are in accordance with the experimental expectation.

3.5. References

- Abdallah EB, Abuarab ME (2013) Soil moisture distribution patterns under surface and subsurface drip irrigation systems in sandy soil using neutron scattering technique. *Irrig Sci* 31:317–332. doi 10.1007/s00271-011-0306-0
- AggieAir, (2015) A Remote Sensing Unmanned Aerial System for Scientific Applications, <http://aggieair.usu.edu/>
- Albergel C, Rüdiger C, Pellarin T, Calvet JC, Fritz N, Froissard F, Suquia D, Petitpa, A, Piguet, B, Martin E (2008) From near-surface to root-zone soil moisture using an exponential filter: an assessment of the method based on in-situ observations and model simulations. *Hydrol Earth Syst Sc* 12: 1323–1337. doi:10.5194/hess-12-1323-2008,2008

- Ben-Dor E, Chabrillat S, Demattê JAM, Taylor GR, Hill J, Whiting ML, Sommer S (2009) Using Imaging Spectroscopy to study soil properties. *Remote Sens Environ* 113: S38-S55
- Bhuiyan C, Singha RP, Koganc FN (2006) Monitoring drought dynamics in the Aravalli region (India) using different indices based on ground and remote sensing data. *Int J Appl Earth Obs* 8: 289–302
- Costa A, Albuquerque JA, Costa A, Pértile P, Ranciani Rodrigues R (2013) Water retention and availability in soils of the state of Santa Catarina-Brazil: effect of textural classes, soil classes and lithology. *Brazilian Soil Science Society* 37: 1535-1548
- Crosson WL, Limaye AS, Laymon CA (2005) Parameter sensitivity of soil moisture retrievals from airborne C- and X-band radiometer measurements in SMEX02. *IEEE Trans Geosci Remote Sens* 43(12): 2842– 2853
- Crow WT, Chan TK, Entekhabi D, Houser PR, Hsu AY, Jackson TJ (2005) An observing system simulation experiment for Hydros radiometer-only soil moisture products. *IEEE Trans Geosci Remote Sens* 43(6): 1289–1303
- Decagon Devices, Inc. 2015. “Decagon Devices, Inc”. 20 Nov. 2014
<http://www.decagon.com/>
- Donahue, R. L., Miller, R.W., Shickluna, J.C. (1983) *Soils: an introduction to soils and plant growth*. Prentice- Hall, London
- Entekhabi D, Njoku EG, O'Neill PE, Kellogg KH, Crow WT, Edelstein WN, Entin JK, Goodman SD, Jackson TJ (2010) The Soil Moisture Active Passive (SMAP) mission. *Proceedings of the IEEE* 98(5): 704–716

- Escorihuela M, Chanzy A, Wigneron J, Kerr Y (2010) Effective soil moisture sampling depth of L-band radiometry: a case study. *Remote Sens Environ* 995–1001.
- European Space Agency. 2015. www.esa.int/ESA
- Famiglietti JS, Ryu AD, Berg A, Rodell M, Jackson TJ (2008) Field observations of soil moisture variability across scales. *Water Resour Res* 44. doi:10.1029/2006WR005804
- Gao H, Wood EF, Jackson TJ, Drusch M, Bindlish R (2006) Using TRMM/TMI to retrieve surface soil moisture over the southern United States from 1998 to 2002, *J Hydrometeorol* 7: 23–38
- Geisser, S. (1993) *Predictive Inference*. New York, NY, Chapman and Hall
- Gill K, Kemblowski M, McKee M (2007) Soil moisture data assimilation using support vector machines and ensemble Kalman filter. *JAWRA* 43: 1004–1015
- Gillies RR, Carlson TN (1995) Thermal remote sensing of surface soil water content with partial vegetation cover for incorporation into climate models. *J Appl Meteorol* 34: 745–756
- Glover DM, Jenkins WJ, Doney SC (2008) *Least Squares and regression techniques, goodness of fit and tests, non-linear least squares techniques*. Woods Hole Oceanographic Institute
- Guyon I (2003) An introduction to variable and feature selection. *J Mach Learn Res* 3: 1157-1182.
- Hassan QK, Bourque CPA, Meng FR, Cox RM (2007) A Wetness Index Using Terrain-Corrected Surface Temperature and Normalized Difference Vegetation Index

- Derived from Standard MODIS Products: An Evaluation of Its Use in a Humid Forest-Dominated Region of Eastern Canada. *Ah S Sens* 7: 2028-2048
- Hassan-Esfahani L, Torres-Rua A, Jensen A, MacKee M (2014) Topsoil moisture estimation for precision agriculture using unmanned aerial vehicle multispectral imagery. in *Proc. IEEE Int. Geoscience and Remote Sensing Symp. (IGARSS)*, 2014
- Haubrock S, Chabrillat S, Lemmnitz C Kaufmann H (2008) Surface soil moisture quantification models from reflectance data under field conditions, *Int. J. Rem. Sens.* 29(1): 3-29
- Hirschi M, Muellerr B, Dorigo W, Seneviratne SI (2014) Using remotely sensed soil moisture for land-atmosphere coupling diagnostics: The role of surface vs. root-zone soil moisture variability. *Remote Sens Environ* 154: 246-252
- Jensen AM (2009) A geospatial real-time aerial image display for a low-cost autonomous multispectral remote sensing. Master Thesis, Utah State University, USA, 2009. Paper 497. <http://aggieair.usu.edu/>
- Jiang H, Cotton W (2004) Soil moisture estimation using an artificial neural network: a feasibility study. *Can J Remote Sens* 30: 827–839
- Kaleita A, Tian L, Hirschi M (2005) Relationship between soil moisture content and soil surface reflectance. *Trans ASAE*, 48: 1979–1986
- Kerr YH, Waldteufel P, Wigneron JP, Delwart S, Cabot F, Boutin J, Escorihuela MJ, Font J, Reul N, Gruhier C, Juglea SE, Drinkwater MR, Hahne A, Martín-Neira M, Mecklenburg S (2010) The SMOS mission: New tool for monitoring key elements

- of the global water cycle. *Proc IEEE*, 98(5): 666–687, doi:10.1109/JPROC.2010.2043032
- Khalil A, Gill MK, McKee M (2005) New applications for information fusion and soil moisture forecasting. In: 8th International Conference on Information Fusion. Philadelphia, PA, USA, 1622–1628. Piscataway, NJ: IEEE, July25–28, 2005
- Kohavi R (1995) A study of cross-validation and bootstrap for accuracy estimation and model selection. *Proceedings of the Fourteenth International Joint Conference on Artificial Intelligence*, 12: 1137–1143
- Kohavi R, John GH (1997) Wrappers for feature subset selection. *Artificial Intelligence* 273-324
- Kogan FN (1995) Droughts of the Late 1980s in the United States as Derived from NOAA Polar-Orbiting Satellite Data. *Bull Am Meteorological Soc*, 76: 655–668
- Koksal ES, Cemek B, Artik C, Temizel KE ,Tasan M (2011) A new approach for neutron moisture meter calibration: artificial neural network. *Irrig Sci* 29:369–377
- Laio F (2006) A vertically extended stochastic model of soil moisture in the root zone, *Water Resour Res* 42, W02406, doi:10.1029/2005WR004502
- Liang S, Rui S, Xiaowen L, Shunlin L, Renhua Z (2012) Monitoring surface soil moisture status based on remotely sensed surface temperature and vegetation index information. *Agr Forest Meteorol* 166: 175–187
- Liu W, Baret F, Gu X, Zhang B, Tong Q, Zheng L (2003) Evaluation of methods for soil surface moisture estimation from reflectance data. *Int J Remote Sens* 24: 2069–2083

- MacKay D (1992) A practical Bayesian framework for backpropagation networks. *Neural Comput* 4(3): 448–472
- MacKay DJC (1994) Bayesian methods for back-propagation networks. In: Domany E, van Hemmen JL, Schulten K, (eds) *Models of Neural Networks III*; Springer, New York, pp 211-254
- Maier RM, Dandy CD (2000) Neural Networks for the prediction and forecasting of water resources variables: a review of modeling issues and applications. *Environ Modell Softw* 15(1): 101–124
- Mallick K, Bhattacharya BK, Patel NK (2009) Estimating volumetric surface moisture content for cropped soils using a soil wetness index based on surface temperature and NDVI. *Agr Forest Meteorol* 149: 1327–1342
- Manfreda S, Brocca L, Moramarco T, Melone F, Sheffield J (2014) A physically based approach for the estimation of root-zone soil moisture from surface measurements. *Hydrol Earth Syst Sc* 18: 1199–1212
- Manfreda S, Fiorentino M (2008) A stochastic approach for the description of the water balance dynamics in a river basin. *Hydrol Earth Syst Sc* 12: 1189–1200. doi:10.5194/hess-12-1189-2008
- MosaicMill EnsoMOSAIC(2012) <http://www.ensomosaic.com>, Accessed 6 May 2012
- Nabney IT (2001) *NETLAB algorithms for pattern recognition*. Springer Verlag, London
- NASA (2015) http://www.nasa.gov/centers/marshall/home/index.html#.VOZk9PnF_Ns
- Neal RM (1996) *Bayesian Learning for Neural Networks*; Springer: New York
- Njoku EG, Jackson TJ, Lakshmi V, Chan TK, Nghiem SV (2003) Soil moisture retrieval from AMSR-E. *IEEE T Geosci Remote* 41(2): 215–229

- Njoku EG, Ashcroft P, Chan TK, Li L (2005) Global survey and statistics of radio-frequency interference in AMSR-E land observations. *IEEE T Geosci Remote* 43(5): 938–947
- Pierce SG, Worden K, Bezazi A (2008) Uncertainty analysis of a neural network used for fatigue lifetime prediction. *Mech Syst Signal Pr* 22 (6): 1395–1411 (Special Issue: Mechatronics)
- Ragab R (1995) Towards a continuous operational system to estimate the root zone soil moisture from intermittent remotely sensed surface moisture. *J Hydrol* 173: 1–25
- Sabater JM, Jarlan L, Calvet JC, Bouyssel F, De Rosnay P (2007) From Near-Surface to Root-Zone Soil Moisture Using Different Assimilation Techniques. *J Hydrometeorol* 8: 194–206
- Seneviratne SI, Corti T, Davin EL, Hirschi M, Jaeger EB, Lehner I, Orlowsky B, Teuling AJ (2010) Investigating soil moisture-climate interactions in a changing climate: A review, *Earth Sci Rev* 99: 125–161
- SMAP Handbook, Soil Moisture Active Passive Mapping Soil Moisture and Freeze/Thaw from Space. (2014)
- Torres AF, Walker WR, McKee M (2011) Forecasting daily potential evapotranspiration using machine learning and limited climatic data. *Agric Water Manage* 98: (4), 553–562
- Titterton DM (2004) Bayesian methods for neural networks and related models. *Stat Sci* 19: 128–139

- Vinnikov KY, Robock A, Qiu S, Entin JK (1999) Optimal design of surface networks for observation of soil moisture. *J Geophys Res* 104: 19743–19749
doi:10.1029/1999JD900060
- Wagner W, Bloschl G, Pampaloni P, Calvet JC, Bizzarri B, Wigneron JP, Kerr Y (2007) Operational readiness of microwave remote sensing of soil moisture for hydrologic applications. *Hydrol Res* 38: 1–20
- Wetzel PJ, Woodward RH (1987) Soil moisture estimation using GOES-VISSR infrared data: A case study with a simple statistical method. *J Clim Appl Meteorol* 26: 107–117
- Zaman B, McKee M, Neale CMU (2012) Fusion of remotely sensed data for soil moisture estimation using relevance vector and support vector machines. *Int J Remote Sens* 33: 6516-6552

CHAPTER 4

ASSESSMENT OF OPTIMAL IRRIGATION WATER ALLOCATION FOR
PRESSURIZED IRRIGATION SYSTEM USING WATER BALANCE APPROACH,
LEARNING MACHINES, AND REMOTELY SENSED DATA²

ABSTRACT

Efficient irrigation can help avoid crop water stress, undesirable levels of nutrient leaching, and yield reduction due to water shortage, runoff or over irrigation. Gains in water use efficiency can be achieved when water application is precisely matched to the spatially distributed crop water demand. Thus, greater irrigation efficiency will facilitate quality crops and help to minimize additional agricultural and financial inputs. Irrigation efficiency is defined based on indicators such as irrigation uniformity, crop production, economic return, and water resources sustainability. This paper introduces a modeling approach for optimal water allocation relative to maximizing irrigation uniformity and minimizing yield reduction. Landsat images, local weather data, and field measurements were used to develop a model that describes field conditions using a soil water balance approach. The model includes two main modules: optimization of water allocation and forecasting the components of the soil water balance model. Each module includes two sub-modules that consider two objectives. The optimization sub-module use Genetic Algorithms (GA) to identify optimal crop water application rates based on the crop type, growing stage, and sensitivity to water stress. Results from the optimization module are passed to

²Reprinted from Agricultural water Management Journal, Vol. 153, Leila Hassan-Esfahani, Alfonso Torres-Rua, Mac McKee, “Assessment of optimal irrigation water allocation for pressurized irrigation system using water balance approach, learning machines, and remotely sensed data” pages 42-50, Copyright (2015), with permission from Elsevier.

the forecasting sub-module, which allocate water through time across the area covered by the center pivot based on the results from the previous period of irrigation (previous day) and the operational capacity of the center pivot irrigation system. The model was tested for a farm installed with alfalfa and oats and equipped with a center pivot in Scipio, Utah. The model products were assessed based on ground data (soil moisture measurements) under optimized and simulated (irrigator decisions) center pivot operations. Based on the simulation and optimization results obtained from the model, study area irrigator could use up to 20 percent less water (saved quantity over total quantity of water) over the growing season, compared to traditional operating procedures, without reducing the benefits.

4.1. Introduction

Irrigation plays an essential role in the agricultural productivity of a farm, especially in arid areas. Gains in water use efficiency can be achieved when water application is precisely matched to the spatially and temporally distributed crop water demand. In the past few decades, new technologies have played an important role in improving irrigation water allocation. For example, precision agriculture technologies have significantly advanced irrigation scheduling. Electronic devices for continuous monitoring of soil moisture and climatic conditions are widely used for more precise irrigation management of hay as a source of food for animals (Sammis, 1981; Irmak et al., 2008; Cruz-Blanco et al., 2014). Satellite sensors, such as MODIS, Landsat, and GOES, and remote sensing technology can be used to estimate crop water use and offer the potential for better water management in irrigated areas as a continuous, automated, and easy-to-use source of information (Fares et al., 2006). Optical and thermal remote sensing data from ground-

based and space-borne platforms have been used to quantify water stress and evapotranspiration at field and district scales (Taghvaeian et al., 2013). Infrared thermometry has been used in conjunction with a few weather parameters to develop non-water-stressed and non-transpiring baselines for irrigated maize in a semi-arid region. Taghvaeian et al. (2012), Torres et al. (2011), Allen et al. (2007), and Bastiaanssen et al. (2005) have used remotely sensed data to calculate daily evapotranspiration.

In addition to new technologies and satellite information, computer modeling have become popular for irrigation management. Many existing models have been developed to simulate on-farm irrigation water demands based on climate-soil-plant systems (Ahmadi and Merkle, 2009). Some optimizing irrigation planning models attempt to obtain the optimum irrigation quantity values to satisfy the objective function and constraints. These optimization models for irrigation planning have received extensive interest. Kuo et al. (2000) developed a model based on on-farm irrigation scheduling and a simple Genetic Algorithm (GA) optimization method for decision support in irrigation project planning. Delavar et al. (2012) developed a real-time modeling approach for optimal water allocation during a drought. Moghaddasi et al. (2009) developed a model for optimal allocation of water among different crops and irrigation units. Ines et al. (2004) presented an innovative approach to explore water management options in irrigated agriculture using combined remote sensing-simulation modeling and genetic algorithm optimization.

Learning machines have also been used to solve problems related to water resources management. Pulido-Calvo and Gutierrez-Estrada (2008) used computational neural networks (CNNs) to model irrigation demand and forecast water demand. Kashif Gill et

al. (2007) presented soil moisture data assimilation research that employed learning machines and a soil moisture prediction model using support vector machines.

The present work uses Landsat satellite images, field measurements, and crop-related remote sensing algorithms to demonstrate the adequacy and accuracy of a model for optimizing irrigation water allocation and simulating soil moisture conditions among the 24 irrigation sectors in the study area. The accuracy of the model was checked using a soil water balance approach for the crop growing cycle.

4.2. Model Components Review

4.2.1. Irrigation Scheduling

Irrigation managers use a process called irrigation scheduling to determine the frequency and duration of irrigation events, based on the application rate of the irrigation equipment, distribution uniformity (Delavar et al., 2012), soil infiltration rate, available water capacity (Moghaddasi et al., 2009), soil water holding capacity, and crop characteristics.

4.2.2. Irrigation Scheduling Based on Models

Optimization is the process of choosing the best solution (considering some criteria) from a set of available alternatives. In a common case, an optimization problem includes maximizing or minimizing a real function by systematically selecting input values from within an available set and computing the value of the objective function (Bradley et al.,

1997). In the current study, the spatially distributed values for irrigation rates are optimized based on specific criteria.

4.2.2.1. Genetic Algorithms

Genetic algorithms have been applied in many studies as search heuristics to find optimal solutions to non-linear problems, and they constitute a routinely used and useful method that mimic the process of natural selection. The priorities of GA over other potential algorithms are stated best by Goldberg. GAs differ from conventional optimization and search procedures in the following ways: (1) GAs work with a coding of the parameter set, not the parameters themselves; (2) GAs search from a population of points, not a single point; (3) GAs use objective function information, not derivatives or other auxiliary knowledge; and (4) GAs use probabilistic transition rules.

4.2.2.2. Optimization Objectives

In the current study, the spatially distributed values for irrigation rates are optimized considering two different objectives targeted toward saving water. These objectives were selected based on criteria regarding crop type, soil texture type, availability of water, irrigation system capacity and restrictions, growing stage, or sensitivity to water stress. Both are fundamental approaches to optimize irrigation water allocation and are summarized as follows:

- Maximizing soil moisture uniformity
- Minimizing yield reduction

4.2.2.2.1. Gini Coefficient

The Gini coefficient is a measure of statistical dispersion. It ranges from 0 to 1 and measures the inequality among values of a frequency distribution. It was first introduced for measuring the inequality of income distribution of a nation's residents and was later applied in other fields of studies (Cullis and van Koppen, 2007). A Gini coefficient of zero describes perfect equality, where all values are the same (everyone has the same income), and a Gini coefficient of one (or 100%) expresses maximal inequality among values (where only one person has all the income). Equation 1 represents this concept as the objective function (Gini, 1912).

Equation 1:
$$GINI = \frac{2 \sum_{i=1}^n i \times y_i}{n \sum_{i=1}^n y_i} - \frac{n+1}{n}$$

where n is the number of measurements and y is the measured values. The GA minimizes the Gini coefficient to seek a uniform water application distribution by changing irrigation rates in space and time, subject to system operational constraints.

4.2.2.2.2. Yield Function

The second objective function was based on a yield function. FAO No. 66 (Steduto et al., 2012) presented a linear relationship between crop yield and water use by an equation where relative yield reduction is related to the corresponding relative reduction in evapotranspiration (ET). Equation 2 represents this relationship as the objective function (FAO. Paper No. 66). This function has been used in other studies (Moghaddasi et al., 2009; Delavar et al., 2012):

Equation 2:
$$\left(1 - \frac{Y_a}{Y_x}\right) = K_y \left(1 - \frac{ET_a}{ET_x}\right)$$

where K_c is the crop coefficient and Y_a, Y_x , ET_a and ET_x are actual and maximum yield and actual and maximum evapotranspiration, respectively. As with the spatial uniformity objective, the GA minimizes yield reduction by changing irrigation rates in space and time, subject to system operational constraints.

4.3. Materials and Methods

4.3.1. Study Area

The study area is a farm of approximately 84 acres in Scipio, Utah, equipped with a modern center pivot sprinkler irrigation system with the capacity of 610 GPM. The crops for this farm, grown from April to October, are alfalfa in three-quarters of the field and oats in the north-east quarter (Fig. 4.1). Generally, the center pivot lateral rotates clockwise at a constant speed and supplies irrigation water from an upstream reservoir. The center pivot is computer programmable, and the smallest portion of the farm that can be individually irrigated is a 15 degree arc, which is considered as an irrigation sector in this study. These 15 degree arcs were numbered from 1 to 24. This study was performed for the crop growing cycle starting September 2, 2012 and ending October 4, 2012. This growing cycle was chosen among four alternative growing cycles in the entire growing season based on the availability of Landsat images covering all growing stages.

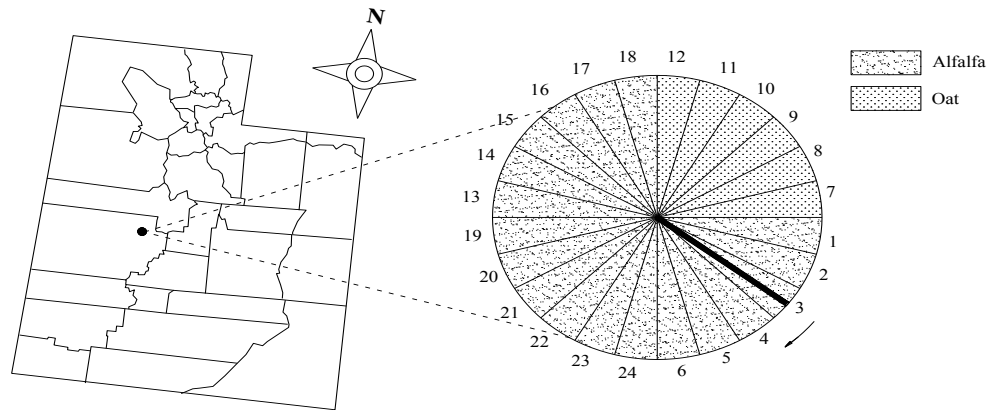


Fig. 4.1. The location of the study area in Utah, USA (schematic Utah counties map (on the right) and cropping pattern for 2013 irrigation season (on the left)), ($39^{\circ}14'N$ $112^{\circ}6'W$).

4.3.2. Soil Moisture Water Balance (SMWB)

Agricultural soil water refers to the amount of water that is held in the crop root zone at a given time. It is the difference between the water added and water withdrawn and is presented in Equation 3 as follows (Hillel, 1971),

$$\text{Equation 3:} \quad \text{Change in soil water} = (P + I + C) - (ET + D + RO)$$

where P is precipitation, I is the irrigation quantity, C is ground water contribution, ET is evapotranspiration, D is deep percolations, and RO is runoff losses. The optimal solution for the amount of water that should be applied to irrigate each 15 degree arc covered by the center pivot is obtained using Equation 3. The cropping pattern, irrigation schedule for supplying crop water requirements, crop type, crop sensitivity to water stress, and soil texture are additional considerations. Figure 4.2 illustrates the entire procedure for calculating soil moisture water balance model components:

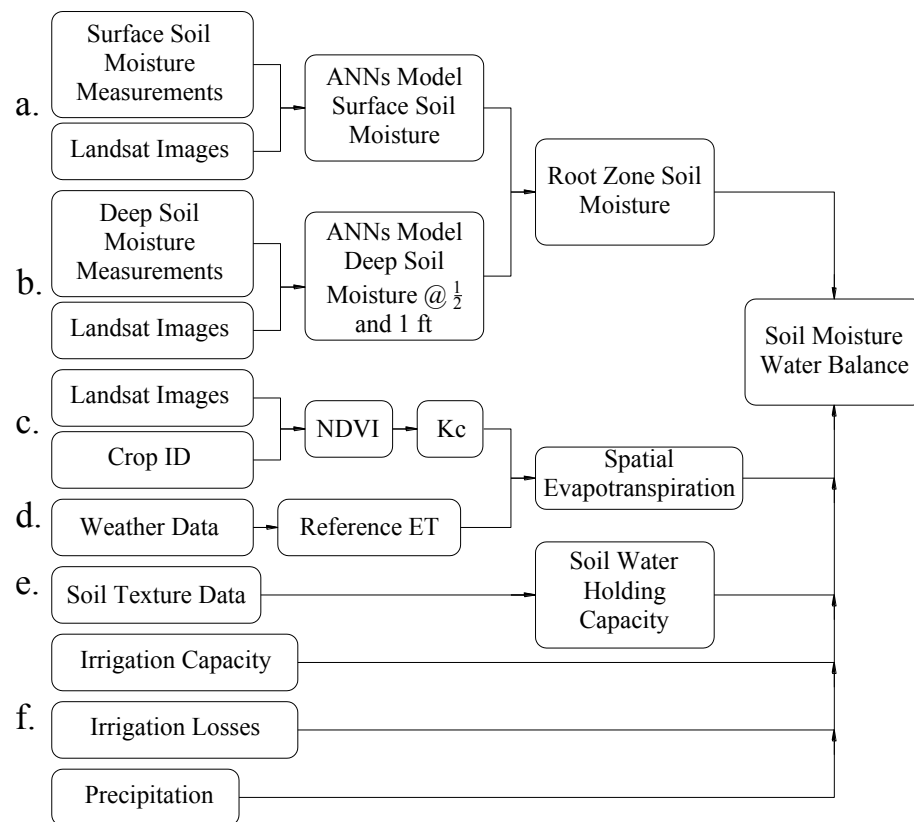


Fig. 4.2. Flowchart of soil moisture water balance calculation (SMWB) for the first time step.

Satellite images for three different dates in the growing cycle, September 2nd, September 18th, and October 4th, were downloaded from Landsat, to represent early growing stage, full growth, and after-cut conditions, respectively. The 30-meter resolution images consisted of visible bands, near-infrared (NIR), and thermal. The digital numbers (DN) of downloaded Landsat raw images were converted to reflectance values using the approach recommended in the Landsat 7 Handbook (Irish, 2000). A Matlab model was developed to compute the Normalized Difference Vegetation Index (NDVI) on a pixel-by-pixel basis for those three dates, and the crop coefficient, K_c , was calculated using the

calculated NDVI image and available experimental equations from the literature (Figure 4.2.c.). The equations are as follow (Ines et al., 2006; Rafn et al., 2008):

$$\text{Equation 4} \quad K_c = 1.1875NDVI + 0.05 \quad \text{for full cover of alfalfa}$$

$$\text{Equation 5} \quad K_c = 1.2246NDVI - 0.2203 \quad \text{for full cover of oat}$$

$$\text{Equation 6} \quad K_c = 1.25 NDVI + 0.2 \quad \text{for bare soil}$$

These equations were selected from among those available for their compatibility with crop type, climate, and irrigation conditions. In order to get daily K_c values, a spline interpolation method was applied, considering the information for Landsat overpasses on the dates right before and after the growing cycle as the boundary conditions. Meanwhile, a weather station near the farm supplied data about wind, radiation, humidity, temperature, and precipitation. Daily reference evapotranspiration values were determined by the RefET software which is based on the Penman-Monteith ET approach (Allen et al., 1998 and 2013) (Figure 4.2.d.). Multiplying daily reference evapotranspiration and K_c values supplied daily crop evapotranspiration values (ET_{daily}).

Intensive ground sampling was conducted simultaneously with Landsat overpasses at georeferenced locations. The research crew collected soil samples from the top and root zone soil, and gravimetric soil moisture values were determined from laboratory tests. The crew also used a hand held measurement device called pro-check to obtain on-field measurements of soil moisture and double check the lab results (Figure 4.2.a. and 4.2.b.). Soil moisture probes were installed at 1 and 2 feet deep to provide hourly information about soil moisture, soil temperature, and soil electrical conductivity (Figure 4.3). Following the methodology described by Pulido-Calvo and Gutierrez-Estrada (2008), the visible, NIR, IR, and thermal bands of the Landsat 7 satellite images for September 2nd, along with

surface soil moisture measurements, were used to calibrate an Artificial Neural Network (ANN) model to estimate surface soil moisture using Landsat data as inputs. The specific Landsat spectral bands used in the model were selected after an intensive trial-and-error procedure. Once calibrated, the ANN model was applied to the entire field image to obtain a soil moisture map of the farm (Figure 4.2.a.). The same procedure was executed to develop a root zone soil moisture map at 0.5 and 1 ft. depth with the same inputs and surface soil moisture from the last step. The deep and surface soil moisture values were used to estimate the volumetric available water content in the root zone.

In order to determine the water holding capacity of different soil types within the field, soil samples within the farm were collected from 14 different points and from three depths at each point. After soil type determination, the corresponding field capacity values were derived from previously published values and used as model inputs (Costa et al., 2013). Figure 4.3 illustrates the soil field capacity map developed by utilizing a Spherical Kriging interpolation method for the information from the 14 available sampling locations.

The local weather station provided precipitation data in the study area, which was zero for the growing cycle. The farmer operated the center pivot system at full capacity and constant angular velocity. This approach was also considered in the study in the case of current irrigation management modeling (Figure 4.2.f.). When estimating irrigation water requirements, the on-farm daily soil water balance may be calculated using Equation 7, which is derived from Equation 3.

Equation 7
$$SM_{t+1} = SM_t + Irr_t - ET_t + P_t - Losses$$

where $SM_{(t)}$ and $SM_{(t+1)}$ are the soil moisture values at the (t)th and (t+1)th day, $Irr_{(t)}$ is the depth of irrigation water at the (t)th day, $P_{(t)}$ is the effective rainfall at the jth day, and $ET_{(t)}$ is the evapotranspiration rate at the (t)th day.

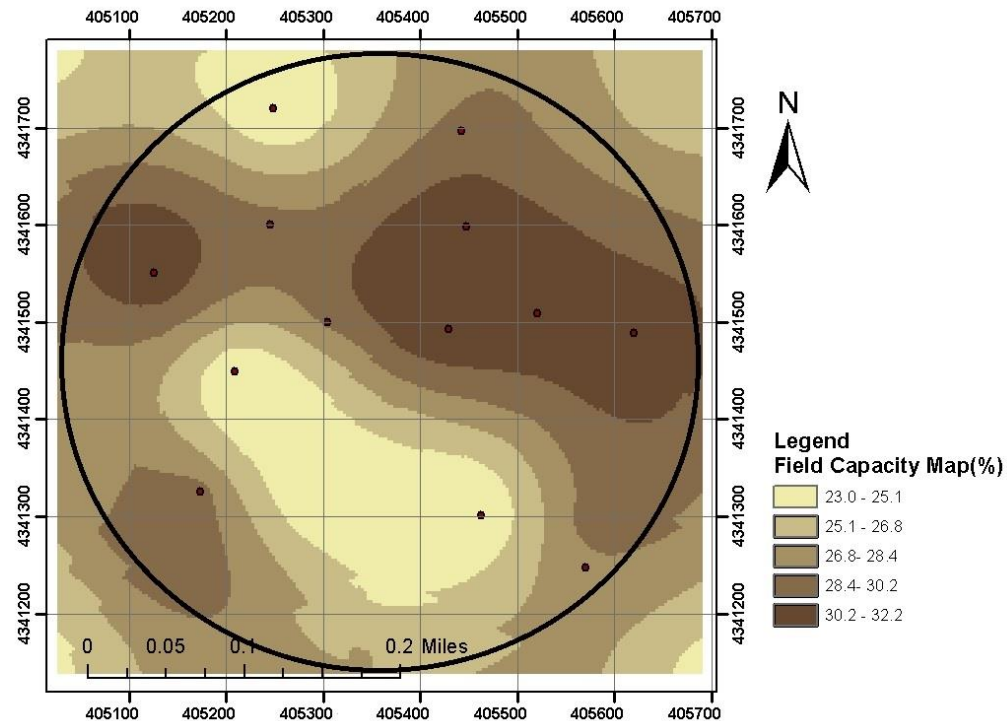


Fig. 4.3. Map of field capacity based on soil texture type and plot of the location of soil moisture sensors.

4.3.3. Optimization

Table 4.1 represents the components of the model based on a water balance approach. Daily root zone soil moisture and evapotranspiration, field capacity, and wilting points are parameters that were considered as inputs in the water balance equation. To ensure correct optimization results, the actual irrigation schedule that was followed by the farmer was previously simulated using the water balance model. Then, the GA model was used to yield optimized irrigation values for the two different objectives.

Table. 4.1. Components of the model based on a water balance approach.

Current water management simulation	Maximizing Soil Moisture Uniformity	Minimizing Crop Yield Reduction
<ul style="list-style-type: none"> • Replicating the current irrigation management using the data derived from soil moisture sensors • Model follows farmers' schedule 	<ul style="list-style-type: none"> • Objective function #1 • Minimizing soil moisture deficit • Applying GA and water balance model • Minimizing GINI coefficient 	<ul style="list-style-type: none"> • Objective function #2 • Minimizing crop yield reduction • Applying GA and water balance model • Minimizing Yield function

4.3.3.1. Objective One: Maximizing Soil Moisture Uniformity

The first objective was based on the concept of the Gini coefficient. This concept was utilized to represent soil moisture uniformity among the 24 arcs, or irrigation sectors, in the farm. As mentioned previously, an arc is the smallest portion of the farm for which the settings of the center pivot are changeable; each such arc is considered as an irrigation sector. The GA was assigned to find the minimum value of this objective by changing irrigation rates for each arc. A Gini coefficient of 0 means all arcs have the same soil moisture, and a Gini coefficient of 1 means one arc gets the entire available soil moisture. Equation 8 represents this concept as the objective function.

Equation 8:
$$GINI = \frac{2 \sum_{i=1}^n i \times Soil\ moisture_i}{n \sum_{i=1}^n Soil\ Moisture_i} - \frac{n+1}{n}$$

4.3.3.2. Objective Two: Minimizing Crop Yield Reduction

The second objective function was based on a yield function. FAO paper No. 66 (Steduto et al., 2012) addressed the relationship between crop yield and water use in the late 1970s, proposing a simple equation where relative yield reduction is related to the corresponding relative reduction in evapotranspiration (ET). This relationship was utilized in the second objective function to calculate yield reduction among the 24 arcs in the farm. Then the GA was assigned to find the minimal yield reduction by changing irrigation rates for each arc.

After receiving the results of the optimization module, the forecasting module allocated water through time across the area covered by the center pivot, considering the results from the previous period of irrigation and the operational capacity of the center pivot irrigation system.

4.4. Results

4.4.1. Soil Moisture Water Balance

4.4.1.1. Root Zone Soil Moisture

After an intensive trial-and-error selection procedure, a network architecture of one hidden layer and six neurons for the surface soil moisture model, and one hidden layer and seven neurons for the deep (root zone) soil moisture were chosen. A division set up of 60:20:20, with trainlm as the training function, worked best for both models.

Estimation of soil moisture produced good results with an R-square value in excess of 0.8 for surface and 0.7 for deep soil moisture. Table 4.2, represents the components of the ANN model for surface and deep soil moisture estimation.

Table. 4.2. Components of the ANN model for surface and deep soil moisture estimation.

Artificial Neural Network for Top Soil Moisture					
Inputs	Hidden Layer	Neurons	Division set up	Training Function	R-Square
Field Measurements, RGB,NIR, Thermal	1	6	60:20:20	trainlm	0.8
Artificial Neural Network for Deep Soil Moisture					
Inputs	Hidden Layer	Neurons	Division set up	Training Function	R-Square
Field Measurements, RGB,NIR, Thermal	1	7	60:20:20	trainlm	0.7

4.4.1.2. Spatial Evapotranspiration

Daily crop evapotranspiration values were calculated on a pixel-by-pixel basis. Figure 4.4 illustrates evapotranspiration values for three sample dates (September 2nd, September 17th and October 4th).

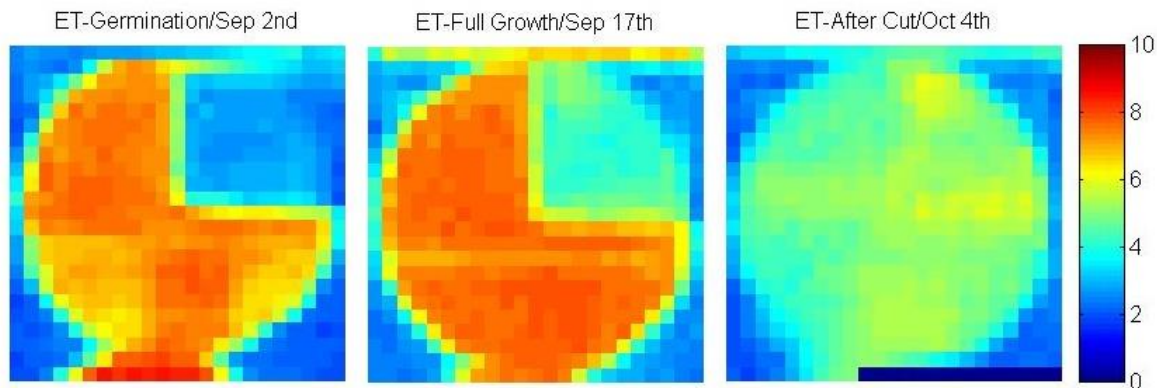


Fig. 4.4. Evapotranspiration map (mm/day).

4.4.2. Current Water Management Simulation

To verify that the model worked properly, the actual irrigation management condition was simulated using a water balance model approach. Figure 4.5.a. shows the results of this simulation for three sample arcs which best represent the modeling approach in the sense of different crop type and soil texture. Table 4.3 represents these results for the same three sample arcs. The ratios of the total volume of water in the root zone for the current irrigation approach and the water balance model is approximately 1, from which it can be concluded that the model is simulating the current approach with good accuracy.

As can be expected from the field capacity map (Figure 4.3), for the same irrigation pattern, arc 9 holds a greater volume of water due to higher water holding capacity. This confirms the significance of soil texture type in irrigation scheduling.

Table. 4.3. Comparison of volume of water in the root zone for current irrigation management and water balance simulation model for three sample arcs.

Total Volume of Water Content (m ³)	Arc#9 (Oats)	Arc#19 (Alfalfa)	Arc#21 (Alfalfa)

Current Irrigation Approach	10967(m ³)	8375(m ³)	9182(m ³)
Water Balance Model Approach	10678(m ³)	8740(m ³)	8717(m ³)
Ratio	1.03	1.04	1.05

4.4.3. Objective One: Maximizing Irrigation Uniformity

The Gini coefficient was utilized to represent soil moisture uniformity among the 24 arcs in the field. The GA found the minimum value of this coefficient by changing irrigation rates for each arc. Figure 4.5.b. shows the soil moisture content of the root zone during the growing cycle for the actual and optimized irrigation management schemes. The ratios of the total available soil moisture in the root zone for the actual irrigation application scheme followed by the farmer over that of the optimized condition are presented in Table 4.4 for the same arcs. Generally these ratios show over-irrigation, and the differences are mainly due to crop and soil texture type changes. As illustrated in Table 4.4, these over-irrigation ratios are 33%, 24% and 4% for arcs number 9, 14 and 21 respectively. The over-irrigation ratios were averaged for the 24 arcs which yielded an average 20% of over-irrigation for the entire field.

Table. 4.4. Comparison of volume of water in the root zone for current and optimized irrigation management for three sample arcs (objective one).

Total Volume of Water Content (m ³)	Arc # 9 (Oats)	Arc # 14 (Alfalfa)	Arc # 21 (Alfalfa)
Current Irrigation Approach	36098(m ³)	31544(m ³)	28570(m ³)
Optimized Irrigation Approach	27101(m ³)	25415(m ³)	27443(m ³)
Ratio	1.33	1.24	1.04

4.4.4. Objective Two: Minimizing Yield Reduction

In this case, the equation that describes the relationship between crop yield and water use is utilized as the objective function (Equation 2). The GA found the minimum value of this objective by changing irrigation rates for each arc. Figure 4.5.c. shows the soil moisture content of the root zone during the growing cycle for actual and optimized irrigation management schemes. The ratios of the total available soil moisture in the root zone for the actual irrigation scheme followed by the farmer over that of the optimized condition are presented in Table 4.5 for the same arcs illustrated earlier. Generally these ratios show over-irrigation (with yield reduction values close to zero) and the differences are again mainly due to crop and soil texture type changes.

Table. 4.5. Comparison of volume of water in the root zone for current and optimized irrigation management for three sample arcs (objective two).

Total Volume of Water Content (m³)	Arc # 9 (Oats)	Arc # 14 (Alfalfa)	Arc # 21 (Alfalfa)
Current Irrigation Approach	36098(m ³)	31544(m ³)	28570(m ³)
Optimized Irrigation Approach	27788(m ³)	26414(m ³)	28383(m ³)
Ratio	1.30	1.19	1.01

As illustrated in Table 4.5, these over-irrigations ratios are 30%, 19% and 1% for arcs number 9, 14 and 21 respectively. The over-irrigation ratios were averaged for the 24 arcs which almost yielded an average 20% of over-irrigation for the entire field.

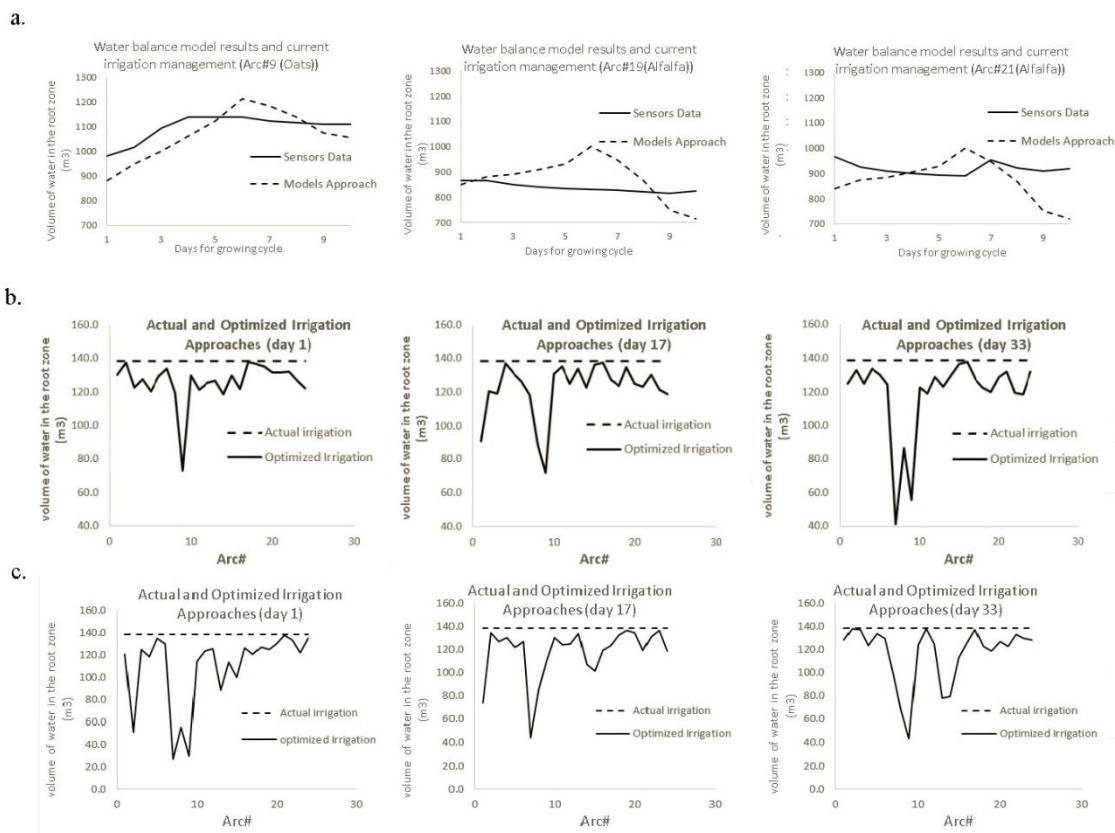


Fig. 4.5. (a) Comparison of volume of water in the root zone for current irrigation management and water balance simulation model, (b) Comparison of volume of water in the root zone for current and optimized irrigation management (objective one), (c) Comparison of volume of water in the root zone for current and optimized irrigation management(objective two).

Fig. 4.6 illustrates the spatial distribution of soil water balance components in the field for both objective functions for a sample day in the growing cycle when the Landsat passed over the field. As the model runs and proceeds forward in terms of time (daily calculations of soil water balance components), it assigns a single value of soil moisture for each arc as well as an irrigation rate. Fig. 4.6 shows soil moisture and irrigation rate distributions on the 17th day are quite similar for both cases which is due to the fact that;

1. Other components of the model such as evapotranspiration and losses are the same,

2. Both objectives are based on the concept of soil water balance. Also, the highest soil moisture values are presented in the north-east quarter where the dominant soil type is finer with higher water holding capacity than other quarters.

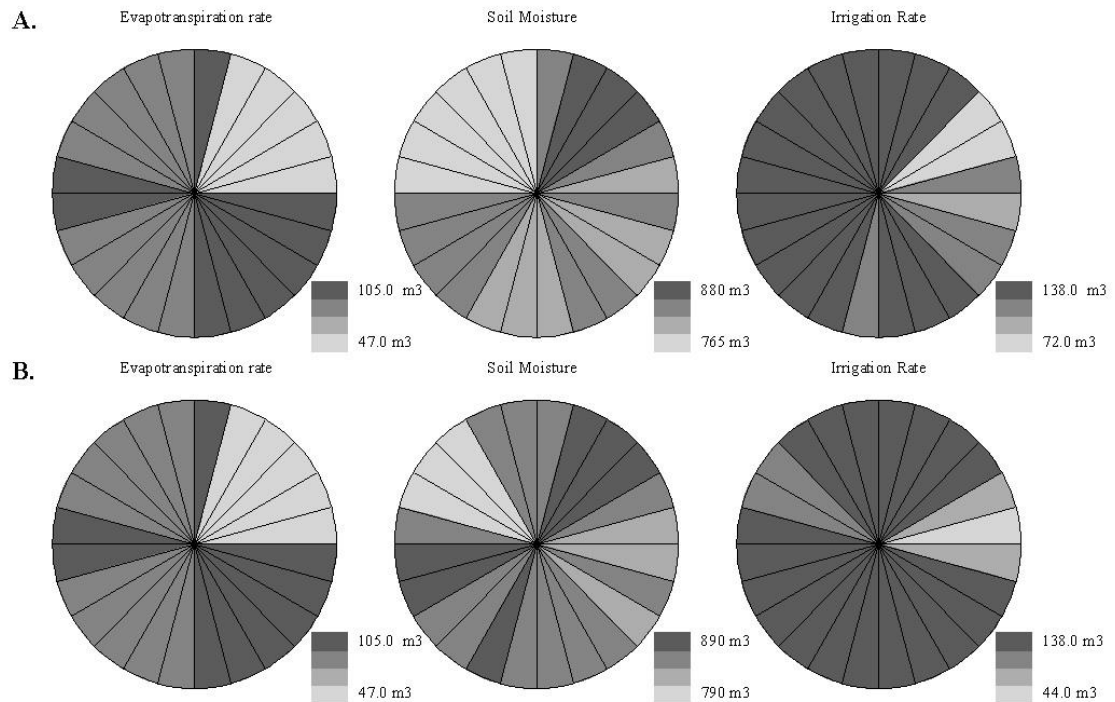


Fig. 4.6. Spatial distribution of soil water balance components in the field for a sample day during the growing cycle (day 17 with Landsat overpass) for objectives one (A) and two (B).

4.5. Conclusions

This study shows the application of water allocation models to achieve more efficient water use in a pressurized irrigation system by use of satellite information, remote sensing models in agriculture, and data mining techniques based on a soil water balance approach. The models were applied to a center pivot for which two different optimization

objectives (water application uniformity and yield reduction minimization) were analyzed and compared against current irrigation schemes for the dates of September 2, 2012 to October 4, 2012.

The results indicate that it is possible to address different actual crop water requirements within the field, given the assessment by the model of soil moisture for each subsector of the farm. These subsectors are the minimal area (or angle) for which the irrigation system can be individually programmed.

The components of the soil moisture balance were modeled based on remote sensing models and field data. Soil moisture data and artificial neural networks were used to develop a customized model for soil moisture estimation that makes use of Landsat imagery to provide soil moisture maps at different depths. The calibration results of the soil moisture models shown in this study indicate good agreement between the model output and the field data.

Actual crop evapotranspiration was calculated following the procedure by Rocha et al. (2010). Potential ET was calculated using the Penman-Monteith approach, while crop coefficients were obtained using NDVI-Kc for alfalfa and oats. Estimation between Landsat passes was made by spline interpolation techniques.

When comparing the results obtained from each optimization objective, it was found that Objectives one and two provide almost the same water savings (up to 20%). This was expected since both objectives functioned based on the concept of soil water balance approach. Other data sources, such as geo-referenced crop harvest information, helped to customize the FAO 56 crop yield equation, which in return shows a different result.

From the analysis of the data collected for the center pivot field, the possible causes for the over-irrigation pattern detected in the optimization model results is mainly due to (1) misinformation about the soil type, (2) low cost of water, (3) desire for a simple program for the center pivot, and (4) lack of attention to the crop type. These possible causes are related to the lack of incentives for achieving more efficient water use.

Keeping in mind the current over-irrigation condition and, in addition, the optimal solutions for the two objectives produced very similar irrigation scheduling, it is possible to present a simple setting for operation of the center pivot that can save significant water and adequately address both objectives.

Still, there are some limitations that restrict the application of remotely sensed data in precision irrigation. Due to the large temporal changes in the field between two consecutive Landsat overpasses and the large pixel size of Landsat images, fine-scale objects are missed. This is a handicap that requires more convenient approaches. Methodologies for using high-resolution, multi-spectral imagery to improve the results might be a solution. Further studies might also address other objectives, such as economical return and improved yield.

4.6. References

- Ahmadi, L., Merkle, G.P., 2009. Planning and management modeling for treated wastewater usage. *Irrig. Drain. Syst* 23, 97–107.
- Allen, R., 2013. REF-ET: Reference Evapotranspiration Calculation Software. University of Idaho Research and Extension Center. Kimberly, ID.

- Allen, R., Pereira, L., Raes, D., Smith, M., 1998. FAO Irrigation and Drainage Paper No. 56. Rome, Italy: FAO; Crop evapotranspiration: guidelines for computing crop water requirements.
- Allen, R., Tasumi, M., Trezza, R., 2007. Satellite-Based Energy Balance for Mapping Evapotranspiration with Internalized Calibration (METRIC)—Model. *J. Irrig. Drain. Eng.* 133(4), 380–394.
- Bastiaanssen, W., Noordman, E., Pelgrum, H., Davids, G., Thoreson, B., Allen, R., 2005. SEBAL Model with Remotely Sensed Data to Improve Water-Resources Management under Actual Field Conditions. *J. Irrig. Drain. Eng.* 131(1), 85–93.
- Bradley, S., Hax, A., Magnanti, T., 1977. *Applied Mathematical Programming*. Addison Wesley.
- Cammalleri, C., Ciraolo, G., 2013. A simple method to directly retrieve reference evapotranspiration from geostationary satellite images. *Int. J. Appl. Earth Obs. Geoinf.* 21, 149-158.
- Costa, A., Albuquerque, J.A., Costa, A., Pértile, P., Ranciani Rodrigues, R., 2013. Water retention and availability in soils of the state of Santa Catarina-Brazil: effect of textural classes, soil classes and lithology. *Braz. Soil Sci. Soc.*, 37:1535-1548.
- Cullis, J., van Koppen, B., 2007. Applying the Gini Coefficient to measure inequality of water use in the Olifants River Water Management Area, South Africa. Colombo, Sri Lanka: International Water Management Institute. 25 p. (IWMI Research Report 113).

- Cruz-Blanco, M., Lorite, I., Santos, C., 2014. An innovative remote sensing based reference evapotranspiration method to support irrigation water management under semi-arid conditions. *Agric. Water Manage.* 131, 135-145.
- Delavar, M., Moghadasi, M., Morid, S., 2012. Real-Time Model for Optimal Water Allocation in Irrigation Systems during Droughts. *J. Irrig. Drain. Eng.* 138(6), 517–524.
- Fares, A., Hamdhani, H., Polyakov, V., 2006. Real-time soil water monitoring for optimum water management. *J. Am. Water Resour. Assoc.*, 42 (2006), pp. 1527–1535.
- Hillel, D., 1971. *Soil and Water: Physical principles and processes*. Academic Press, New York.
- Ines, A., Honda, K., Gupta, A., 2006. Combining remote sensing-simulation modeling and genetic algorithm optimization to explore water management options in irrigated agriculture. *Agric. Water Manage.* 83 (2006) 221–232.
- Irmak, A., Irmak, S., Martin, D., 2008. Reference and Crop Evapotranspiration in South Central Nebraska. I: Comparison and Analysis of Grass and Alfalfa-Reference Evapotranspiration. *J. Irrig. Drain. Eng.* 134(6), 690–699.
- Irish, R.R., 2000. *Landsat 7 Science Data User's Handbook*. National Aeronautics and Space Administration, Report (2000): 430-15.
- Gini, C., 1912. Italian: Variabilità e mutabilità 'Variability and Mutability', C. Cuppini, Bologna, 156 p.
- Goldberg, D.E. 1989. *Genetic Algorithms in Search, Optimization, and Machine Learning*, Addison-Wesley.

- Kashif Gill, M., Kemblowski, M. W., McKee, M., 2007. Soil Moisture Data Assimilation Using Support Vector Machines and Ensemble Kalman Filter. *JAWRA J. Am. Water Resour. Assoc.* 43: 1004–1015.
- Kuo, S.F., Merkley, G.P, Liu, C., 2000. Decision support for irrigation project planning using a genetic algorithm. *Agricultural Water Management* 45 (2000) 243-266.
- Moghaddasi, M., Morid, S., Araghinejad, S., Aghaalikhani, M., 2009. Assessment of irrigation water allocation based on optimization and equitable water reduction approaches to reduce agricultural drought losses: The 1999 drought in the Zayandeh Rud irrigation system (Iran). *J. Irrig. Drain. Eng.* 59 (4), 377–387.
- Pulido-Calvo, I., Gutierrez-Estrada, J.C., 2008. Improved irrigation water demand forecasting using a soft-computing hybrid model. *Biosyst. Eng.* 102 (2009), 202-218.
- Rafn, E.B., Contor, B., Ames, D.P., 2008. Evaluation of a Method for Estimating Irrigated Crop-Evapotranspiration Coefficients from Remotely Sensed Data in Idaho. *J. Irrig. Drain. Eng.* 134(6), 722–729.
- Rocha, J., Perdigao, A., Melo, R., Henriques, C., 2010. Managing water in agriculture through remote sensing application. In: *Proceedings of EARSeL Symposium 2010, 31 May - 3 June 2010, UNESCO, Paris, France.*
- Sammis, T. W., 1981. Yield of Alfalfa and Cotton as Influenced by Irrigation. *Agronomy J.* 1981. 73:323–329.
- Steduto, P., Hsiao, T.C, Fereres, E., Raes, D., 2012. Crop yield response to water. In: *FAO Irrigation and Drainage Paper 66.*

- Taghvaeian, S. Chávez, J., Hattendorf, M., Crookston, M.A., 2013. Optical and thermal remote sensing of turfgrass quality, water stress, and water use under different soil and irrigation treatments. *Remote Sens.* 5(5), 2327-2347.
- Taghvaeian, S., Chavez, J., Hansen, N., 2012. Infrared thermometry to estimate crop water stress index and water use of irrigated maize in northeastern colorado. *Remote Sens.* 2012, 4, 3619-3637.
- The Nature of Mathematical Programming, *Mathematical Programming Glossary*, INFORMS Computing Society. Greenberg, 1999-2006.
- Torres A.F., Walker, R.W., McKee, M., 2011. Forecasting daily potential evapotranspiration using machine learning and limited climatic data. *Agric. Water Manage.* 98 (2011) 553–562.

CHAPTER 5

CONCLUSIONS

5.1. General Conclusions

Remote sensing can provide information for many agricultural management applications. Some currently orbiting satellites provide opportunities of extracting data for free, and many more research opportunities are provided for affordable prices by using sensors aboard small aircraft.

Consecutive Landsat over-passes provide unique imagery that can help monitor agricultural field conditions and crop development stage and site-specific real-time management. Although users benefit from the free Landsat imagery, they have to cope with some existing limitations. Landsat provides imagery from fixed spectral bands which are not necessarily appropriate for agricultural applications. In addition, coarse spatial resolution, inadequate overpasses to monitor variations in agricultural development, and long time periods between image acquisition and delivery to users are other handicaps. Aircraft-based sensors are designed to avoid these limitations but they still suffer from others. They are not free, the imagery is hard to mosaic and ortho-rectify, and can require difficult, site-specific calibration. In this study the application of remote sensing in agriculture was investigated at two different spatial scales: Landsat scale (30m by 30m) and AggieAir scale (0.15m by 0.15) and the advantages and disadvantages of each scale were discussed.

This study presents a solution to the problem of optimally allocating irrigation water over agricultural areas to preserve scarce water resources and help farmers to potentially grow more lands, save on irrigation water expenses and enhance the quality of

the crops. Optimal irrigation water allocation models addressed crop types and growth stages, sensitivity to water stress, and crops water demand.

Application of programmable irrigation systems can improve real-time irrigation water management of a center pivot irrigation system. Remote sensing data at Landsat resolution (30m by 30m pixel size) were used to estimate the components of a soil water balance model including surface and root zone soil moisture and evapotranspiration (ET) rates. Previously developed remote sensing models in agriculture provided us with a wealth of information on how to translate spectral reflectance from Landsat imagery to agricultural information. A non-linear regression model (in the form of Artificial Neural Networks (ANNs)) was used to retrieve soil moisture values from remotely sensed data. Intensive ground-sampling supported the study in terms of modeling the current irrigation management status, evaluating irrigation losses and training, testing and validating the regression model. Putting all these components together provided a soil water balance model which was optimized using two different criteria to yield more efficient water use in the study area where it is equipped with a modern programmable, pressurized irrigation system. The experiment was designed to cover an entire growing cycle of alfalfa and was carried out on three dates in 2012; September 2nd and 18th and October 4th. The results indicate the possibility of presenting a simple setting that can significantly save water. More precisely, the model was optimized regarding two different objectives (maximizing irrigation uniformity and minimizing yield reduction) and illustrated that it is able to calculate optimal irrigation rate (based on each objective) for the subsectors of the study area for which the irrigation system can be individually programmed. The results from the soil moisture modeling approach using ANNs in this study indicate good agreement

between the model output and the field data. Actual crop evapotranspiration, potential crop ET and crop coefficient were calculated following a procedure that was published previously, Penman-Monteith approach and NDVI-Kc for alfalfa and oats, respectively. The results from optimization phase, including both objectives, show almost the same water saving amount (up to 20%). This is expected because both objectives functioned based on the concept of soil water balance approach. Among the field experiments, soil texture analysis wiped out some questions about over-irrigation causes. The farmer was misinformed about the soil type and it negatively affected his decision making quality in terms on irrigation rate and scheduling. Desire for a simple irrigation pattern for the entire field that lacks the attention to crop type variation, is another reason for inefficient irrigation application. Generally, these factors are related to the lack of incentives for achieving more efficient water use. Other than the optimal solutions presented it is possible to construct a simple, single setting for operation of the center pivot that can save significant water and adequately address both objectives (Hassan-Esfahani et al., 2015a).

The limitations of applying remote sensing in agriculture could be due to its temporal scale. Landsat over-passes have sixteen days offset which includes large variation in terms of the growing stage of crops. Also, each Landsat pixel (30m by 30m) covers 900m² of the ground and potentially underestimates the heterogeneities within the footprint and degrades the quality of estimations which can be critical for regression models, retrieving algorithms, and validating the ground truthing data. This is a handicap that requires more convenient approaches. Methodologies for using high-resolution, multi-spectral imagery to improve the results might be a solution.

This study also developed surface soil moisture estimations as a key piece of information in irrigation water management. High-resolution multi-spectral imagery in conjunction with data mining algorithms and ground-truthing data provided the required information to estimate spatially distributed surface soil moisture. The model is a site-and time-specific model and was calibrated using on-site information such as soil moisture measurements, soil texture, crop type information, and high resolution multi-spectral imagery. Although the calibrated ANNs model cannot be used for other study areas, the methodology, data collection procedure, and application of data mining algorithm offers new ideas to further studies.

One of the limitations of remote sensing data is the available spectral bands are limited and might not be quite compatible with the research purpose. In order to check the significance of each individual existing band in surface soil moisture estimations, an intensive modeling procedure examined all individual bands and all possible combinations of them as candidate inputs to the model. The thermal (infrared) and NIR bands contained the most significant information in the surface soil moisture estimations.

In general, surface soil moisture estimations at the high-resolution AggieAir scale provides farmers with far more precise information in identifying stressed crops, hot and dry spots, and water holding capacity of the soil. With this information, farmers do not need to make decisions on irrigation scheduling only based on their visual perceptions or a few soil moisture samples averaged across the farm. It can be concluded that the application of data mining algorithms to AggieAir aerial imagery allows for quantification of actionable information for precision agriculture in terms of soil moisture values across

the field. The soil moisture maps that are produced can be further related to irrigation water management for scheduling and determination of application rates (see chapter 3).

After estimating surface soil moisture at high spatial resolution, research was conducted to estimate root zone soil moisture as a key component in a soil water balance model that supports agricultural water management. A Bayesian-based model was applied to in-field data of root zone soil moisture. This model used surface soil moisture measurements from the previous model as boundary conditions for the calculations. The model output was presented as the spatially distributed root zone soil volumetric water content. The same methodology has been applied at this stage in terms of training, testing and validating the data mining algorithm. In the model development procedure, in-field conditions such as soil texture, crop type, growing stage and location of lateral at the time of imagery have been noted. Although this model is site-and time-specific, it offers insight into a process for identifying model inputs that contain the most information for estimating soil moisture. Also, using all the data (i.e. data for four different sampling dates) in modeling captures information about four different moisture states for each sample point; this lessens the limitations of the “time-specific” adjective of the model. Four different moisture states for each point is enough information to represent soil moisture variation in the temporal scale. The statistical matrices that have been applied to check the goodness of fit of the model indicate good accuracy in their geospatial estimation of soil moisture. Instead of visual perception of soil moisture by farmers, this study provides a means whereby farmers might gain information about actual soil moisture distribution over the farms, which could help in irrigation scheduling and enable greater precision in the application of irrigation water by identifying dry/wet spots. The significance of the thermal

(infrared) band and soil texture type are identified as the main conclusion of this study. Since soil texture type is the main parameter in determining soil water holding capacity, these results were expected and meaningful.

In addition to individual spectral bands, vegetation indices were also used as model inputs to the neural net models. The results show these indices could selectively improve the model performance statistics (see chapter 2).

5.2. Future Work

Further studies might generate the same sort of estimates using other data mining algorithms. The root zone soil moisture results could be used to produce remotely sensed estimates of crop water requirements useful for prescriptive irrigation scheduling with the same resolution in time and space. Pixelwise estimation of root zone soil moisture could also be applied in a water balance model for forecasting short-term future conditions.

Accurate high-resolution soil moisture data are needed for a range of agricultural and hydrologic activities. To improve the spatial resolution of soil moisture estimates derived from Landsat imagery (30 m resolution), a methodology to derive soil moisture estimates based on airborne imagery (15 cm resolution) has been implemented. These two sets of analogous information (at two different spatial scales, Landsat and AggieAir) could be compared. Also, these two sets could be used for further calculations on downscaling/upscaling issues.

APPENDICES

ESEVIER LICENSE

This is a License Agreement between LEILA HASSAN ("You") and Elsevier ("Elsevier") provided by Copyright Clearance Center ("CCC"). The license consists of your order details, the terms and conditions provided by Elsevier, and the payment terms and conditions.

License number	3654311488301
License date	Jun 22, 2015
Licensed content publisher	Elsevier
Licensed content publication	Agricultural Water Management
Licensed content title	Assessment of optimal irrigation water allocation for pressurized irrigation system using water balance approach, learning machines, and remotely sensed data
Licensed content author	Leila Hassan-Esfahani,Alfonso Torres-Rua,Mac McKee
Licensed content date	1 May 2015
Licensed content volume number	153
Licensed content issue number	n/a
Number of pages	9

Start Page	42
End Page	50
Type of Use	reuse in a thesis/dissertation
Portion	full article
Format	print
Are you the author of this Elsevier article?	Yes
Will you be translating?	No
Title of your thesis/dissertation	HIGH RESOLUTION MULTI-SPECTRAL IMAGERY AND LEARNING MACHINES IN PRECISION IRRIGATION WATER MANAGEMENT
Expected completion date	Jun 2015
Estimated size (number of pages)	150
Elsevier VAT number	GB 494 6272 12
Permissions price	0.00 USD
VAT/Local Sales Tax	0.00 USD / 0.00 GBP
Total	0.00 USD

ESEVIER LICENSE

TERMS AND CONDITIONS

INTRODUCTION

1. The publisher for this copyrighted material is Elsevier. By clicking "accept" in connection with completing this licensing transaction, you agree that the following terms and conditions apply to this transaction (along with the Billing and Payment terms and conditions established by Copyright Clearance Center, Inc. ("CCC"), at the time that you opened your Rightslink account and that are available at any time at <http://myaccount.copyright.com>).

GENERAL TERMS

2. Elsevier hereby grants you permission to reproduce the aforementioned material subject to the terms and conditions indicated.

3. Acknowledgement: If any part of the material to be used (for example, figures) has appeared in our publication with credit or acknowledgement to another source, permission must also be sought from that source. If such permission is not obtained then that material may not be included in your publication/copies. Suitable acknowledgement to the source must be made, either as a footnote or in a reference list at the end of your publication, as follows:

"Reprinted from Publication title, Vol /edition number, Author(s), Title of article / title of chapter, Pages No., Copyright (Year), with permission from Elsevier [OR APPLICABLE

SOCIETY COPYRIGHT OWNER]." Also Lancet special credit - "Reprinted from The Lancet, Vol. number, Author(s), Title of article, Pages No., Copyright (Year), with permission from Elsevier."

4. Reproduction of this material is confined to the purpose and/or media for which permission is hereby given.

5. Altering/Modifying Material: Not Permitted. However figures and illustrations may be altered/adapted minimally to serve your work. Any other abbreviations, additions, deletions and/or any other alterations shall be made only with prior written authorization of Elsevier Ltd. (Please contact Elsevier at permissions@elsevier.com)

6. If the permission fee for the requested use of our material is waived in this instance, please be advised that your future requests for Elsevier materials may attract a fee.

7. Reservation of Rights: Publisher reserves all rights not specifically granted in the combination of (i) the license details provided by you and accepted in the course of this licensing transaction, (ii) these terms and conditions and (iii) CCC's Billing and Payment terms and conditions.

8. License Contingent Upon Payment: While you may exercise the rights licensed immediately upon issuance of the license at the end of the licensing process for the transaction, provided that you have disclosed complete and accurate details of your proposed use, no license is finally effective unless and until full payment is received from you (either by publisher or by CCC) as provided in CCC's Billing and Payment terms and conditions. If full payment is not received on a timely basis, then any license preliminarily granted shall be deemed automatically revoked and shall be void as if never

granted. Further, in the event that you breach any of these terms and conditions or any of CCC's Billing and Payment terms and conditions, the license is automatically revoked and shall be void as if never granted. Use of materials as described in a revoked license, as well as any use of the materials beyond the scope of an unrevoked license, may constitute copyright infringement and publisher reserves the right to take any and all action to protect its copyright in the materials.

9. Warranties: Publisher makes no representations or warranties with respect to the licensed material.

10. Indemnity: You hereby indemnify and agree to hold harmless publisher and CCC, and their respective officers, directors, employees and agents, from and against any and all claims arising out of your use of the licensed material other than as specifically authorized pursuant to this license.

11. No Transfer of License: This license is personal to you and may not be sublicensed, assigned, or transferred by you to any other person without publisher's written permission.

12. No Amendment Except in Writing: This license may not be amended except in a writing signed by both parties (or, in the case of publisher, by CCC on publisher's behalf).

13. Objection to Contrary Terms: Publisher hereby objects to any terms contained in any purchase order, acknowledgment, check endorsement or other writing prepared by you, which terms are inconsistent with these terms and conditions or CCC's Billing and Payment terms and conditions. These terms and conditions, together with CCC's Billing

and Payment terms and conditions (which are incorporated herein), comprise the entire agreement between you and publisher (and CCC) concerning this licensing transaction. In the event of any conflict between your obligations established by these terms and conditions and those established by CCC's Billing and Payment terms and conditions, these terms and conditions shall control.

14. Revocation: Elsevier or Copyright Clearance Center may deny the permissions described in this License at their sole discretion, for any reason or no reason, with a full refund payable to you. Notice of such denial will be made using the contact information provided by you. Failure to receive such notice will not alter or invalidate the denial. In no event will Elsevier or Copyright Clearance Center be responsible or liable for any costs, expenses or damage incurred by you as a result of a denial of your permission request, other than a refund of the amount(s) paid by you to Elsevier and/or Copyright Clearance Center for denied permissions.

LIMITED LICENSE

The following terms and conditions apply only to specific license types:

15. Translation: This permission is granted for non-exclusive world English rights only unless your license was granted for translation rights. If you licensed translation rights you may only translate this content into the languages you requested. A professional translator must perform all translations and reproduce the content word for word preserving the integrity of the article. If this license is to re-use 1 or 2 figures then permission is granted for non-exclusive world rights in all languages.

16. Posting licensed content on any Website: The following terms and conditions apply as follows: Licensing material from an Elsevier journal: All content posted to the web site must maintain the copyright information line on the bottom of each image; A hyper-text must be included to the Homepage of the journal from which you are licensing at <http://www.sciencedirect.com/science/journal/xxxxx> or the Elsevier homepage for books at <http://www.elsevier.com>; Central Storage: This license does not include permission for a scanned version of the material to be stored in a central repository such as that provided by Heron/XanEdu.

Licensing material from an Elsevier book: A hyper-text link must be included to the Elsevier homepage at <http://www.elsevier.com> . All content posted to the web site must maintain the copyright information line on the bottom of each image.

Posting licensed content on Electronic reserve: In addition to the above the following clauses are applicable: The web site must be password-protected and made available only to bona fide students registered on a relevant course. This permission is granted for 1 year only. You may obtain a new license for future website posting.

17. For journal authors: the following clauses are applicable in addition to the above:

Preprints:

A preprint is an author's own write-up of research results and analysis, it has not been peer-reviewed, nor has it had any other value added to it by a publisher (such as formatting, copyright, technical enhancement etc.).

Authors can share their preprints anywhere at any time. Preprints should not be added to or enhanced in any way in order to appear more like, or to substitute for, the final versions of articles however authors can update their preprints on arXiv or RePEc with their Accepted Author Manuscript (see below).

If accepted for publication, we encourage authors to link from the preprint to their formal publication via its DOI. Millions of researchers have access to the formal publications on ScienceDirect, and so links will help users to find, access, cite and use the best available version. Please note that Cell Press, The Lancet and some society-owned have different preprint policies. Information on these policies is available on the journal homepage.

Accepted Author Manuscripts: An accepted author manuscript is the manuscript of an article that has been accepted for publication and which typically includes author-incorporated changes suggested during submission, peer review and editor-author communications.

Authors can share their accepted author manuscript:

- – immediately
 - via their non-commercial person homepage or blog
 - by updating a preprint in arXiv or RePEc with the accepted manuscript
 - via their research institute or institutional repository for internal institutional uses or as part of an invitation-only research collaboration work-group

- directly by providing copies to their students or to research collaborators for their personal use
- for private scholarly sharing as part of an invitation-only work group on commercial sites with which Elsevier has an agreement
- – after the embargo period
 - via non-commercial hosting platforms such as their institutional repository
 - via commercial sites with which Elsevier has an agreement

In all cases accepted manuscripts should:

- – link to the formal publication via its DOI
- – bear a CC-BY-NC-ND license - this is easy to do
- – if aggregated with other manuscripts, for example in a repository or other site, be shared in alignment with our hosting policy not be added to or enhanced in any way to appear more like, or to substitute for, the published journal article.

Published journal article (JPA): A published journal article (PJA) is the definitive final record of published research that appears or will appear in the journal and embodies all

value-adding publishing activities including peer review co-ordination, copy-editing, formatting, (if relevant) pagination and online enrichment.

Policies for sharing publishing journal articles differ for subscription and gold open access articles:

Subscription Articles: If you are an author, please share a link to your article rather than the full-text. Millions of researchers have access to the formal publications on ScienceDirect, and so links will help your users to find, access, cite, and use the best available version.

Theses and dissertations which contain embedded PJAs as part of the formal submission can be posted publicly by the awarding institution with DOI links back to the formal publications on ScienceDirect.

If you are affiliated with a library that subscribes to ScienceDirect you have additional private sharing rights for others' research accessed under that agreement. This includes use for classroom teaching and internal training at the institution (including use in course packs and courseware programs), and inclusion of the article for grant funding purposes.

Gold Open Access Articles: May be shared according to the author-selected end-user license and should contain a CrossMark logo, the end user license, and a DOI link to the formal publication on ScienceDirect.

Please refer to Elsevier's posting policy for further information.

18. For book authors the following clauses are applicable in addition to the above: Authors are permitted to place a brief summary of their work online only. You

are not allowed to download and post the published electronic version of your chapter, nor may you scan the printed edition to create an electronic version. Posting to a repository: Authors are permitted to post a summary of their chapter only in their institution's repository.

19. Thesis/Dissertation: If your license is for use in a thesis/dissertation your thesis may be submitted to your institution in either print or electronic form. Should your thesis be published commercially, please reapply for permission. These requirements include permission for the Library and Archives of Canada to supply single copies, on demand, of the complete thesis and include permission for Proquest/UMI to supply single copies, on demand, of the complete thesis. Should your thesis be published commercially, please reapply for permission. Theses and dissertations which contain embedded PJAs as part of the formal submission can be posted publicly by the awarding institution with DOI links back to the formal publications on ScienceDirect.

20. Other Conditions:

v1.7

Questions? customercare@copyright.com or +1-855-239-3415 (toll free in the US) or +1-978-646-2777.

Permission to include papers in dissertation

Alfonso Torres-Rua <a.torres@aggiemail.usu.edu

Jun 18

to me

I hereby give permission to Leila Hassan-Esfahani to reprint the following material in her dissertation.

Hassan Esfahani, L. Torres-Rua A., and McKee, M. (2015)." Assessment of optimal irrigation water allocation for pressurized irrigation system using water balance approach, learning machines, and remotely sensed data". Agricultural Water Management. 2015, 153, 42-50.
doi:10.1016/j.agwat.2015.02.005

Hassan Esfahani, L. Torres-Rua A., Jensen A., and McKee, M. (2015)." Assessment of Surface Soil Moisture Using High-Resolution Multi-Spectral Imagery and Artificial Neural Networks". Remote Sensing 2015; 7(3):2627-2646. doi:10.3390/rs70302627

Hassan Esfahani, L. Torres-Rua A., Jensen A., and McKee, M. (2015)." High-Resolution Root-Zone Soil Water Content Estimation Using Bayesian-Based Artificial Neural Networks and High Resolution Visual, NIR, and Thermal Imagery". Under review in Irrigation Science

Best,

Alfonso

Alfonso Torres-Rua, Ph.D

Research Engineer

Utah Water Research Laboratory

Utah State University

Alfonso.Torres@usu.edu

Tel: +1 (435) 890-0196

Fax: +1 (435) 797-3663

Austin Jensen Austin.Jensen@usu.edu

Jun 16

to me

I hereby give permission to Leila Hassan-Esfahani to reprint the following material in her dissertation.

Hassan Esfahani, L. Torres-Rua A., Jensen A., and McKee, M. (2015)." Assessment of Surface Soil Moisture Using High-Resolution Multi-Spectral Imagery and Artificial Neural Networks". Remote Sensing 2015; 7(3):2627-2646. doi:10.3390/rs70302627

Hassan Esfahani, L. Torres-Rua A., Jensen A., and McKee, M. (2015)." High-Resolution Root-Zone Soil Water Content Estimation Using Bayesian-Based Artificial Neural Networks and High Resolution Visual, NIR, and Thermal Imagery". Under review in Irrigation Science

Thanks!

Austin

Austin Jensen, Ph.D., Research Engineer
Utah Water Research Laboratory (UWRL)
Utah State University, 8200 Old Main Hill
Logan, UT, 84322-8200, USA
W: <http://aggieair.usu.edu>

E: Austin.Jensen@usu.edu

T: (435)797-3315

CURRICULUM VITAE

Leila Hassan Esfahani

Ph.D Research Assistant

Department of Civil and Environmental Engineering

Utah State University

EDUCATION

Postdoctoral Fellow

June 2015 – present

Utah State University, Logan, Utah, USA

Research focus: “Remote sensing of agricultural field conditions” Adviser: Dr. Mac

McKee

PhD, Civil and Environmental Engineering

January 2011 – June 2015

Utah State University, Logan, Utah, USA

Thesis: “High resolution multi-spectral imagery and learning machines in precision

irrigation water management” Adviser: Dr. Mac McKee

M.S., Civil Engineering

September 2005 – December 2007

Tabriz University, Tabriz, Iran

Thesis: “Evaluation of Gstars model for simulation of sedimentation in detention basins”

Adviser: Dr. M.E. Banihabib

Graduated with honors

B.S. Agricultural Engineering – Irrigation

September 2001 – September 2005

Mazandaran University, Sari, Iran

Adviser: Mirkhalegh Z. Ahmadi

RESEARCH INTERESTS

- Remote sensing of agricultural fields condition
- Data mining analysis
- Modeling agricultural fields condition
- Sediment and flood control analysis

CONSULTING EXPERIENCE

Title: Civil Engineer

December 2007 – January

2011

- Gave consultancy to manager for decision making
- Used hec– ras 4.0 (beta), hec ras 3.1.2, and gstars 3.0
- Analyzed different proposed options for special cases
- Analyzed trap efficiency of reservoirs, sediment concentration ratio, and sediment storage rate
- Analyzed sedimentation and river morphology changes

Organization: Ide Pardazen Company, Tehran, Iran. <http://www.idehpardazan.ir/>

Title: Civil Engineer

July 2006 – December 2007

- Designed hydraulic structures
- Designed water conveyance structures

- Modeled hydrological processes in catchments

Organization: NETPA Company, Tehran, Iran

COMPUTER SKILLS

- Microsoft office
- GSTARS
- Auto Cad
- Autodesk Land Desktop
- HEC-HMS and HEC-RAS
- ArcGIS
- ERDAS
- MATLAB Programming

RESEARCH EXPERIENCE

2011-

PRESENT

- Remote sensing of agricultural fields condition
- Precision agriculture
- Data mining
- Evaluating irrigation performance and presenting optimal irrigation schedule as an application of remote sensing instrumentation
- Modeling of surface/root zone soil moisture as an application of remote sensing instrumentation

Specialties: Remote sensing, GIS, Agricultural hydrology, Matlab programming,
ERDAS

RESEARCH EXPERIENCE

2005-2009

- Numerical simulation of flow
- Sediment transport & water quality
- Mechanism & occurrence of mud and debris flow
- Simulation of sedimentation in settling basins and detention basins

Specialties: GSTARS, HEC-RAS, HEC-HMS- Auto-CAD

PUBLICATIONS

Journals

1. Hassan Esfahani, L. Torres-Rua A., Jensen A., and McKee, M. (2014)." Top soil moisture estimation for precision agriculture using unmanned aerial vehicle multispectral imagery". *Geoscience and Remote Sensing Symposium (IGARSS), 2014 IEEE International*
2. Hassan Esfahani, L. Torres-Rua A., and McKee, M. (2015)." Assessment of optimal irrigation water allocation for pressurized irrigation system using water balance approach, learning machines, and remotely sensed data". *Agricultural Water Management*. 2015, 153, 42-50. [doi:10.1016/j.agwat.2015.02.005](https://doi.org/10.1016/j.agwat.2015.02.005)
3. Hassan Esfahani, L. Torres-Rua A., Jensen A., and McKee, M. (2015)." Assessment of Surface Soil Moisture Using High-Resolution Multi-Spectral

- Imagery and Artificial Neural Networks". *Remote Sensing* 2015; 7(3):2627-2646. doi:10.3390/rs70302627
4. Hassan-Esfahani and L Banihabib, M.E. (2014). "Fusion of a physical model for assessment of gstars3.0 ability to simulate debris flows control by slit and classic retention dams". Under review in *Environmental Earth Science*.
 5. Hassan Esfahani, L. Torres-Rua A., Jensen A., and McKee, M. (2015). " High-Resolution Root-Zone Soil Water Content Estimation Using Bayesian-Based Artificial Neural Networks and High Resolution Visual, NIR, and Thermal Imagery". Under review in *Irrigation Science*

Conferences

1. Banihabib, M.E., Hassanzadeh, Y. and Hassan Esfahani, L. (2006). "Evaluation of GSTARS Model for Simulation of Sedimentation in Detention Basins". *7th Iranian Hydraulic Conference*. Tehran, Iran
2. Banihabib, M.E., Hassanzadeh, Y. and Hassan Esfahani, L. (2005). "Evaluation of HEC-RAS Model for Simulation of Sedimentation in Detention Basins". *4th National Conference of Watershed Engineering and Management*. Tehran, Iran
3. Hassan Esfahani, L. and McKee, M. (2013). " Optimal irrigation water allocation for a center pivot using remotely sensed data". *AGU Fall meeting 2013*. San Francisco CA.
4. Hassan Esfahani, L. Torres-Rua A., Jensen A., and McKee, M. (2014). " Fusion of high resolution multi-spectral imagery for surface soil moisture estimation using

- learning machines". *Spring runoff conference, 2014*. Utah State University, Logan, Utah.
5. Hassan Esfahani, L. Torres-Rua A., Jensen A., and McKee, M. (2014)." Retrieving High-Resolution Root-Zone Soil Moisture from Remotely Sensed Surface Soil Moisture, Multispectral Unmanned Aerial Vehicle Imagery, and Data Mining Algorithms". *American Water Resources Association, AWRA 2014*. Tyson Corner, Virginia.
 6. Hassan Esfahani, L. Torres-Rua A., Jensen A., and McKee, M. (2014)." Spatial Scaling Assessment of Surface Soil Moisture Estimations Using Remotely Sensed Data for Precision Agriculture". *AGU Fall meeting 2014*. San Francisco CA.
 7. Hassan Esfahani, L. Torres-Rua A., Jensen A., and McKee, M. (2014)." The Contributions of High Resolution Multispectral Imagery to Precision Agriculture: A Case Study of Soil Moisture Estimations". *Spring runoff conference, 2015*. Utah State University, Logan, Utah.
 8. Leila Hassae-Esfahani. (2015).The Contributions of Landsat and Airborne Products in Monitoring Surface Soil Moisture. *10th Annual J. Paul Riley AWRA-Utah Section Student Conference and Paper Competition, Brigham Young University, Salt Lake Center*
 9. Torres-Rua A., El-arab, M., Hassan Esfahani, L., Jensen, A., and McKee, M. (2015). Development of Unmanned Aerial Systems for Use in Precision Agriculture: The AggieAir Experience. *2015 IEEE Conference on Technologies for Sustainability (SusTech)*

Awards

1. Graduate student travel assistance award, Utah State University, Sep 2014
2. Winner of scholarship award for 10th Annual J. Paul Riley AWRA-Utah Section Student Conference and Paper Competition